

Convection and Chemistry in the Atmospheric Boundary Layer

Arthur C. Petersen

Cover design by Marijke Jansen
Photography by Laurens Ganzeveld
Printed by Ponsen & Looijen, Wageningen

ISBN 90-393-2082-9

Convection and Chemistry in the Atmospheric Boundary Layer

**Convectie en Chemie in de Atmosferische
Grenslaag**

(met een samenvatting in het Nederlands)

PROEFSCHRIFT

TER VERKRIJGING VAN DE GRAAD VAN DOCTOR AAN
DE UNIVERSITEIT UTRECHT OP GEZAG VAN DE RECTOR
MAGNIFICUS, PROF. DR. H.O. VOORMA, INGEVOLGE HET
BESLUIT VAN HET COLLEGE VOOR PROMOTIES IN HET
OPENBAAR TE VERDEDIGEN OP MAANDAG 7 JUNI 1999
DES NAMIDDAGS TE 4.15 UUR

door

Arthur Caesar Petersen

geboren op 29 september 1970, te Amsterdam

promotoren: **Prof. dr. A.A.M. Holtslag**
Faculteit Natuur- en Sterrenkunde, Universiteit Utrecht
Prof. dr. J. Lelieveld
Faculteit Natuur- en Sterrenkunde, Universiteit Utrecht
co-promotor: **Dr. H. van Dop**
Faculteit Natuur- en Sterrenkunde, Universiteit Utrecht

The work presented in this dissertation was supported by the Netherlands Earth and Life Sciences Foundation (ALW) with financial aid from the Netherlands Organization for Scientific Research (NWO).

Preface

The work presented here forms part of a PhD research project that started in January 1995 under the supervision of Han van Dop at the Institute for Marine and Atmospheric Research Utrecht (IMAU). The project's aim was to study—and possibly improve—the description of physical processes that affect atmospheric chemistry, especially those processes that cannot be resolved by large-scale atmospheric chemistry models (with grid sizes ranging from 10 to 1000 km).

From a range of possible topics indicated in the original project proposal the turbulent transport–reaction problem in the atmospheric boundary layer was chosen as the primary focus of my research. This choice was to some extent coincidental but to a large extent the result of the presence of a research program on this topic at Utrecht University (involving Peter Buitjes, Jordi Vilà-Guerau de Arellano, Peter Duynkerke, Kees Beets, Han van Dop, Stefano Galmarini, Lianne Crone, Maarten Krol, and Laurens Ganzeveld) and the Royal Netherlands Meteorological Institute (KNMI; involving Gé Verver). These colleagues were all studying specific aspects of the turbulent transport–reaction problem and some had put forth evidence that current large-scale atmospheric chemistry models are in error due to some simplifying assumptions contained in these models. However, the precise contribution of the neglected aspects of the turbulent transport–reaction problem to inaccuracies in the models was still unknown, since no simple “parameterizations” of these effects were available for inclusion in the models. Thus the aim of my studies became the development of a simple parameterization for one aspect (“segregation effects”) of the mentioned problem.

I have greatly profited from the encouragement, help, and comments from the colleagues that are mentioned in the above. Peter Buitjes was involved from the start and stimulated the participation in a European research network, Peter Duynkerke suggested to me the usefulness of the mass-flux approach for the problem at hand, Kees Beets assisted with the numerical implementation of the mass-flux schemes and transferred his large-eddy simu-

lation code to me, Jordi Vilà-Guerau de Arellano gave stimulating comments throughout the whole project and helped with debugging a large-eddy simulation code used in chapters 3 and 4, Maarten Krol critically followed the whole project and gave access to his large-eddy simulation results for the photochemistry case studied in chapters 3 and 4, Laurens Ganzeveld implemented chemistry in the single-column climate model and made it possible to run the model with output from global climate and chemistry models, and Gé Verver was willing to answer the challenges that I (not always rightly) made to his model (which led to fruitful discussions on both our models' deficiencies).

I thank my co-authors Kees Beets, Han van Dop, Peter Duynkerke, Bert Holtslag, and Pier Siebesma for their contributions to this dissertation. Furthermore, I particularly want to thank my three advisers. Bert Holtslag was enthusiastic about applying meteorological knowledge to atmospheric chemistry problems, he stimulated and helped me a lot with the writing, especially by suggesting some structural changes in the different chapters. Jos Lelieveld became involved when the project was already well underway. He was very interested to know the errors associated with neglecting some aspects of the turbulent transport–reaction problem in global atmospheric chemistry models, he stimulated the development of the single-column chemistry–climate model, and commented on the manuscript. Finally, Han van Dop stimulated me to become an independent scientist and trusted me with pursuing this research direction, he organized a fruitful cooperation with the National Research Institute for Mathematics and Computer Science (CWI), and he gave many incisive comments on the manuscript.

I finally wish to thank Pier Siebesma for enhancing my insight in mass-flux modeling, Harm Jonker for his comments on chapter 1 and his calculation of the spectra in appendix B, Peter Bechtold, Aad van Ulden, and two anonymous reviewers for their comments on chapter 2, Hans Cuijpers for providing his large-eddy simulation code, two anonymous reviewers for their comments on chapter 3, Stephan de Roode for his comments on chapter 4, and Erik van Meijgaard for providing the single-column climate model used in chapter 5.

At seminars, conferences, courses, and short working visits in Europe and North America I received stimulating input to my research from the many contacts I had there with atmospheric scientists. Closer to home, at IMAU and KNMI, I had many conversations with PhD students, postdocs, and faculty of both the boundary-layer meteorology and the atmospheric chemistry groups. The comments received at working group sessions have also been valuable.

This PhD project was part of an effort, named CIRK, by the three partners of the Netherlands Centre for Climate Research (CKO)—IMAU, KNMI, and the National Institute of Public Health and the Environment (RIVM)—together with CWI, to join forces in the de-

velopment of global atmospheric chemistry models. The global atmospheric tracer model TM2, and its successor TM3, in use at CKO, was chosen as the model of interest. The areas of model development were the numerics and the treatment of subgrid-scale processes. I spent most of my research time on subgrid-scale processes (the subject of this dissertation) and part of my time on the development and implementation of new advection schemes (see Petersen et al. 1998). The following people at CWI are thanked for their leading role in the second part of my job: Edwin Spee, Willem Hundsdorfer, Joke Blom, and Jan Verwer.

During the four years that the project lasted I stayed with the group of Bert Holtslag at KNMI for 18 months (winter 1996–summer 1997). The facilities offered by KNMI are gratefully acknowledged. Chapter 2 is the result of this period at KNMI. The year before and the 18 months following this visit were spent at IMAU. For the whole project support by the Netherlands Earth and Life Sciences Foundation (ALW, formerly the Geosciences Foundation, GOA) is acknowledged, with financial aid from the Netherlands Organization for Scientific Research (NWO). This work was sponsored by the National Computing Facilities Foundation (NCF) for the use of supercomputing facilities.

Utrecht

ARTHUR PETERSEN

Contents

1	General introduction	1
1.1	The CABL as a manifestation of turbulence	5
1.2	The CABL with reacting chemical species	10
1.3	Models for atmospheric transport and chemistry	13
1.3.1	LES models including chemistry	14
1.3.2	Single-column chemistry models	17
1.3.3	Large-scale chemical transport models	19
1.4	Research questions and outline of the dissertation	20
2	Mass-flux characteristics of reactive scalars in the convective boundary layer	21
2.1	Introduction	23
2.2	Description of LES and cases	25
2.2.1	LES of the solid-lid CABL	25
2.2.2	Cases	28
2.3	Scalar plume budgets	30
2.3.1	Basic equations	30
2.3.2	Subplume contributions to the plume-budget equations	32
2.3.3	Lateral-exchange terms	35
2.3.4	Mass-flux schemes for scalar transport	37
2.4	LES results for nonreactive scalars	39
2.4.1	Scalar profiles $\overline{s_{BU}}$ and $\overline{s_{TD}}$	39
2.4.2	Fluxes $\overline{w's'_{BU}}$ and $\overline{w's'_{TD}}$	39
2.4.3	Lateral entrainment and detrainment rates E_{BU} , D_{BU} , E_{TD} , and D_{TD}	41
2.5	LES results for reactive scalars	42
2.5.1	Steady-state scalar values $\overline{s_A}$ and $\overline{s_B}$	42
2.5.2	Fluxes $\overline{w's'_A}$ and $\overline{w's'_B}$	44

2.5.3	Covariance $\overline{s'_A s'_B}$	46
2.5.4	Lateral entrainment and detrainment rates E_A , D_A , E_B , and D_B	47
2.6	Results of mass-flux schemes	49
2.6.1	Non-reactive case BUTD	49
2.6.2	Reactive cases AB1, AB2, and AB3	49
2.7	Summary and discussion	52
3	A first-order closure for covariances and fluxes of reactive species in the convective boundary layer	55
3.1	Introduction	57
3.2	Theory and background	59
3.3	First-order closures	63
3.3.1	Covariances	63
3.3.2	Fluxes	66
3.3.3	Incorporation in a 1-D model	67
3.4	Simple cases with one irreversible, binary reaction	68
3.4.1	Description and LES results	68
3.4.2	Closure evaluations	73
3.5	Photochemistry case	75
3.5.1	Description and LES results	75
3.5.2	Closure evaluations	79
3.5.3	Sensitivity runs	83
3.6	Summary and discussion	84
4	The impact of chemistry on flux estimates in the convective boundary layer	87
4.1	Introduction	89
4.2	Theory	90
4.3	Second-order closure formulation	91
4.4	Mass-flux closure formulation	92
4.5	Intercomparison of formulations using LES	95
4.5.1	Description of cases	95
4.5.2	Results	98
4.6	Summary and discussion	99
5	Segregation effects in atmospheric chemistry related to boundary-layer convection	101
5.1	Introduction	103

5.2	Model description	104
5.3	Results for different cases	105
5.4	Summary and discussion	107
6	Summary and discussion	109
6.1	Summary	111
6.2	Discussion	113
A	Fractional top-hat contribution to the covariance κ_{12}	115
B	Spectral behavior of $\overline{s'_1 s'_2}$	119
C	Top-hat formulas for a and M	121
D	Implementing the covariance closure	125
E	Specification of LES runs used in chapter 3	129
	Bibliography	133
	Samenvatting	143
	Curriculum vitae	147

Chapter 1

General introduction

The earth's troposphere is the lowest layer of the atmosphere and has a thickness of about 10 km. It is the layer that contains most of the mass (80%) of the atmosphere. All weather phenomena that we experience have their origin in the troposphere. It is the stage for some well-known environmental problems: climate change, ozone smog, and acidification. These problems are related to the trace amount of gases that are emitted into the troposphere from anthropogenic sources. Although these emissions do not significantly change the composition of the atmosphere (78% stays N_2 , and 21% stays O_2) the trace amounts of the emitted gases, such as CO_2 , CH_4 , NO , NO_2 , nonmethane hydrocarbons (NMHC), and SO_2 , either have an impact on the radiative balance in the atmosphere, or are reactive and can be transformed into other gases and aerosols that, in their turn, can have an impact on climate, acidification, plant stress, or human health—all depending on the type of the species and the concentration. Clearly, society has an interest to obtain knowledge on the tropospheric chemical composition and on the physical and chemical processes that control the fate of emitted gases in the atmosphere. Of course atmospheric physics and chemistry is an interesting topic for academic research for its own sake.

Much of the atmospheric chemistry of, especially, short-lived trace gases (with lifetimes of several hours) takes place predominantly in the atmospheric boundary layer. The atmospheric boundary layer is defined as the layer of the atmosphere which is directly influenced by the earth's surface. Since many of the relevant chemical reactions take place during daytime under the influence of sunlight, the so-called "convective atmospheric boundary layer" (CABL) is an important layer in the troposphere. It is in this layer that—under clear-sky conditions and significant heating of the surface—reactive gases are emitted and become involved in photochemical reactions. The turbulent mixing of chemically reactive gases in the CABL is the subject of this dissertation.

First we introduce here the turbulent motions that characterize the CABL. Thermal convection is a common physical phenomenon occurring in the boundary layer, and is driven by the transfer (flux) of heat from the surface to the air above it. This flux results from a temperature difference between the surface and the overlying atmosphere (the temperature difference is typically caused by solar heating of the land surface or a relatively warm sea surface). The heat flux to the atmosphere leads to an increase in temperature, expansion,

and associated with that to a decrease of the density and to buoyancy forces which cause an upward acceleration of air mass. A very well-known example of thermal convection is that over land on sunny days with little or no wind (so that surface friction is not the most important source of atmospheric turbulence). The solar energy absorbed at the surface is transferred to the atmosphere as heat in turbulent buoyant plumes. The CABL that then develops typically reaches a height of the order of 1 to 2 km over land in the middle of the day and is fully turbulent.

In this dissertation, the CABL is studied as a medium for turbulent transport and chemical transformation of reactive gases. We are specifically interested in the time evolution of the concentrations of these gases in the CABL, and in their exchange between the CABL and the earth's surface and biosphere. Gas emissions to the atmosphere take place through both natural processes and human activities. The focus is on ozone chemistry under different chemical conditions. In summer strong anthropogenic emissions of ozone precursors can lead to photochemical smog formation (i.e., high concentrations of ozone). The chemical destruction of ozone precursors, like hydrocarbons and nitrogen oxides, is specifically studied—both for anthropogenically perturbed and for background conditions. The goal of this dissertation is to gain increased understanding of processes that determine atmospheric chemistry and transport on regional and global scales. Two related matters are also addressed: first, how we can incorporate chemistry in a conceptually 'simple' dynamic model of the CABL, and second, what the impact of this description is in the context of large-scale atmospheric chemistry models. We will focus on one of the unresolved topics in atmospheric chemistry modeling, that deal with the time evolution of moderately fast and fast reacting species in the CABL. Here "moderately fast" and "fast" are defined relative to the turbulent mixing timescale (which is of the order of 10 min).

As an introduction to the topic, we will first describe the turbulent nature of the CABL. For this purpose we exploit the similarities between convection in the atmospheric boundary layer and Rayleigh-Bénard convection in the limit of fully developed turbulence. Subsequently, we will elaborate on the central problem of the turbulent mixing of moderately fast and fast reacting chemical species in the CABL. After that, the tools that are used in this study—i.e., the models—will be introduced. Finally, we will formulate the research questions and outline the structure of this dissertation. Most references are to early articles on a certain topic, review articles, and text books, and are not intended to be exhaustive.

1.1 The CABL as a manifestation of turbulence

While at the end of the 1960s still relatively little was known about the CABL, the knowledge about the CABL (including its transport properties for nonreactive scalars) has expanded considerably since then, and the CABL is now relatively well understood. This has been achieved through both fine-scale numerical simulation, atmospheric measurements, and laboratory experiments (e.g., Deardorff 1966, 1970, 1972, 1973; Tennekes 1970; Willis and Deardorff 1974; Kaimal et al. 1976; Nieuwstadt and van Dop 1982; Stull 1988; Garratt 1992; Holtslag and Duynkerke 1998).

It is fruitful to apply the concepts of chaos theory to the CABL. The CABL can be treated as the fully developed turbulence limit of Rayleigh-Bénard convection. Rayleigh-Bénard convection is the archetype of thermal convection. It is the type of convection found in a fluid residing between two horizontal isothermal heat-conducting plates (the bottom one being hotter) in a gravity field (Rayleigh 1916; Lorenz 1963; Busse 1978). One can cause a transition in the flow from a state of rest to a state of fully developed turbulence by increasing a single parameter, the Rayleigh number, defined as

$$\text{Ra} \equiv g \frac{\Delta T}{T_r} \frac{z_i^3}{\nu \kappa}, \quad (1.1)$$

where z_i is the height of the layer, ΔT is the temperature difference between top and bottom of the layer, g is the gravitational acceleration, ν is the kinematic viscosity, κ is the thermal diffusivity, and T_r is a reference temperature. For a small temperature difference molecular thermal diffusivity is able to carry the heat flux from bottom to top plate and the fluid stays at rest. At a certain threshold value of Ra, the so-called critical Ra, a supercritical bifurcation is encountered (signifying a continuous phase transition) between the state of rest and two convective states, of equal velocity but opposite direction. A regular structure of rolls with parallel horizontal axes is formed above this threshold. When Ra is further increased more bifurcations follow, and already after the third bifurcation the fluid can show chaotic behavior (Ruelle and Takens 1971; Bergé et al. 1984). As Ra further increases the number of degrees of freedom increases too, and less and less structure remains to be seen in the fluid. For very high Ra the fluid has become fully turbulent. However, even Rayleigh-Bénard convection at very high Ra retains a typical structure of relatively steady large-scale cells in which highly fluctuating (both in space and time) small-scale convection elements are embedded (“spoke-pattern convection,” Busse 1978). Thus a large variety of possible structures is captured by Rayleigh-Bénard convection if we vary Ra from zero to infinity.

Also in the CABL (having even a much higher Ra), convective cells have been observed (e.g., Hardy and Ottersten 1969). The pattern is that of cells with a sinking motion, covering

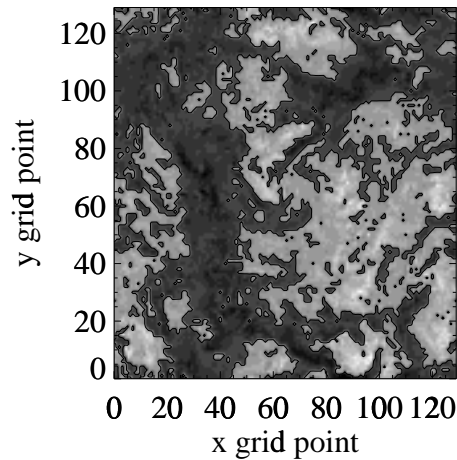


Figure 1.1: LES horizontal cross-section (xy -plot) of the instantaneous vertical velocity field w at height $z/z_i = 0.86$. A linear scale of gray shades is used with a discontinuity at $w = 0$. Light shades correspond to upward velocities. An insulating, frictionless, solid lid is used on top of the CABL and a constant heat flux prescribed at the surface. The spatial resolution of the LES is $130 \times 130 \times 66$ grid cells on a $6 \text{ km} \times 6 \text{ km} \times 1.5 \text{ km}$ spatial domain. See section 1.3 and chapter 2 for details of the LES model.

the largest horizontal area, at the cell center. A polygonal spoke pattern is induced near the surface by the wide downdrafts; the fluid converges towards lines—the “spokes”—moves along the spokes towards the hubs of the spoke pattern, and then goes upwards, as concluded from a fine-scale numerical simulation—a “large-eddy simulation” (LES, discussed below)—of the CABL by Schmidt and Schumann (1989).

In order to provide some visualization of the above-mentioned structures, we show in Figs. 1.1, 1.2, and 1.3 instantaneous horizontal cross-sections of vertical velocity, taken from an LES of a CABL. Both the spoke pattern near the surface (Fig. 1.3) and the large-scale organization of air that is moving upwards, in “updrafts,” and air that is moving downwards, in “downdrafts,” are clearly visible. Halfway the CABL the horizontal scale of the large-scale organization is about $2z_i$ (see Fig. 1.2), where here z_i is the depth of the CABL. Furthermore, updraft and downdraft cores are visible as white spots within the updraft and

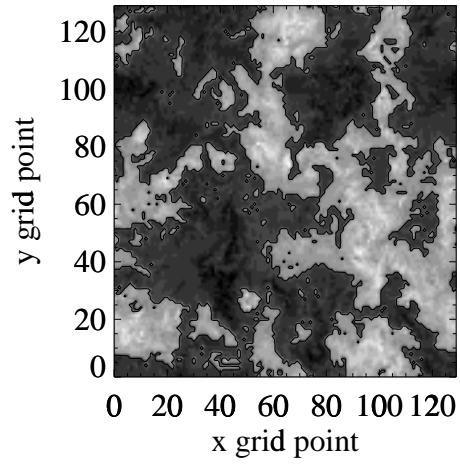


Figure 1.2: Same as Fig. 1.1 for height $z/z_i = 0.5$.

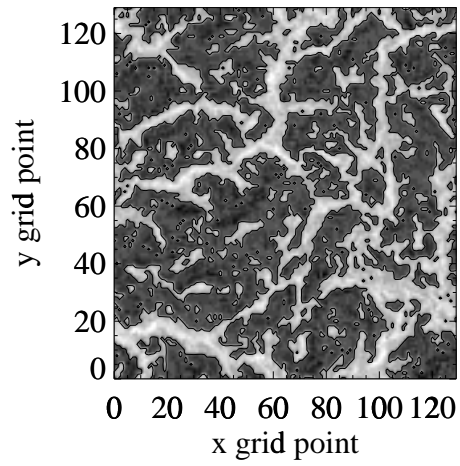


Figure 1.3: Same as Fig. 1.1 for height $z/z_i = 0.06$.

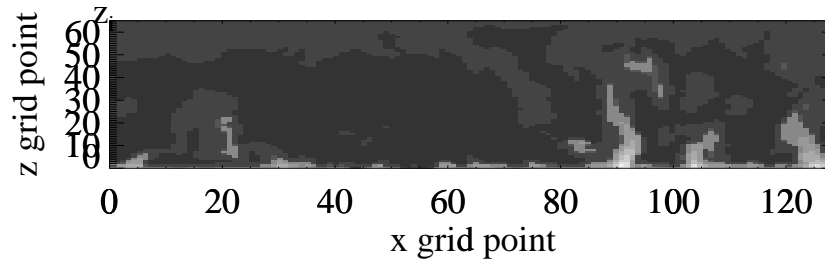


Figure 1.4: LES cross-section (xz -plot) of the instantaneous potential temperature field θ at the middle of the domain in the y -dimension. A linear scale of gray grades is used with an artificial discontinuity located at the borders of the highest-temperature plumes.

as black spots within the downdraft. The boundaries between updrafts and downdrafts are highly convoluted. In Fig. 1.4, a vertical cross-section of potential temperature is shown (the potential temperature of an air parcel is the temperature that the same air parcel would have at a reference pressure—by convention the surface pressure). Visible on the right are some strong thermals, extending high up into the CABL. From Fig. 1.4 one can also conclude that the horizontally averaged potential temperature is higher at the top than in the middle of the CABL (while the heat flux is linearly decreasing with height from its positive value at the surface to zero at the top). This is a manifestation of the countergradient heat flux that is observed for heat in the CABL (e.g., Ertel 1942; Deardorff 1966; Holtslag and Moeng 1991), and illustrates the advective rather than diffusive character of buoyant convection.

The problem of thermal convection belongs to the domain of fluid dynamics. The fundamental equations of fluid dynamics are given and discussed in section 1.3. Here we elaborate on aspects of chaos related to these equations, starting with a discussion of the computability of solutions to the Navier–Stokes equations. Tennekes and Lumley (1972) plainly stated that since one characteristic of turbulent flows is their irregularity, their randomness, a deterministic approach to turbulence problems is impossible and that, instead, one has to rely on statistical methods. A quantitative estimate of the total number of degrees of freedom for a turbulent flow results in a value of the order of $\text{Re}^{9/4}$, where Re is the Reynolds number,

a number based on the integral velocity and length scales \mathcal{V} and \mathcal{L} . Re is defined as

$$\text{Re} = \frac{\mathcal{V}\mathcal{L}}{\nu}. \quad (1.2)$$

Compared to the resolution needed to compute fully turbulent flows directly, the improvement in resolution of direct numerical simulation (DNS) has been very slow over the past ten years; in simulations Re is still many orders of magnitude too low to simulate all turbulent scales (Lesieur 1997). Wyngaard (1982) expressed the current consensus view that, although we cannot solve the Navier–Stokes equations for fully developed turbulence flow directly on the computer (due to the limited computer capacity) and have to be satisfied with some averaging of flow fields, one possibility to compute the flow is by means of LES. The philosophy behind LES is that the explicit description of the large scales suffices if one is interested in transport problems and that the processes at the subgrid scales can be described in a statistical manner. In this way an enormous reduction in the simulated number of degrees of freedom is achieved (e.g., the LES used in this chapter has 10^6 grid cells, which can be run on many computers nowadays).

After having mentioned the sheer size of the computational task that accompanies a solution to thermal convection, we have to notice that the tools that have been developed in dynamical systems theory for lower-dimensional dynamical systems (bifurcations, Lyapunov exponents, dimension of attractors, etc.) have so far not been very successful for fully developed turbulence. In fact, severe practical limitations exist on measuring the dimensions of attractors when these are too high, as is pointed out by, e.g., Frisch (1995). Still, the theory of dynamical systems is conceptually helpful for understanding the CABL, because it shows that no singularities or external noise are needed to explain its unpredictable behavior. One must further note that the practical applicability of dynamical systems theory to the CABL is still under debate. The presence of coherent structures in the flow is often seen as a clue that lower-dimensional theories of the turbulent flow can be developed. The skeptical position holds that even if fully developed turbulence has a strange attractor, the system will still be too complex to compute on the basis of dynamical systems theory (Guckenheimer 1986). There is also discussion on the question whether fully developed turbulence has a strange attractor at all. This discussion has gone back and forth since the seminal paper by Ruelle and Takens (1971). The strange-attractor view has both strong proponents (e.g., Lanford 1982) and opponents (e.g., Crutchfield and Kaneko 1988).

Researchers in the turbulence research community have tried to reduce the number of dimensions needed to describe fully developed turbulence, since the first significant developments made in the field of dynamical systems and chaos in the 1970s. Connected to this there is currently a keen interest in the study of coherent structures in turbulent flow (like

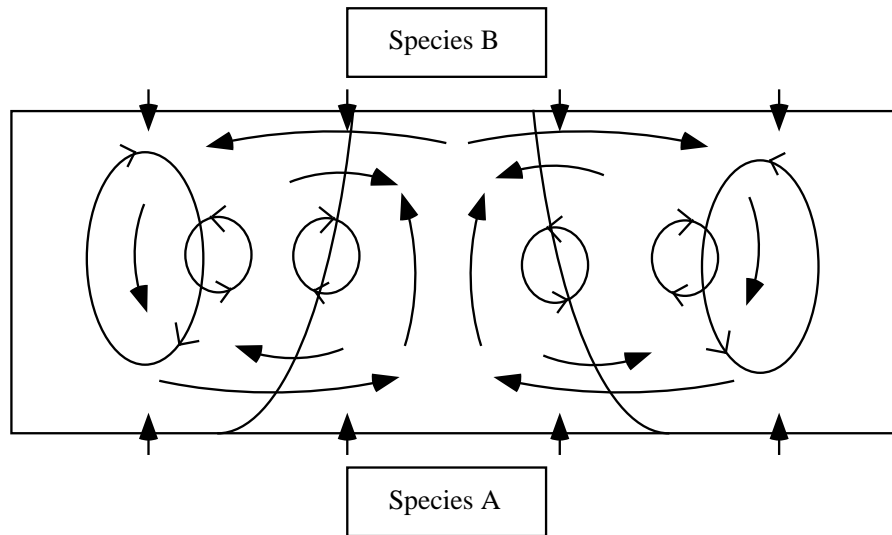


Figure 1.5: Two pictures of turbulence in the CABL superimposed: (i) schematic view based on the updraft–downdraft decomposition (plumes and full arrows) and (ii) the presence of eddies at all scales (designated by some larger and smaller eddies with open arrows). Also shown are the boundary conditions for a simple chemistry case.

the structures we discussed in the above). Lumley (1990) observed that the existence of coherent structures is not incompatible with a statistical approach. Especially if the coherent structures scale in the same way as the remainder of the flow, they can be combined with the disorganized motion in a statistical description. This is the course we will follow in this dissertation.

1.2 The CABL with reacting chemical species

The central topic of this dissertation is the turbulent transport–reaction problem. For the study of chemically reacting species in the CABL we will make use of the “mass-flux approach.” This approach is illustrated in Fig. 1.5. The air in the CABL can be decomposed into two compartments: upward moving air (updraft) and downward moving air (down-

draft). The structure of the updraft and the downdraft are quite complex, as is evident from Figs. 1.1–1.3. In the mass-flux approach the flow structure is not considered in detail, but instead *statistical* prognostic equations are used for updraft and downdraft quantities, like the equations given by Chatfield and Brost (1987). One should note that this statistical approach is not dependent on the presence of coherent structures. First, no coherent structures are used in the theoretical derivation of the updraft–downdraft approximation to the flux (Wyngaard and Moeng 1992), and second, this approximation also works for the neutral and stable surface layer where no convective coherent structures are present (Businger and Oncley 1990). So in this dissertation we do not continue on the “road to chaos” presented in the previous section, but use a statistical approach instead and calibrate this approach by using LES results. The mass-flux approach—where chemical reactions can be considered separately for updraft and downdraft—is particularly suited for chemically reacting species in the CABL, as will be shown in this dissertation.

The turbulent transport–reaction problem in the atmospheric boundary layer has been studied since the early 1970s (e.g., Donaldson and Hilst 1972; Lamb 1973; Bilger 1978; Lenschow 1982; Fitzjarrald and Lenschow 1983; Schumann 1989). The subject has recently been reviewed by Vilà-Guerau de Arellano and Lelieveld (1998). As an example to illustrate the problem we here consider a simple chemistry case. This case is similar to the one studied by, e.g., Schumann (1989), and consists of an irreversible, binary reaction $A + B \rightarrow C$. In this dissertation also more complex cases are studied, but for this introduction the simple case suffices. Species A is injected at the surface of the CABL and species B is entrained at the top (as shown in Fig. 1.5). The two species react at the local reaction rate $R_A = R_B = -kAB$, where k is the dimensionless reaction rate coefficient (the quantity is made nondimensional using a.o. the convective timescale z_i/w_* , where $w_* \equiv (gHz_i/T_r)^{1/3}$, with H the temperature flux at the surface) and A and B are the local concentrations.

Chemical reactions take place on the molecular scale. So in our example of reacting bottom-up diffusing species A and top-down diffusing species B, the turbulent transport–reaction processes proceed more or less simultaneously: turbulent mixing, molecular diffusion and chemical reaction (for a general description of these processes see Ottino 1989). Since molecular diffusion is not an important mixing mechanism in the CABL, we would expect that it is not necessary to consider molecular diffusion in the turbulent transport–reaction problem. This issue will be discussed explicitly in this dissertation.

In large-scale models of atmospheric chemistry and transport, the modeled concentrations are averages over large grid boxes (ranging in horizontal size from 10 to even 1000 km). Therefore, the horizontal scales of turbulent processes in the CABL that are smaller than the grid size are not represented by these models. Hence, the effects of these smaller

scales on the resolved scales have to be “parameterized” (specified as a function of the variables that are explicitly modeled on the model grid). In the vertical dimension these models typically have several layers in the CABL. Compared to other scalars included in large-scale models, such as temperature and humidity, an accurate representation of the mixing of chemically reacting scalars in the models requires additional information. This can be seen by calculating a horizontal average (denoted by an overbar) over a large grid box (larger than the typical CABL structures) of the chemical reaction rate:

$$\overline{R_A} = \overline{R_B} = -k\overline{AB} = -k\left(\overline{A} \overline{B} + \overline{A'B'}\right), \quad (1.3)$$

where the primes denote local deviations from the horizontal average. The term $\overline{A'B'}$ is the covariance of species A and B, and its influence on the average reaction rate is often expressed using the intensity of segregation

$$I_s = \frac{\overline{A'B'}}{\overline{A} \overline{B}}. \quad (1.4)$$

The term “intensity of segregation” was introduced in the context of engineering applications for binary mixtures by Danckwerts (1952) and applied to chemically reacting binary mixtures by Danckwerts (1958). If $I_s = 0$ then the species are well mixed, if $I_s = -1$ then the species are completely segregated, and if $I_s > 0$ then the species are pre-mixed.

In order to get a grip on the parameters in the turbulent transport–reaction problem that determine the value of I_s , we write (1.4) as follows

$$I_s = \frac{\rho_{AB}\sigma_A\sigma_B}{\overline{A} \overline{B}}, \quad (1.5)$$

where ρ_{AB} is the correlation coefficient for species A and B and σ_A and σ_B are the rms values of the concentration fluctuations of species A and B, respectively. Now suppose in first approximation that ρ_{AB} is of the order of $+1$ or -1 . The intensity of segregation then only approaches an absolute value of the order of 1 if the concentration fluctuations of both species A and B are large compared to the mean concentrations of the respective species. Thus, for segregation effects to be important in atmospheric chemistry, fluctuations of both reacting species have to be relatively large. Due to the way they are set up, most of the simple chemistry cases studied in the first chapters of this dissertation are characterized by large fluctuations compared to the mean concentrations. In the later chapters cases that are more representative for the real chemistry in the atmosphere are also studied. For these cases it is not evident beforehand that the conditions required for large intensities of segregation are fulfilled. If the intensity of segregation stays below an absolute values of the order of 10^{-2} the segregation process can be neglected in atmospheric chemistry modeling.

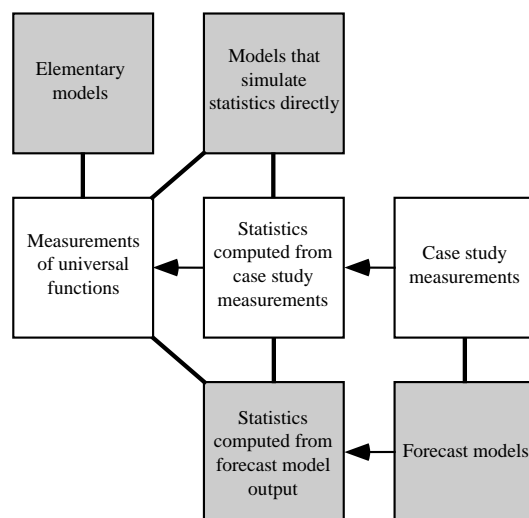


Figure 1.6: Diagram illustrating the relations between measurements and models. The white boxes represent measurements or statistics computed from measurements. The gray boxes represent models or products generated by models. The thick lines represent hypotheses, which bring together models and measurements. From Randall and Wielicki (1997).

We will use LES of chemically reacting species in the CABL to study segregation effects. In choosing this method we have to face a challenge that has been identified by many authors for including chemistry in LES (e.g. Ottino 1989; Cantwell 1990; Lesieur 1997; Moeng 1998). This challenge is the following: since chemical reactions take place at the molecular level, LES can have problems with the simulation of fast reactions (since everything that happens at the molecular level is parameterized in terms of the larger scales).

1.3 Models for atmospheric transport and chemistry

The focus of the current study is on the modeling of covariances of reacting species in the CABL. To this end a parameterization is developed for covariances, using a method based on a hierarchy of models (the concept of ‘model hierarchy’ is discussed for climate models by Petersen 1999a). The method is illustrated in the diagram of Fig. 1.6. A fine-scale modeling technique, LES, is employed to simulate with high resolution CABLs that

contain chemically reacting species. LES can be considered as a forecast model of the turbulent motion in the CABL. It has been tested successfully for dynamics and thermodynamics against case study measurements in the real CABL, especially by comparing the statistics of LES models with the statistics of measurements (see Moeng 1998 for an overview). The concentration fluctuations of the chemically reactive species that are of special interest in this dissertation (e.g., the hydroxyl radical OH, the “tropospheric vacuum cleaner”) and the covariances of concentration fluctuations of reacting species have not sufficiently been studied experimentally to compare models that simulate statistics, i.e. covariances, directly with statistics computed from case study measurements. Therefore, we use LES as a substitute for real measurements in the comparison with our statistical models. One of the models we propose (in chapter 3) for the covariance is actually based on a similarity relation, although it cannot be ascribed the status of an elementary model (which is a model that can be derived from basic physical principles). Again, experimental data that can confirm or refute this similarity relation are lacking, so that for now only a test of this relation can be performed using different cases modeled with LES.

The different kinds of models used in this study describe different (horizontal) spatial scales (and can be ordered according to these scales). The LES models that are used have a horizontal domain of a few kilometers. The single-column models, that should directly simulate the statistics of the LES models, represent columns from large-scale models. The horizontal column size can typically vary between 10 and 500 km. We include the proposed covariance parameterization in a single-column model, initialized by output from global climate and chemistry models, to assess the importance of the effects studied in this dissertation for global atmospheric chemistry. Here we will give general descriptions of the three types of models that are used. More details will follow in the various chapters.

1.3.1 LES models including chemistry

Fundamental equations

The fundamental equations of fluid dynamics, the Navier–Stokes equations, for the velocities u_i , pressure p , virtual potential temperature θ_v (“virtual” means that this temperature also accounts for the buoyancy effects related to humidity), and other (nonreactive or reactive) scalars s_l (scalars are quantities that have no direction, for instance temperature or concentrations of chemical species) read in the so-called Boussinesq approximation:

$$\frac{\partial u_i}{\partial x_i} = 0 \tag{1.6}$$

$$\frac{\partial u_i}{\partial t} + \frac{\partial u_j u_i}{\partial x_j} = -\frac{1}{\rho_r} \frac{\partial p}{\partial x_i} + \frac{g}{\theta_{v,r}} (\theta_v - \overline{\theta_v}) \delta_{i3} + \frac{\partial}{\partial x_j} \left(\nu \frac{\partial u_i}{\partial x_j} \right) \quad (1.7)$$

$$\frac{\partial \theta_v}{\partial t} + \frac{\partial u_j \theta_v}{\partial x_j} = \frac{\partial}{\partial x_j} \left(\kappa \frac{\partial \theta_v}{\partial x_j} \right) \quad (1.8)$$

$$\frac{\partial s_l}{\partial t} + \frac{\partial u_j s_l}{\partial x_j} = \frac{\partial}{\partial x_j} \left(\mathcal{D}_{s_l} \frac{\partial s_l}{\partial x_j} \right) + R_{s_l}. \quad (1.9)$$

Here it is assumed that no clouds are present and that the longwave radiative flux divergence can be neglected. In (1.6)–(1.9), \mathcal{D}_{s_l} are the Fickian diffusion coefficients, R_{s_l} represents sources and sinks of the scalars s_l , $\theta_{v,r}$ is the reference virtual potential temperature, and ρ_r is the reference density. A summation over repeated indices is assumed. The pressure in (1.7) is calculated by enforcing the condition of incompressible flow (1.6). As said, we assume that there are no sources and sinks for virtual potential temperature. In the CABL Re and Ra are extremely high, and therefore the thermal diffusivity κ , and Fickian diffusion coefficients \mathcal{D}_{s_l} are effectively zero in the CABL. Eqs. (1.7)–(1.9) are all nonlinear partial differential equations, with an effectively infinite number of degrees of freedom since the variables are defined for all (x, y, z) in continuous 3-D space.

LES models are based on the Navier–Stokes equations (1.6)–(1.9). These models separate the flow and concentration fields into large-scale (resolved) fields, indicated by $\widehat{}$, and small-scale (unresolved) fields, indicated by $''$, i.e. $u_i = \widehat{u}_i + u_i''$. Usually it is assumed that this decomposition satisfies a set of convenient properties, the Reynolds rules. Substitution of the decomposition in the Navier–Stokes equations then leads to the following set of prognostic equations for the resolved motions:

$$\frac{\partial \widehat{u}_i}{\partial x_i} = 0 \quad (1.10)$$

$$\frac{\partial \widehat{u}_i}{\partial t} = -\frac{\partial \widehat{u}_j \widehat{u}_i}{\partial x_j} - \frac{\partial \widehat{\pi}}{\partial x_i} + \frac{g}{\theta_{v,r}} (\widehat{\theta}_v - \overline{\theta_v}) \delta_{i3} - \frac{\partial (u_j'' u_i'' - \frac{2}{3} e \delta_{ij})}{\partial x_j} \quad (1.11)$$

$$\frac{\partial \widehat{\theta}_v}{\partial t} = -\frac{\partial \widehat{u}_j \widehat{\theta}_v}{\partial x_j} - \frac{\partial u_j'' \theta_v''}{\partial x_j} \quad (1.12)$$

$$\frac{\partial \widehat{s}_l}{\partial t} = -\frac{\partial \widehat{u}_j \widehat{s}_l}{\partial x_j} - \frac{\partial \widehat{u}_j'' s_l''}{\partial x_j} + \widehat{R}_{s_l} + \widehat{R}_{s_l}'', \quad (1.13)$$

where the modified pressure $\widehat{\pi} = \widehat{p}/\rho_r + 2e/3$, and $e = \frac{1}{2}\widehat{u}_i'' u_i''$ is the subgrid-scale kinetic energy. The quantity R_{s_l} represents sources and sinks of the scalars s_l . Different models are used in this dissertation for the subgrid-scale quantities appearing in (1.11)–(1.13). For the numerical techniques used we refer to the details in chapters 2 and 3.

Strengths and weaknesses of LES

As we have already mentioned, it is difficult to study the covariances of chemically reacting species in the CABL experimentally. LES can provide us with a ‘database’ of numerical results that can be used to develop and test parameterizations. The CABL is relatively easy to simulate with LES. Different LES codes give excellent agreement for the CABL and their results lie within the range of available observations (Nieuwstadt et al. 1993). Since the details of the subgrid model do not significantly affect the flow structure in the CABL—except near the boundaries—we even employ results in this dissertation generated using a LES model version with constant subgrid diffusivities. Such a model approach is similar to a DNS approach, but the smallest resolved scales are several tens of meters instead of the smallest turbulent scale—the Kolmogorov scale. The Kolmogorov scale is formally implied as smallest scale by the definition of DNS. The use of a LES with a constant subgrid diffusivity as one of the LES model versions that appear in chapters 3 and 4 can be defended by the observation that the eddy structure of the CABL at very high Re and Rayleigh-Bénard convection at lower Re are quite similar (Moeng and Rotunno 1990; Nieuwstadt 1990). The differences between the two types of flow—which we argued before belong to a continuum of flow types—have been quantified by Beets et al. (1996). These authors found that the spectra at large scales from LES and DNS behave similarly and that—as was to be expected—the differences are confined to the small scales where more variability is observed in the CABL as compared to Rayleigh-Bénard convection. However, the contribution of these small scales of the flow to the ensemble-averaged fluxes and covariances is small. Wyngaard (1998a) warned that the differences in fine structure between high and low Re flow may be important. He observed that not many problems have been identified for which this might be the case. We already pointed out that several authors have identified chemistry in turbulent flow as just such a problem.

A major weakness of LES is that these models have, up till now, almost exclusively been applied to idealized, horizontally homogeneous boundary layers, mainly due to the size limitation of the numerical domain and the assumed periodic lateral boundary conditions

(Moeng 1998). And even for such idealized boundary layers the domains that have been used are typically too small, since mesoscale fluctuations can be generated by turbulence even on the largest scales in the LES model (Jonker et al. 1999): for some types of scalars there appears to be no spectral gap and mesoscale phenomena have to be considered in conjunction with the smaller-scale turbulence—or they could even dominate the spectra.

Another weakness of LES that is often identified is that assumptions, incorporated in subgrid models, are made about the smallest scales of the turbulent motion. These assumptions can lead to errors (e.g., Mason 1994). However, for the CABL this should not be considered a problem (Nieuwstadt et al. 1993). What remains a potential weakness of LES at the smallest scales is the possible importance of these scales for chemistry, as we mentioned before.

1.3.2 Single-column chemistry models

Closures and their statistical order

In contrast with LES the ensemble averages (for instance over a horizontal grid area of a large-scale model) are modeled directly in single-column models. Single-column models for reactive gases in the CABL solve the following budget equation for chemical species (we do not give details here on the the single-column modeling of the dynamical and thermodynamical quantities):

$$\frac{\partial \overline{s}_l}{\partial t} = -\frac{\partial \overline{w's'_l}}{\partial z} + \overline{R_{s_l}}, \quad (1.14)$$

where for simplicity we have assumed horizontal homogeneity and $\overline{w} = 0$. For a simple, binary reaction $A + B \rightarrow C$ the chemical reaction rates $\overline{R_A}$ and $\overline{R_B}$ are given by (1.3). The covariance $\overline{A'B'}$ appears in (1.3), as was mentioned in the above. More detailed expressions for more reactions will be given in chapter 3.

The fluxes and the covariances in (1.14) can be modeled in several ways in a single-column model. For the turbulent transport–reaction problem either first-order closure (local or nonlocal) or higher-order closure (second-order, third-order, and so forth) can be used. The statistical order of the closure is here defined as the highest order of the moments involving species concentration fluctuations that are prognostically modeled. In this dissertation only first- and second-order closures are discussed.

We will start, in chapter 2, with 1-D models based on the updraft–downdraft decomposition, mass-flux schemes. The mass-flux schemes will be used to model these fluxes and covariances. The mass-flux closure is typically categorized as a first-order closure (e.g. by Stull 1998). However, since two prognostic equations are carried—one for the updraft

concentration and one for the downdraft concentration—which can be transformed into a prognostic equation for the mean concentration and a prognostic equation for a higher moment involving the concentration (e.g., the flux), one could argue that mass-flux closure can be considered a higher-order closure (albeit not a full second-order closure, since the higher moments are all coupled to each other and the second moments are not independent variables as in a full second-order closure).

We use several kinds of flux closures in the other chapters, some in combination with a first-order covariance closure. In chapter 3 this is developed and combined with a nonlocal first-order closure for the fluxes. In chapter 4 the full second-order closure equations are studied and the chemical corrections they contain for the flux are compared to those of mass-flux schemes, and also to first-order closure. Finally, in chapter 5 again a first-order closure is used for the scalar fluxes.

Strengths and weaknesses of single-column models

The main reason why single-column models are used in atmospheric chemistry is that they are computationally inexpensive. The turbulent scales smaller than the grid scales of large-scale models are important and must be taken into account (for instance, most of the vertical transport of chemical species in the lower atmosphere takes place at these small scales). So if one is interested in large-scale budgets of chemical species (see the next section) one cannot get around single-column models. But single-column models are also very powerful research tools, especially because of the relatively low computational cost of running such a model: one can quickly see the impact of new parameterizations. Using, for instance, LES results as a benchmark one can try to improve on the modeling of a certain process.

Major drawbacks of single-column models for turbulence, as summarized by Wyngaard (1998b)—although he considers dynamics and not scalar transport—are that they are (i) calibrated surrogates for turbulence; (ii) not predictive tools; (iii) not based on a theory of turbulence; and (iv) rest on observational work (the drawback being that there are insufficient observations: there is a “fact gap,” hampering the development of turbulence models). Indeed, all these drawbacks apply to our covariance closure: it is calibrated using a few LES cases, may not be applicable to some other cases, is not derived from the Navier–Stokes equations, and is severely limited by the fact that experimental measurements of covariances of reacting species in the CABL are not available. Still, based on our physical intuition, we have confidence in the parameterization, but it should be used with a critical sense.

1.3.3 Large-scale chemical transport models

Large-scale tropospheric species budgets (and related concentrations, deposition fluxes, shortwave and longwave radiative fluxes and transport to the stratosphere) can be modeled using large-scale chemical transport models. Such models have a horizontal grid size varying from 10 to 1000 km. To give an example, global models solve the following equation for the resolved chemical species concentrations \tilde{s}_l :

$$\frac{\partial \tilde{s}_l}{\partial t} + \frac{1}{a \cos \phi} \left[\frac{\partial(\tilde{u} \tilde{s}_l)}{\partial \lambda} + \frac{\partial(\tilde{v} \cos \phi \tilde{s}_l)}{\partial \phi} \right] + \frac{1}{h_\eta} \frac{\partial(\tilde{w} \tilde{s}_l)}{\partial \eta} = R(\tilde{s}_l) + S(\tilde{s}_l), \quad (1.15)$$

where λ , ϕ , and η are the coordinates in the longitudinal, latitudinal, and vertical direction (pressure-based, terrain-following hybrid coordinates are used here); \tilde{u} , \tilde{v} , and \tilde{w} are the resolved velocity components in the λ , ϕ , and η direction; a is the radius of the earth; and h_η is a scale factor from the coordinate transformation. The term S represents the parameterized subgrid-scale transport in the vertical direction and the term R represent all sources and sinks, including deposition and chemical transformations. The description for boundary-layer turbulent transport and chemical reactions in a large-scale model is like (1.14) for every column in the model. The strength of large-scale models is that they are comprehensive and allow for assessments of regional or global scale environmental problems. The major weakness is the relatively low resolution (and the neglect or parameterization of processes that occur on subgrid scales).

Due to the nonlinearity of chemistry and the spatial heterogeneity of anthropogenic trace gas sources, a tendency toward higher spatial resolution and a higher number of chemical species can be recognized in global atmospheric chemistry modeling. For models designed to run for several years with a large number of chemical species and using monthly averaged climatological meteorology, the horizontal resolution, the vertical resolution, and the number of transported species have recently doubled from (latitude \times longitude) $10^\circ \times 10^\circ$, 10 layers, and 10 species in MOGUNTIA (Crutzen and Zimmermann 1991) to $5^\circ \times 5^\circ$, 25 layers, and 19 species in IMAGES (Müller and Brasseur 1995), respectively. Models that use a higher meteorological time resolution exist in two types: on-line models (which calculate the meteorology at every time step) and off-line models (which use climate or weather forecast model output at a time resolution of 4 to 12 hours). Such models at this moment typically use a resolution between 2° and 5° , 19 vertical layers, and up to 70 reactive species to simulate ozone chemistry (Roelofs et al. 1997; Houweling et al. 1998). According to Peters et al. (1995), horizontal grid resolutions of 0.5° or better, at least 20 layers, and 40 to 100 species are necessary for an adequate modeling of anthropogenic perturbations to global atmospheric chemistry. The numerical solution of (1.15) amounts to a tremendous

task, given the desired resolution and number of species. Some aspects of the numerics—both chemistry solvers and advection schemes—have been studied and new methods have been developed recently by Spee (1998) and Petersen et al. (1998).

All three different types of transport models described in this section, are used in this dissertation: three-dimensional (3-D) LES models, one-dimensional (1-D) models, and 3-D global transport models (which in a sense encompass the second type).

1.4 Research questions and outline of the dissertation

We will now formulate more specifically the questions that are addressed in this dissertation—the corresponding chapters are added between parentheses:

- Can we adequately describe the mixing of moderately and fast reacting species using a statistical analysis of the coherent structure of updrafts and downdrafts in the CABL, as simulated by LES? (Chapter 2, “Mass-flux characteristics of reactive scalars in the convective boundary layer.”) The following issues will also be addressed:
 1. Can the covariance be accurately estimated using updraft and downdraft concentrations? Accurate means accurate enough to lead to an improvement of modeled reaction rates in large-scale models of atmospheric chemistry and transport.
 2. Do fast reactions constitute a problem for LES?
- How can we develop a simple parameterization for the covariances of reactive species based on mass-flux characteristics? Simple means simpler than a prognostic mass-flux scheme or second-order closure scheme for the scalars, but more elaborate than current practice. (Chapter 3, “A first-order closure for covariances and fluxes of reactive species in the convective boundary layer.”)
- How do second-order closures and mass-flux closures compare for the contribution of chemical higher-order moments to the flux? Do we need to take these chemical higher-order moments into account or is a first-order closure approach for the flux sufficiently accurate? (Chapter 4, “The impact of chemistry on flux estimates in the convective boundary layer.”)
- What is the importance of segregation effects, related to the covariances of reactive species, for global-scale atmospheric chemistry modeling? (Chapter 5, “Segregation effects in atmospheric chemistry related to boundary-layer convection.”)

Chapter 2

Mass-flux characteristics of reactive scalars in the convective boundary layer*

*The material contained in this chapter has been published in *Journal of the Atmospheric Sciences* (**56**, 37–56, 1999), with C. Beets, H. van Dop, P. G. Duynkerke, and A. P. Siebesma as co-authors.

Abstract

The transport of nonreactive and reactive bottom-up and top-down diffusing scalars in a solid-lid convective boundary layer is studied using large-eddy simulation (LES). The chemistry considered consists of an irreversible, binary reaction involving the bottom-up and top-down diffusing scalars. The mass-flux or top-hat characteristics of the reactive flow are determined. Also, several mass-flux schemes are run in an off-line mode, that is, with prescribed profiles of the mass flux and the updraft area fraction, and are compared to the LES. Top-hat approximations are found to capture about 25% of the covariance between two arbitrary (nonreacting or reacting) scalars and about 65% of the flux. Subplume fluxes are located either in the updraft for bottom-up diffusing scalars or in the downdraft for top-down diffusing scalars. The mass-flux scheme that is nearly identical to the exact plume-budget equations gives the best performance. For the parametrization of lateral exchange this mass-flux scheme includes gross exchange across the interface between updrafts and downdrafts, that is, includes also subinterface-scale exchange processes (like the other dynamical quantities also prescribed in an off-line mode using LES data). A simpler mass-flux scheme, which does not include the more sophisticated parametrizations of subplume fluxes and subinterface-scale lateral exchange, is found to perform only slightly worse. The results of this chapter are also valid for the surface layer and lower mixed layer of the entraining convective boundary layer but not for the entrainment zone.

2.1 Introduction

For many years mass-flux schemes have been applied successfully in the parameterization of scalar transport by cumulus convection (e.g., Arakawa and Schubert 1974; Tiedtke 1989). More recently, mass-flux schemes have been proposed as attractive candidates for the parameterization of transport in convective atmospheric boundary layers (CABLs)—both the dry CABL and the stratocumulus-topped CABL—for instance by Chatfield and Brost (1987) and Randall et al. (1992). The main difference between mass-flux schemes for cumulus and for the CABL is the decomposition that is applied: cloud–environment for cumulus and updraft–downdraft for the CABL. Another difference is that mass-flux formulas for the flux in cumulus resolve 80%–90% of the total flux (except near cloud base), as shown by Siebesma and Cuijpers (1995) for shallow cumulus, whereas mass-flux formulas for the flux in CABLs resolve about 65% of the total flux (Young 1988a; Schumann and Moeng 1991a, Wyngaard and Moeng 1992; de Laat and Duynkerke 1998). This difference is related to the presence of a potential barrier in cumulus convection. As a consequence, cloud updrafts occur in bursts in an otherwise quiet cloud layer and the vertical velocity distribution is highly positively skewed. Mass-flux schemes for the CABL are sensitive to the parameterization of the parts of the total flux that are not resolved by mass-flux formulas. These unresolved parts are called “subplume fluxes.”

In this chapter we study the scalar transport characteristics of different mass-flux schemes for transport of nonreactive and reactive scalars in the CABL. This study is part of the development of a new boundary-layer parameterization for large-scale atmospheric chemistry–transport models (with horizontal grid sizes ranging from 50 to 500 km) that is suitable for the turbulent transport–chemistry problem (discussed below). The mass-flux schemes proposed earlier in the literature for transport of scalars, both in cumulus clouds and in CABLs, are combined, categorized, and evaluated using statistics from large-eddy simulation (LES) of a solid-lid CABL. The scalars studied are bottom-up and top-down diffusing scalars, either nonreacting or quickly reacting away. We run the mass-flux schemes in an off-line mode, that is, we prescribe the boundary-layer height and the vertical profiles of

the mass flux and the updraft area fraction (both determined from LES). Furthermore, we prescribe identical scalar surface fluxes and identical scalar entrainment fluxes (at the top of the CABL) in both the LES and the mass-flux schemes.

Previous studies have shown that LES is able to provide detailed and realistic statistics for the CABL (Nieuwstadt et al. 1993). LES models are able to compute explicitly the most important lengths and timescales of the CABL (typically 25–1000 m and 10–10 000 s respectively). The small turbulence scales below the LES grid size of about 25 m have been found to have only a minor influence on the dynamics of the CABL, and therefore can be parameterized with a relatively simple LES subgrid-scale model. Simulating a solid-lid CABL rather than an entraining CABL allows for integration towards a (quasi-)steady state of the scalar profiles, facilitating the comparison with (quasi-)steady state solutions of the mass-flux schemes (see also Brown 1996, who used a solid-lid CABL instead of an entraining CABL for similar reasons).

We categorize the differences between the mass-flux schemes in terms of the parameterization of the different component processes that appear in the plume-budget equations for scalars. Two components are relevant to transport of both nonreactive and reactive scalars, namely the parameterization of subplume fluxes and the parameterization of lateral-exchange processes between the updrafts and the downdrafts. Another component only pertains to reactive scalars, namely the parameterization of subplume covariances of reacting scalars. New parameterizations are proposed for the subplume fluxes and the subplume covariances.

In our view the attractiveness of mass-flux schemes for scalar transport in the CABL is threefold, compared to the first-order closure schemes that are currently used in large-scale atmospheric chemistry–transport models. First, nonlocal transport effects are clearly embodied in mass-flux schemes, which is attractive compared to the often used local first-order closure schemes (cf. Holtslag and Moeng 1991; Stull 1993). Second, the effects of a continuous distribution of fast chemical sources and sinks on the fluxes are taken into account (Fitzjarrald and Lenschow 1983; Schumann 1989; Sykes et al. 1994; Gao and Wesely 1994; Vilà-Guerau de Arellano et al. 1995; Galmarini et al. 1997; Verver et al. 1997). And third, the effects of horizontal segregation of reactive scalars on the mean reaction rates are represented (Schumann 1989; Vilà-Guerau de Arellano and Duynkerke 1993; Sykes et al. 1994; Beets et al. 1996; Verver et al. 1997; Molemaker and Vilà-Guerau de Arellano 1998).

We here briefly explain the two last mentioned advantages of mass-flux schemes for the transport of reactive scalars in the CABL. In the mass-flux schemes that we study in this chapter we use the updraft–downdraft decomposition and treat both updraft and downdraft scalar quantities as prognostic variables. Therefore the mass-flux schemes considered

here can be compared to higher-order (but not fully second-order) closure schemes in the sense that they contain two prognostic variables that provide a model for all higher-order moments. The mean scalar value and the scalar flux (a second moment) in a mass-flux scheme can for instance be written in terms of these updraft and downdraft quantities, and can replace these as independent variables. The prognostic equations for the mean scalar values include a direct influence of the covariances, and the prognostic equations for the fluxes include a direct influence of the chemistry on the fluxes. In contrast to mass-flux schemes, first-order closure schemes do not implicitly include these two aspects of the turbulent transport–chemistry problem.

As already stated in the above, we do not evaluate complete mass-flux schemes in this chapter, that is, we do not deal with questions concerning the parameterization of the mass flux and the updraft area fraction. Instead of this, we are concerned with evaluating the scalar transport–reaction characteristics of mass-flux schemes.

This chapter is organized as follows. The LES of the solid-lid CABL, including the studied cases of scalar transport, is described in section 2.2. In section 2.3 we present the scalar plume-budget equations and the mass-flux schemes that can be derived from these. The LES results for the scalars appear in sections 2.4 and 2.5. In section 2.6 we present the results of the mass-flux schemes. Finally, we briefly summarize and discuss the results in section 2.7.

2.2 Description of LES and cases

2.2.1 LES of the solid-lid CABL

The type of boundary layer studied here is a solid-lid CABL (without entrainment of heat at the top of the CABL as opposed to the entraining CABL), which was also used for studying transport of reactive scalars by Beets et al. (1996) and Molemaker and Vilà-Guerau de Arellano (1998). The dynamics and thermodynamics of the solid-lid CABL was studied with LES by Schumann (1993). He found that LES compares favorably with laboratory measurements. Sorbjan (1996) studied the differences between solid-lid and entraining CABLs, of which the last one is more representative for the real atmosphere. Both convection experiments in tanks and numerical studies have shown that various turbulence statistics in the lower portion of the solid-lid CABL resemble those of the entraining CABL. Differences in the dynamics caused by the inclusion of entrainment of heat in the entraining CABL are reflected in a lower updraft area fraction a in the upper-part of the CABL. Sorbjan (1996) found that a is approximately 0.45 throughout the whole mixed layer for the

solid-lid CABL but decreases to a minimum of 0.25 near the top of the mixed layer for the entraining CABL. Here it must be borne in mind that, as shown by Nieuwstadt et al. (1993), the minimum value of a differs substantially among LES models of the entraining CABL: in their simulations the minimum value of a varies roughly from 0.3 (model of Schumann) to 0.4 (model of Moeng). Furthermore, Sorbjan (1996) found that the average updraft vertical velocity $\overline{w^u}$ is almost the same for both types of CABL at every height.

Since the aim of this chapter is the study of transport of dynamically passive scalars (with varying chemical reaction rates) in the CABL, we may exploit the ease with which fixed fluxes can be implemented at the top of the solid-lid CABL (identical to the top of the LES domain). The flux at the top is zero for potential temperature and zero or a finite constant for other scalars of interest. According to the results shown in Sorbjan (1996) the second (and third) moments in the surface layer (and for some variables also in the lower mixed layer) do not differ between the solid-lid and the entraining CABL. We have verified that conclusions reached in this study concerning mass-flux characteristics of second moments involving scalars in the solid-lid CABL can be extrapolated to the lower parts of the entraining CABL (surface layer and lower mixed layer), but certainly not to the entrainment layer at the top of the entraining CABL. The study of entrainment processes at the top of the CABL is not part of this work.

The algorithm for the large-eddy simulations performed in this study has been derived from a model used in earlier studies (Nieuwstadt and Brost 1986; van Haren and Nieuwstadt 1989; Nieuwstadt et al. 1993) and was previously used in Beets et al. (1996). The general LES modeling approach was described in chapter 1. Here we will only describe details pertaining to the specific LES model used in this chapter. In this LES model the constant reference density ρ_r is taken equal to 1 kg m^{-3} , the gravitational acceleration $g = 9.8 \text{ m s}^{-2}$, and the reference temperature $T_r = 300 \text{ K}$. No-slip and free-slip boundary conditions are prescribed at the surface and top of the domain, respectively. The surface roughness length z_0 is set to 0.16 m. The boundary-layer height $z_i = 1500 \text{ m}$, the convective velocity scale $w_\star \equiv \left(g \overline{w'\theta'_0} z_i / T_r \right)^{1/3} = 1.5 \text{ m s}^{-1}$ and $\overline{w'\theta'_0} = 0.069 \text{ K m s}^{-1}$ the surface potential temperature flux. The resulting convective timescale is $t_\star = z_i / w_\star = 1000 \text{ s}$.

As will be discussed in the next subsection, in this chapter we consider chemical sink terms for two species (labelled l and m) reacting away in a binary reaction with reaction rate coefficient k'_{lm} . The resolved and subgrid-scale source and sink terms in the studied chemistry cases read

$$\widehat{S}_l = \widehat{S}_m = -k'_{lm} \widehat{s}_l \widehat{s}_m \quad (2.1)$$

$$\widehat{S}_l'' = \widehat{S}_m'' \equiv -k'_{lm} \widehat{s}_l'' \widehat{s}_m'' \quad (2.2)$$

The equations for the resolved quantities (1.10)–(1.13) are solved explicitly. The subgrid-scale Reynolds stresses, subgrid-scale temperature flux, subgrid-scale scalar fluxes and subgrid-scale covariances that appear in these equations are parameterized as a function of the resolved quantities, the normal stresses, and a timescale of subgrid scale turbulence τ according to

$$\widehat{u}_i'' \widehat{u}_j'' = -C_1 \tau \left(\widehat{u}_i'' \widehat{u}_i'' \frac{\partial \widehat{u}_j}{\partial x_i} + \widehat{u}_j'' \widehat{u}_j'' \frac{\partial \widehat{u}_i}{\partial x_j} \right) \quad i \neq j, \quad (2.3)$$

$$\widehat{u}_i'' \widehat{\theta}'' = -C_2 \tau \left(\widehat{u}_i'' \widehat{u}_i'' \frac{\partial \widehat{\theta}}{\partial x_i} \right) \quad (2.4)$$

$$\widehat{u}_i'' \widehat{s}_l'' = -C_2 \tau \left(\widehat{u}_i'' \widehat{u}_i'' \frac{\partial \widehat{s}_l}{\partial x_i} \right) \quad (2.5)$$

$$\widehat{s}_l'' \widehat{s}_m'' = -C_3 \tau \left(\widehat{u}_i'' \widehat{s}_l'' \frac{\partial \widehat{s}_m}{\partial x_i} + \widehat{u}_i'' \widehat{s}_m'' \frac{\partial \widehat{s}_l}{\partial x_i} \right), \quad (2.6)$$

where τ is the ratio of the characteristic grid size Δ and the square root of the subgrid-scale kinetic energy e . A modeled conservation equation for all normal stresses is solved explicitly. The constants C_1 , C_2 , and C_3 in (2.3)–(2.6) are derived from inertial-subrange theory, and can be expressed as

$$C_1 = \frac{l_f}{2\pi \Delta} (1.5\alpha)^{-1.5} \quad (2.7)$$

$$C_2 = \frac{\alpha}{\beta} C_1 \quad (2.8)$$

$$C_3 = \frac{\beta}{\alpha} C_1, \quad (2.9)$$

where α and β are constants which appear in the expressions for the inertial subrange energy and concentration variance spectra. The following values that are typical for these constants are used: $\alpha = 1.5$ and $\beta = 0.7$. The filter length scale l_f is taken equal to twice the characteristic grid size ($l_f = 2\Delta$).

The governing equations for the resolved field are solved explicitly using a finite-volume technique. All terms in the filtered momentum equations are discretized using straightforward second-order central differences, except for the advective terms which are discretized using the method of Piacsek and Williams (1970). The leap-frog scheme, with an Asselin filter to prevent decoupling of odd and even time levels, is used for the time integration of the momentum equations. Conservation of mass is obtained by solving a diagnostic equation for the pressure. For the advection and diffusion of temperature and the other scalars we use the limited $\kappa = \frac{1}{3}$ scheme (Koren 1993) for the spatial discretization, and a two-stage Runge–Kutta method for the time integration (Hundsdorfer et al. 1995). For the time advancement of chemistry we use the routine Twostep (Verwer and Simpson 1995), and straightforward second-order central differences for the discretization of the subgrid-scale covariance. The entire numerical discretization for temperature and the other scalars satisfies three important properties: it is conservative, positive, and monotone.

The grid used has $130 \times 130 \times 66$ grid points in the horizontal and vertical directions, respectively, representing a $6.0 \text{ km} \times 6.0 \text{ km} \times 1.5 \text{ km}$ physical domain, thus employing a higher resolution than in previous studies with the LES model. The time step in the model is approximately 0.6 s. A grid domain of $32 \times 32 \times 30$ was used by Sorbjan (1996), but although the associated resolution is generally considered to be sufficient for the representation of basic turbulence characteristics of the CABL, we use a relatively high spatial resolution to minimize the LES unresolved covariance contribution to the chemical sink term and to be able to perform spectral investigations on very small scales. The unresolved covariance contribution is nearly zero in the bulk and much smaller than the resolved covariance near the bottom and top boundaries (this can also be checked by comparing Figs. 2.7a and 2.8).

2.2.2 Cases

For the nonreactive case, called BUTD, we have introduced in our LES a passive bottom-up diffusing scalar (BU) and a passive top-down diffusing scalar (TD). The flux of BU at the top of the CABL is put to zero, as is the flux of TD at the bottom. Choosing a flux scale F_* , the constant input fluxes of BU and TD are set to F_* and $-F_*$, respectively. Using the convective velocity scale w_* , a scalar-value scale can then be defined as $s_* = F_*/w_*$. If later in this chapter no units are assigned to specific quantities, it is assumed that these quantities have been made dimensionless using the scales defined here.

The reactive cases, called AB1, AB2, AB3, and AB_∞ , are of the following type: they consist of bottom-up (A) and top-down (B) scalars reacting away in a second-order reaction ($A + B \rightarrow C$).

To illustrate the effect of horizontal segregation on the mean reaction rate we write the sink term for species A and B due to the reaction $A + B \rightarrow C$ as

$$\begin{aligned} S &= -k'_{A+B \rightarrow C} \overline{s_A s_B} \\ &= -k'_{A+B \rightarrow C} \left(\overline{s_A} \overline{s_B} + \overline{s'_A s'_B} \right), \end{aligned} \quad (2.10)$$

where s_A and s_B are the scalar values (concentrations) of chemical species A and B. Here and throughout the rest of this chapter overbars denote horizontal ensemble averages and primes denote fluctuations from these averages. The intensity of segregation, defined as

$$I_s = \frac{\overline{s'_A s'_B}}{\overline{s_A} \overline{s_B}}, \quad (2.11)$$

is a measure of the importance of the covariance term $\overline{s'_A s'_B}$ appearing in (2.10). The intensity of segregation obeys the inequality $I_s \geq -1$. The reaction-rate coefficient k' that appears in (2.10) can be made nondimensional in the following way:

$$k_{A+B \rightarrow C} = s_* t_* k'_{A+B \rightarrow C}. \quad (2.12)$$

The nondimensional reaction-rate coefficient is also called the ‘‘flux Damk€ohler number.’’ We expect the largest segregation effects for fast chemical reactions ($k \gg 1$), and we will vary the flux Damk€ohler number from zero (nonreactive case) to infinity. The three nondimensional reaction-rate coefficients used in cases AB1, AB2, and AB3 are 0.2, 1.0, and 5.0 respectively.

As in the nonreactive case, for all reactive cases only two boundary fluxes are nonzero. These are the constant fluxes of scalars A and B into the boundary layer with values F_* at the bottom and $-F_*$ at the top, respectively. The other two flux boundary conditions are put to zero. The concentrations of scalars A and B reach a steady state due to the presence of the chemical sink.

A rather special case is AB_∞ , for which one does not have to do a chemistry run nor a series of runs to approximate the infinite reaction rate limit. Instead, we can diagnose the A and B scalar fields for case AB_∞ from the BU and TD scalar fields in the nonreactive case. As was also done by Schumann (1989), we may use $|s_{BU} - s_{TD}|$ as a substitute for s_A if $s_{BU} \geq s_{TD}$ (s_B is then set to zero) and for s_B if $s_{BU} < s_{TD}$ (s_A is then set to zero). In other words, we can regard scalars A and B as diffusing from their respective sources at the bottom and top of the CABL (without reacting) to a highly complex reaction interface of zero thickness. At one side of this interface surface only scalar B is present and at the other side of this interface only scalar A. To defend the above outlined procedure for case AB_∞ , we show in appendix B that the scalars A and B become uncorrelated at the smallest

scale that is resolved in the LES model when we increase the reaction-rate coefficient from moderate to infinite values. Correspondingly, the unresolved covariance contribution will become negligible for very high reaction-rate coefficients (as it is for nonreactive scalars).

Each LES run is started with a well-developed turbulent layer and varying initial scalar profiles (always with equal total amounts of both species present in the CABL). For cases with a chemical timescale smaller than the convective timescale the scalars come close to a steady state after several convective turnovers (turbulent mixing being the limiting factor). For slower chemistry, the dimensionless chemical timescale k^{-1} determines the number of required turnovers. The averaging process is not started before it has been verified that the scalars have nearly reached their steady-state values (in case BUTD the scalars will reach a quasi-steady state characterized by a linear flux profile). Then the averaging takes place using eight consecutive snapshots (with a time separation of $0.25t_*$) during an integration of length $2t_*$. The only exception to this procedure is case $AB\infty$: we perform the calculations for this case only on the final field of case BUTD. Therefore the profiles for case $AB\infty$ are somewhat less smooth than the other profiles.

2.3 Scalar plume budgets

2.3.1 Basic equations

Firstly, we introduce the convective mass flux M :

$$M = \rho a (\overline{w^u} - \overline{w}), \quad (2.13)$$

with a the updraft area fraction, $\overline{w^u}$ the updraft velocity, and \overline{w} the mean vertical velocity. As stated before, we take the density $\rho = 1 \text{ kg m}^{-3}$ and we therefore do not explicitly include ρ in our equations below.

We use the following decomposition of the scalar flux:

$$\begin{aligned} \overline{w's'} &= a(\overline{w^u} - \overline{w})(\overline{s^u} - \overline{s}) + (1 - a)(\overline{w^d} - \overline{w})(\overline{s^d} - \overline{s}) + a\overline{w's'^u} + (1 - a)\overline{w's'^d} \\ &= M(\overline{s^u} - \overline{s^d}) + a\overline{w's'^u} + (1 - a)\overline{w's'^d}, \end{aligned} \quad (2.14)$$

as is done by Siebesma and Cuijpers (1995). The indices u and d indicate that the averaging areas consist of updrafts and downdrafts, respectively. In decomposition (2.14) we can distinguish between mass-flux (also called “top-hat”) and subplume contributions to the total flux, and the decomposition is exact. The terms $\overline{w's'^u}$ and $\overline{w's'^d}$ represent fluxes associated with subplume correlations of vertical velocity and scalar quantities and are defined as $\overline{w's'^u} \equiv \overline{(w - \overline{w^u})(s - \overline{s^u})^u}$ and $\overline{w's'^d} \equiv \overline{(w - \overline{w^d})(s - \overline{s^d})^d}$.

Using a and M we can write the following mass-conservation equation, or continuity equation:

$$\frac{\partial a}{\partial t} = -\frac{\partial M}{\partial z} + E_m - D_m, \quad (2.15)$$

where, following Siebesma (1997), we have used the gross lateral mass-exchange rates E_m and D_m , also called entrainment and detrainment rates, respectively (the terms entrainment and detrainment are defined relative to the updraft). These are defined as

$$E_m \equiv -\frac{1}{A} \int_{\mathbf{n} \cdot (\mathbf{u} - \mathbf{u}_i) < 0} \mathbf{n} \cdot (\mathbf{u} - \mathbf{u}_i) dl \quad (2.16)$$

$$D_m \equiv \frac{1}{A} \int_{\mathbf{n} \cdot (\mathbf{u} - \mathbf{u}_i) > 0} \mathbf{n} \cdot (\mathbf{u} - \mathbf{u}_i) dl, \quad (2.17)$$

where the integrals are over specific segments of all the interfaces between updrafts and downdrafts in a horizontal domain, A , \mathbf{n} is an outward directed unit normal vector at the interface (outward is defined relative to the updraft), \mathbf{u} the 3-D flow velocity field and \mathbf{u}_i the 3-D interface velocity field. This formulation is generally valid for any interface. Since in the case of an interface between updrafts and downdrafts $w = w_i = 0$ the integrals contain only horizontal contributions.

The exact updraft and downdraft scalar plume-budget equations can be written, again following Siebesma (1997), as

$$\begin{aligned} \frac{\partial a \bar{s}^u}{\partial t} = & -\frac{\partial M \bar{s}^u}{\partial z} + \frac{1}{A} \oint_{\text{interface}} \mathbf{n} \cdot (\mathbf{u} - \mathbf{u}_i) s dl - \frac{\partial a \overline{w' s'^u}}{\partial z} \\ & + a(S_u + S_{u, \text{subplume}}) \end{aligned} \quad (2.18)$$

$$\begin{aligned} \frac{\partial (1-a) \bar{s}^d}{\partial t} = & +\frac{\partial M \bar{s}^d}{\partial z} - \frac{1}{A} \oint_{\text{interface}} \mathbf{n} \cdot (\mathbf{u} - \mathbf{u}_i) s dl - \frac{\partial (1-a) \overline{w' s'^d}}{\partial z} \\ & + (1-a)(S_d + S_{d, \text{subplume}}). \end{aligned} \quad (2.19)$$

The term containing the contour integral represents lateral-exchange processes and the last terms in (2.18) and (2.19) correspond to sources and sinks, being subdivided into a plume mean and a subplume part (to be discussed below).

Below we will first discuss various parameterizations for the two types of subplume contributions to the plume-budget equations. This is followed by a discussion of parameterizations for the contour integral representing lateral-exchange processes. At the end of this

section we will define the five mass-flux schemes for scalar transport that are studied in this chapter as different combinations of the various parameterizations presented below.

2.3.2 Subplume contributions to the plume-budget equations

Subplume fluxes $\overline{w's'^u}$ and $\overline{w's'^d}$

In the past it has been found by Businger and Oncley (1990) for the surface layer and by Young (1988a), Schumann and Moeng (1991a), Wyngaard and Moeng (1992), and de Laet and Duynkerke (1998) for the CABL that the top-hat contribution to the flux, $M(\bar{s}^u - \bar{s}^d)$, is a constant fraction κ_{ws} of the total flux, in formula form:

$$\overline{w's'} \approx \kappa_{ws}^{-1} M(\bar{s}^u - \bar{s}^d). \quad (2.20)$$

We can give a theoretical estimate of κ_{ws} , as shown by Wyngaard and Moeng (1992), provided that the joint probability density function (pdf) $P(w', s')$ of vertical velocity and scalar fluctuations is a Gaussian function. In that case $\kappa_{ws} = 4/(2\pi) = 0.64$.

In the mass-flux schemes for scalar transport studied in this chapter the subplume fluxes are treated in three different ways. First, they can be assumed to be zero:

$$\overline{w's'^u} = \overline{w's'^d} = 0. \quad (2.21)$$

For a given total scalar flux and a given mass flux this will result in an overestimation of $(\bar{s}^u - \bar{s}^d)$ in (2.14) by a factor κ_{ws}^{-1} , according to (2.20).

Second, the subplume fluxes can be assumed to be proportional to the gross plume-scale top-hat contributions $M\bar{s}^u$ and $M\bar{s}^d$, respectively, as implicitly done by Randall et al. (1992):

$$\overline{w's'^u} = \frac{1 - \kappa_{ws}}{a\kappa_{ws}} M\bar{s}^u \quad (2.22)$$

$$\overline{w's'^d} = - \frac{1 - \kappa_{ws}}{(1 - a)\kappa_{ws}} M\bar{s}^d. \quad (2.23)$$

In this parameterization it is assumed that the subplume fluxes can be absorbed into the top-hat flux terms by using $\kappa_{ws}^{-1}M$ instead of M in (2.14). Eqs. (2.22) and (2.23) are consistent with (2.20).

Third, we propose a new subplume fluxes parameterization based on the results shown in Figs. 2.4a,b (to be discussed in section 2.4). This new parameterization makes use of the fact that purely bottom-up diffusing scalars only have a subplume flux in the updraft and

purely top-down diffusing scalars only have a subplume flux in the downdraft. According to the superposition hypothesis of Wyngaard and Brost (1984), any nonreactive passive scalar can be written as a linear combination of bottom-up and top-down diffusing scalar fields:

$$s = \alpha s_{\text{BU}} + \beta s_{\text{TD}}, \quad (2.24)$$

where the scalars BU and TD are assumed to have equal but opposite input fluxes for BU at the bottom of the CABL and for TD at the top of the CABL. If we assume quasi-steady conditions, the fractional contributions of both component fields to the total flux at a certain height, γ_{BU} and γ_{TD} , are

$$\gamma_{\text{BU}} \equiv 1 - \gamma_{\text{TD}} = \frac{|\alpha| \left(1 - \frac{z}{z_i}\right)}{|\alpha| \left(1 - \frac{z}{z_i}\right) + |\beta| \frac{z}{z_i}}. \quad (2.25)$$

The new subplume-fluxes parameterization reads:

$$\overline{w's'^u} = \gamma_{\text{BU}} \frac{1 - \kappa_{ws}}{a\kappa_{ws}} M(\bar{s}^u - \bar{s}^d) \quad (2.26)$$

$$\overline{w's'^d} = \gamma_{\text{TD}} \frac{1 - \kappa_{ws}}{(1 - a)\kappa_{ws}} M(\bar{s}^u - \bar{s}^d), \quad (2.27)$$

which is also consistent with (2.20). For scalars that have a continuous distribution of sources and sinks in the CABL, the flux profile can deviate from linearity and the decomposition of the scalar field in bottom-up and top-down components is not strictly valid anymore. However, we will apply (2.26) and (2.27) also in our reactive cases, since we also found for these cases that bottom-up species have subplume fluxes in the updraft only and top-down species have subplume fluxes in the downdraft only.

Subplume covariances $\overline{s'_A s'_B{}^u}$ and $\overline{s'_A s'_B{}^d}$

In the same manner as we did in (2.14) for the flux, we write the following decomposition of the covariance:

$$\begin{aligned} \overline{s'_A s'_B} &= a(\overline{s_A^u} - \overline{s_A})(\overline{s_B^u} - \overline{s_B}) + (1 - a)(\overline{s_A^d} - \overline{s_A})(\overline{s_B^d} - \overline{s_B}) \\ &\quad + a\overline{s'_A s'_B{}^u} + (1 - a)\overline{s'_A s'_B{}^d}. \end{aligned} \quad (2.28)$$

The first two terms on the rhs together constitute the top-hat contribution to the covariance and the last two terms contain the subplume covariances. These subplume covariances appear in the formulas for the subplume contributions to chemical sinks and sources,

$S_{u,\text{subplume}}$ and $S_{d,\text{subplume}}$. The subplume contributions are relevant only to sinks and sources related to second-order chemical reactions. In the two plume-budget equations (2.18) and (2.19) the chemical sink terms for our type of reactive cases look as follows:

$$S_u = -k\overline{s_A^u} \overline{s_B^u} \quad (2.29)$$

$$S_d = -k\overline{s_A^d} \overline{s_B^d} \quad (2.30)$$

$$S_{u,\text{subplume}} = -k\overline{s_A' s_B'^u} \equiv -k\overline{(s_A - \overline{s_A^u})(s_B - \overline{s_B^u})} \quad (2.31)$$

$$S_{d,\text{subplume}} = -k\overline{s_A' s_B'^d} \equiv -k\overline{(s_A - \overline{s_A^d})(s_B - \overline{s_B^d})}. \quad (2.32)$$

As we will show in this chapter the subplume contributions to the total chemical sinks and sources are substantial, so they must be parameterized.

We will treat subplume covariances in two ways in the mass-flux schemes studied in this chapter. Firstly, we can assume them to be zero:

$$\overline{s_A' s_B'^u} = \overline{s_A' s_B'^d} = 0. \quad (2.33)$$

For our reactive cases, the use of (2.33) will lead to underestimating the absolute value of the intensity of segregation I_s (it will be less negative) and consequently to overestimating the mean reaction rate, resulting in lower steady-state concentrations of scalars A and B.

Second, we propose a new parameterization for the subplume covariances based on the results shown in Fig. 2.7b (to be discussed in section 2.5). Analogous to the fluxes, we assume that the top-hat contribution to the total covariance is a constant fraction κ_{AB} of the total covariance:

$$\begin{aligned} \overline{s_A' s_B'^u} &\approx \kappa_{AB}^{-1} \left[a\overline{s_A^u} \overline{s_B^u} + (1-a)\overline{s_A^d} \overline{s_B^d} - \overline{s_A} \overline{s_B} \right] \\ &\equiv \kappa_{AB}^{-1} \overline{s_A' s_B'^{\text{top-hat}}}. \end{aligned} \quad (2.34)$$

The value of κ_{AB} is approximately 0.25: only 25% of the total covariance is resolved by the top-hat term. The experimental backing for this value of κ_{AB} is discussed extensively in section 2.5 (where Fig. 2.7b is discussed) and appendix A. We propose the following parameterization for the subplume covariances on the basis of this result:

$$\overline{s_A' s_B'^u} = \frac{1 - \kappa_{AB}}{2a\kappa_{AB}} \overline{s_A' s_B'^{\text{top-hat}}} \quad (2.35)$$

$$\overline{s'_A s'_B{}^d} = \frac{1 - \kappa_{AB}}{2(1 - a)\kappa_{AB}} \overline{s'_A s'_B{}^{\text{top-hat}}}, \quad (2.36)$$

limiting the values of $\overline{s'_A s'_B{}^u}$ and $\overline{s'_A s'_B{}^d}$ on the negative side to $-\overline{s_A} \overline{s_B}^u$ and $-\overline{s_A} \overline{s_B}^d$, respectively. Eqs. (2.35) and (2.36) are similar to (2.26) and (2.27) for the subplume fluxes, except for the fact that in (2.35) and (2.36) it is assumed that the contributions of the updraft and the downdraft subplume covariances to the total covariance are equal. This is why the factor 2 appears in the denominators of (2.35) and (2.36). As said in the above the parameterization proposed here for the subplume covariances will be defended on the basis of LES results in section 2.5.

2.3.3 Lateral-exchange terms

The contour integral for the lateral scalar exchange processes, appearing in (2.18) and (2.19), can be written as a sum of two terms:

$$\frac{1}{A} \oint_{\text{interface}} \mathbf{n} \cdot (\mathbf{u} - \mathbf{u}_i) s \, dl = (E_m - D_m) \overline{s}^i + a_i \overline{v'_R s'^i}, \quad (2.37)$$

where \overline{s}^i is the mean scalar value at the interface between updrafts and downdrafts, a_i is the perimeter/area ratio of the updrafts, v_R is shorthand for $\mathbf{n} \cdot (\mathbf{u} - \mathbf{u}_i)$, and the primes denote fluctuations relative to the interface average, which is denoted by the overbar with index i . The first term on the rhs of (2.37) is an interface-scale term and the second term is a subinterface-scale term.

In our mass-flux schemes for scalar transport we will use two parameterizations of the lateral-exchange terms. Both parameterizations provide a closure for the rhs of (2.37) in terms of the updraft and downdraft quantities \overline{s}^u and \overline{s}^d .

First, we follow Chatfield and Brost (1987) and write

$$(E_m - D_m) \overline{s}^i + a_i \overline{v'_R s'^i} = r_d \overline{s}^d - r_u \overline{s}^u, \quad (2.38)$$

with

$$r_u = \max \left\{ -\frac{\partial M}{\partial z}, 0 \right\} \quad (2.39)$$

$$r_d = \max \left\{ \frac{\partial M}{\partial z}, 0 \right\}. \quad (2.40)$$

In this parameterization only net advection occurs from one draft to the other (with the direction depending on the sign of $\partial M / \partial z$). This can be regarded as a parameterization

of the interface-scale lateral exchange only, substituting \bar{s}^u and \bar{s}^d for \bar{s}^i depending on the direction of the net mass exchange.

Second, we include the parameterization used extensively in cumulus schemes (e.g., Arakawa and Schubert 1974; Tiedtke 1989):

$$(E_m - D_m)\bar{s}^i + a_i \overline{v'_R s'^i} = E_s \bar{s}^d - D_s \bar{s}^u, \quad (2.41)$$

with E_s and D_s being “scalar entrainment” and “scalar detrainment” quantities. The difference between (2.38) and (2.41) is that E_s and D_s —provided that they are assigned positive values—are related to gross exchange, E_s to advection from downdraft to updraft and D_s to simultaneous advection from updraft to downdraft. Thus, contrary to (2.38), (2.41) does include a parameterization for the subinterface-scale lateral-exchange process. The plume-budget equations (2.18) and (2.19) now become

$$\frac{\partial a \bar{s}^u}{\partial t} = - \frac{\partial M \bar{s}^u}{\partial z} + E_s \bar{s}^d - D_s \bar{s}^u - \frac{\partial a \overline{w' s'^u}}{\partial z} + a(S_u + S_{u,\text{subplume}}) \quad (2.42)$$

$$\begin{aligned} \frac{\partial (1-a) \bar{s}^d}{\partial t} = &+ \frac{\partial M \bar{s}^d}{\partial z} - E_s \bar{s}^d + D_s \bar{s}^u - \frac{\partial (1-a) \overline{w' s'^d}}{\partial z} \\ &+ (1-a)(S_d + S_{d,\text{subplume}}). \end{aligned} \quad (2.43)$$

As Young (1988b) and Schumann and Moeng (1991b) did, we can determine ($E_s \bar{s}^d - D_s \bar{s}^u$) as a residual term of either (2.42) or (2.43). However, it is also possible to determine unique profiles of E_s and D_s , provided that we impose some constraint. It is convenient to impose, as is implicitly done by Siebesma and Cuijpers (1995),

$$E_s - D_s = E_m - D_m. \quad (2.44)$$

Substituting the continuity equation (2.15) in (2.42) and (2.43), and noting that we have $\overline{w} = 0$ in our LES, results in

$$E_s(\bar{s}^u - \bar{s}^d) = \bar{s}^u \frac{\partial M}{\partial z} - \frac{a \overline{w s^u}}{\partial z} - a \frac{\partial \bar{s}^u}{\partial t} + a(S_u + S_{u,\text{subplume}}) \quad (2.45)$$

$$\begin{aligned} D_s(\bar{s}^u - \bar{s}^d) = &\bar{s}^d \frac{\partial M}{\partial z} + \frac{(1-a) \overline{w s^d}}{\partial z} + (1-a) \frac{\partial \bar{s}^d}{\partial t} \\ &- (1-a)(S_d + S_{d,\text{subplume}}). \end{aligned} \quad (2.46)$$

We must be aware that the quantities E_s and D_s defined by (2.41) and (2.44) are not guaranteed to be scalar-independent. Also, E_s and D_s do not have to be positive. The closure

Scheme	Lateral-exchange terms $(E_m - D_m)\bar{s}^i + a_i \overline{v'_R s'^i}$	Subplume fluxes $\overline{w' s'^u}$ and $\overline{w' s'^d}$	Subplume covariances $\overline{s'_A s'_B'^u}$ and $\overline{s'_A s'_B'^d}$
MF1	(2.41), (2.45), and (2.46) SC95	(2.26) and (2.27) this chapter (new)	(2.35) and (2.36) this chapter (new)
MF2	(2.38), (2.39), and (2.40) CB87	(2.26) and (2.27) this chapter (new)	(2.35) and (2.36) this chapter (new)
MF3	(2.38), (2.39), and (2.40) CB87	(2.22) and (2.23) RSM92	(2.35) and (2.36) this chapter (new)
MF4	(2.38), (2.39), and (2.40) CB87	(2.21) no ref. (zero)	(2.33) no ref. (zero)
MF5	(2.38), (2.39), and (2.40) CB87	(2.22) and (2.23) RSM92	(2.33) no ref. (zero)

Table 2.1: Composition of mass-flux schemes for scalar transport with reference to equations in this chapter and with reference to corresponding literature: Chatfield and Brost 1987 (CB87), Randall et al. 1992 (RSM92), and Siebesma and Cuijpers 1995 (SC95).

assumption (2.41), in combination with determining E_s and D_s from (2.45) and (2.46), might even lead to plume-budget equations that do not have stable solutions (due to negative E_s and D_s). In sections 2.4 and 2.5 we will determine the behavior of E_s and D_s for different types of scalars from LES. Also we will specify there which profiles of E_s and D_s are used in our most comprehensive mass-flux scheme for scalar transport.

2.3.4 Mass-flux schemes for scalar transport

Now we have come to the point where we can define the mass-flux schemes that we will evaluate in this study. The mass-flux schemes can be considered as composed of the basic scalar plume-budget equations (2.18) and (2.19) with different permutations of the parametrizations presented in the above for the subplume fluxes, the subplume covariances, and the lateral-exchange terms. As said before, the mass-flux schemes are run in an off-line mode.

In Table 2.1 we define five mass-flux schemes (MF1 up to MF5) for transport of nonreactive and reactive scalars in the CABL. The column pertaining to the subplume covariance parametrization is only relevant to the reactive cases, so for the nonreactive case BUTD we

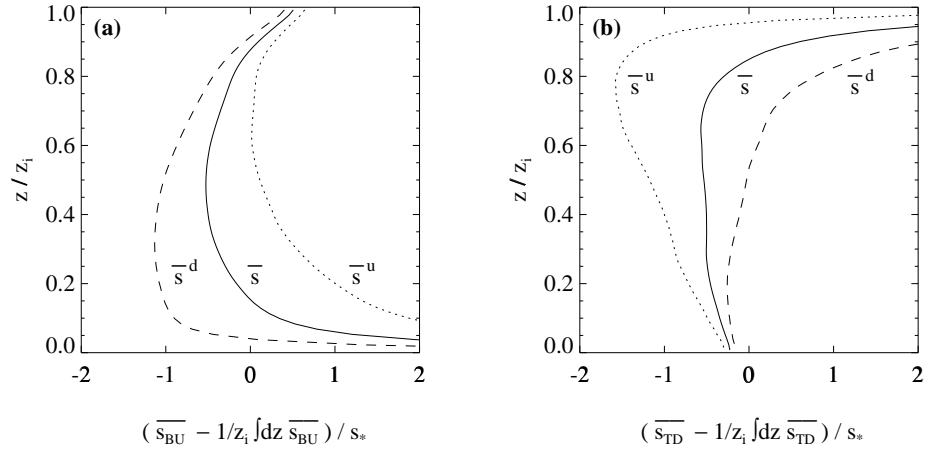


Figure 2.1: Profiles of (a) bottom-up diffusing scalar BU and (b) top-down diffusing scalar TD, determined from LES; the steady deviation from the bulk value is plotted, calculated by subtracting the vertically integrated (and steadily increasing) scalar quantities from the vertical profiles. Mean, updraft, and downdraft values are shown.

effectively have four different mass-flux schemes (for this case MF5 is identical to MF3). We use the same vertical grid resolution in the mass-flux schemes as in the LES, namely 66 layers.

Since the new proposals for the parameterization of subplume fluxes and subplume covariances are based on LES results (to be presented in sections 2.4 and 2.5) and since the parameterization of lateral exchange according to Siebesma and Cuijpers (1995) also uses LES results as input, scheme MF1 has the closest resemblance to the exact plume-budget equations. Going down the list of schemes, less sophisticated parameterizations are used for the three component processes and we expect in general that the performance will become worse (although, as it turns out there can be “compensating errors” at play, resulting in a better performance of a relatively simple scheme compared to a relatively complex scheme).

2.4 LES results for nonreactive scalars

2.4.1 Scalar profiles $\overline{s_{BU}}$ and $\overline{s_{TD}}$

Updraft and downdraft profiles of bottom-up and top-down diffusing scalars BU and TD, obtained from the LES by way of conditional sampling (averaging over areas with respectively positive and negative vertical velocities), are shown in Figs. 2.1a,b. The BU and TD scalar profiles are in quasi-steady state (with the gradients not changing in time), since there is a constant influx at either the bottom or the top boundary and there is no sink for each of the two scalars. Therefore we have subtracted the (steadily increasing) boundary-layer averaged scalar values from the profiles before plotting them in Figs. 2.1a,b, respectively.

A striking (but not perfect) symmetry between bottom-up and top-down transport mechanisms exists in the solid-lid CABL. For both scalars we find countergradient fluxes near their respective zero-flux boundaries: a stronger countergradient flux near the top for the BU scalar and a weaker countergradient flux near the bottom for the TD scalar. The countergradient fluxes of the scalars are caused by the presence of relatively fast cores within both updrafts and downdrafts that quickly vertically transports the scalars through the CABL. In the entraining CABL we do not find a countergradient flux of top-down diffusing scalars, since there is less vertical symmetry in the entraining CABL.

2.4.2 Fluxes $\overline{w's'_{BU}}$ and $\overline{w's'_{TD}}$

The flux profiles for case BUTD plotted in Figs. 2.2a,b are nearly linear, which means that the scalar profiles in Figs. 2.1a,b are close to quasi-steady state.

In Figs. 2.3a,b the ratios of the top-hat contribution to the total flux κ_{ws} are shown for bottom-up and top-down diffusing scalars, respectively. We find that the theoretical estimate (based on Gaussian assumptions) of $\kappa_{ws} = 0.64$ holds quite well for the BU and TD scalars, although the BU scalar shows a somewhat lower value of κ_{ws} near the top, where the fluxes become small. A value of 0.6 for κ_{ws} was also found before by Businger and Oncley (1990) from measurements in the surface layer for all stabilities, by Schumann and Moeng (1991a) and Wyngaard and Moeng (1992) from LES of the clear and stratocumulus-topped CABL, and by de Laat and Duynkerke (1998) from measurements in the stratocumulus-topped CABL. For the solid-lid CABL we do not find the higher value of κ_{ws} for the TD scalar that was found before by Wyngaard and Moeng (1992) for the entraining CABL (which is again due to the fact that the entraining CABL is less symmetrical in the vertical).

In Figs. 2.4a,b the LES results are shown for the decomposition of the total fluxes as

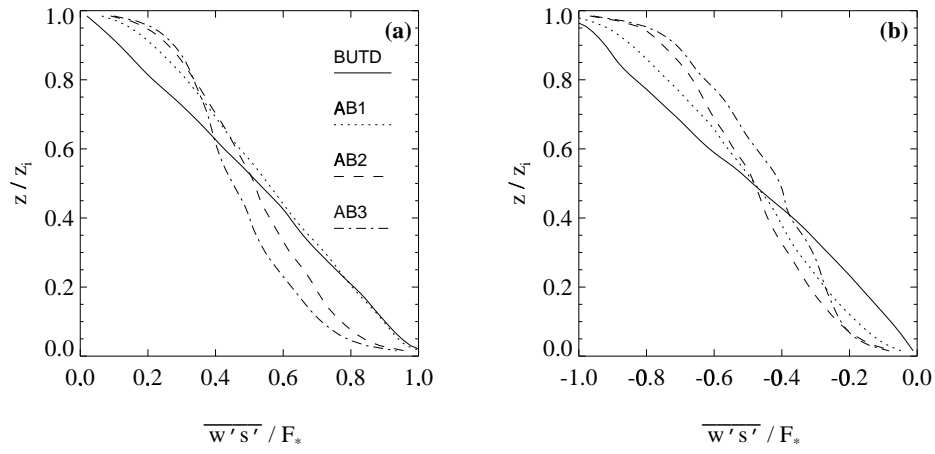


Figure 2.2: Fluxes of (a) bottom-up diffusing scalars BU or A and (b) top-down diffusing scalars TD or B, determined from LES.

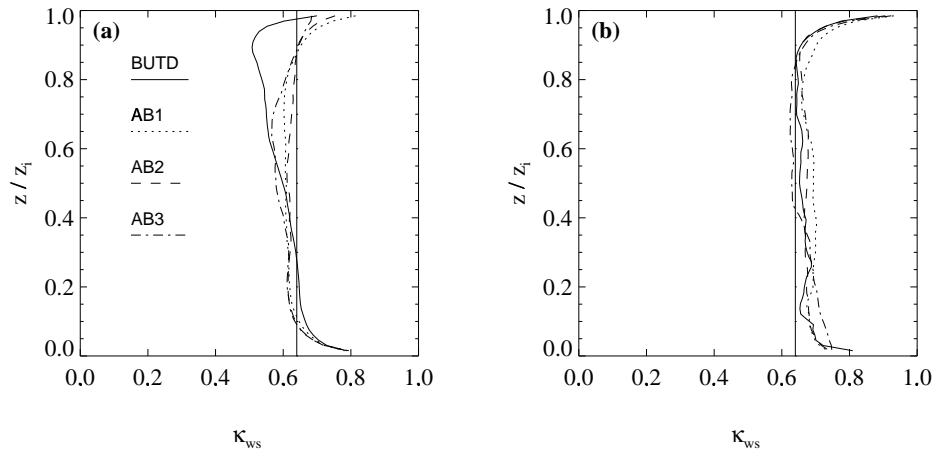


Figure 2.3: Ratios of top-hat contribution to total flux for (a) bottom-up diffusing scalars BU or A and (b) top-down diffusing scalars TD or B, determined from LES. The vertical lines indicate the theoretical value of 0.64 for a Gaussian joint pdf $P(w', s')$.

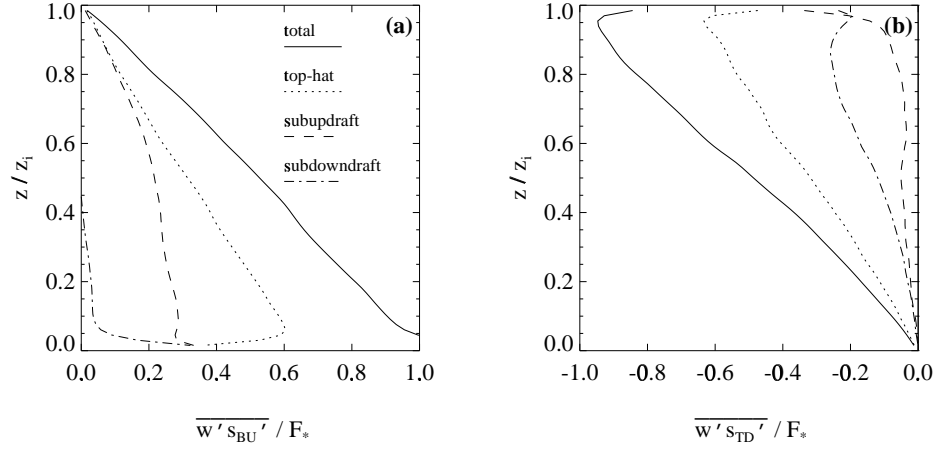


Figure 2.4: Flux decomposition for (a) bottom-up diffusing scalar BU and (b) top-down diffusing scalar TD, determined from LES.

given in (2.14). It turns out that the subplume flux of scalar BU is located only in the updraft and that the subplume flux of scalar TD is located only in the downdraft. This fact was used in our subplume-flux parameterization (2.26) and (2.27). Although Chatfield and Brost (1987) and Hunt et al. (1988) refer only to updrafts and not to downdrafts when dealing with subplume fluxes, our result that the subplume flux of scalar TD is carried almost completely by the downdrafts shows the importance of subdowndraft fluxes for scalar fields which have a significant top-down component. This is also evident in the results presented in Young (1988b) for the vertical velocity budget in the downdrafts present in the entraining CABL.

2.4.3 Lateral entrainment and detrainment rates E_{BU} , D_{BU} , E_{TD} , and D_{TD}

Scalar entrainment and detrainment rates E_{BU} , D_{BU} , E_{TD} , and D_{TD} determined from LES using (2.45) and (2.46) are shown in Figs. 2.5a,b. The breakdown of closure assumption (2.41) is evident from the large negative values of E_s and D_s near the respective zero-flux boundaries (E_{BU} and D_{BU} near the top, and E_{TD} and D_{TD} near the bottom). Using these E_s and D_s profiles in a mass-flux scheme would give rise to unstable solutions. The cause of this problem is the fact that near the problematic boundaries the subinterface-scale lateral-exchange term $\overline{v'_R s'^i}$ gives rise to transport from the draft with the lower mean

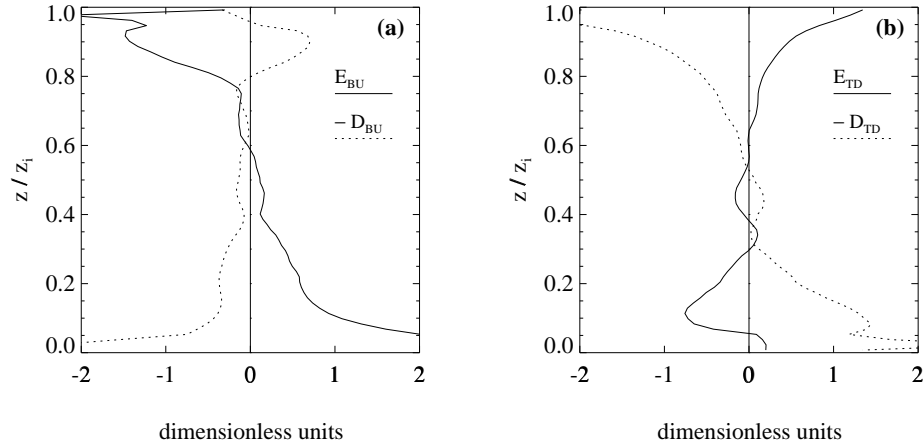


Figure 2.5: Entrainment and detrainment rates, determined from LES case BUTD for (a) bottom-up diffusing scalar BU and (b) top-down diffusing scalar TD.

scalar value to the draft with the higher mean scalar value. This is possible due to the presence of strong countergradient fluxes near those boundaries and the presence of smaller eddies that are not represented in the plume-budget equations. Since in the entraining CABL countergradient fluxes are only found for bottom-up diffusing scalars, this problem would in the real atmosphere only occur for purely bottom-up diffusing scalars and would be confined to the top part of the CABL.

As said, if we try to model this process with (2.41), using unchanged profiles of E_s and D_s , we inevitably get an unstable mass-flux scheme. Since in practice we do not deal with purely bottom-up and top-down diffusing scalar fields we propose the following practical solution to the problem. We will ensure positivity by taking $E = \max(E_{BU}, E_{TD})$ and $D = \max(D_{BU}, D_{TD})$ and use these scalar-independent E and D instead of E_s and D_s in mass-flux scheme MF1.

2.5 LES results for reactive scalars

2.5.1 Steady-state scalar values $\overline{s_A}$ and $\overline{s_B}$

The steady-state scalar values for the reactive cases are listed as boundary-layer averages in Table 2.2. As to be expected, the steady-state scalar values decrease with increasing react-

Case	k	s_A, s_B	Da_t	Da_{eff}	I_s	$\frac{\int \kappa_{AB} \overline{s'_A s'_B} dz}{\int \overline{s'_A s'_B} dz}$
AB1	0.20	2.8	0.55	0.13	-0.34	0.18
AB2	1.0	1.8	1.8	0.32	-0.68	0.22
AB3	5.0	1.4	7.2	0.49	-0.90	0.23
AB ∞	∞	1.4	∞	0.48	-1	0.25

Table 2.2: Dimensionless reaction-rate coefficient (flux Damköhler number) k , and LES results for bulk quantities: mean steady-state concentrations s_A and s_B , turbulent Damköhler number Da_t , effective Damköhler number Da_{eff} , bulk intensity of segregation I_s , and bulk ratio of top-hat contribution to total covariance.

ion-rate coefficients. The variable that ultimately determines the steady-state concentrations is the covariance term $\overline{s'_A s'_B}$ in (2.10). A measure of the importance of this covariance term at each height is the intensity of segregation I_s , defined in (2.11) and plotted in Fig. 2.6. We find that I_s becomes more negative for higher reaction-rate coefficients, slowing down the horizontally averaged reaction rate by as much as 90% (compared to the horizontally well-mixed assumption) in case AB3. In Table 2.2 we have also given for each case the “bulk intensity of segregation,” which represents the fractional change in bulk-averaged reaction rate (compared to the bulk well-mixed assumption). For the cases studied in this chapter, the bulk value of I_s is for the largest part determined by the horizontal segregation plotted in Fig. 2.6. In general, however, vertical segregation may also give an important contribution to the boundary-layer averaged segregation. Concerning the steady-state concentrations listed in Table 2.2, we must be aware that the steady-state concentration of $1.4s_*$ for scalars A and B in case AB ∞ is based on one instantaneous LES field only (as said before). Still we expect the real value to deviate not more than $0.05s_*$ from this value, and we therefore conclude that the reaction-rate coefficient $k = 5.0$ in case AB3 is already “close” to the infinite reaction-rate limit.

The boundary-layer averaged scalar values for the reactive cases shown in Table 2.2 illustrate the limitation of chemical reactions due to incomplete mixing by convective turbulence (cf. Beets et al. 1996; Molemaker and Vilà-Guerau de Arellano 1998). We see that for increasing “turbulent Damköhler number” (defined as $Da_t \equiv k s_A/s_*$), which is based on a well-mixed assumption, the effective Damköhler number, defined as $Da_{\text{eff}} \equiv (1 + I_s) Da_t$, reaches a finite limit. Thus it can be concluded that the convergence of I_s to its limiting value

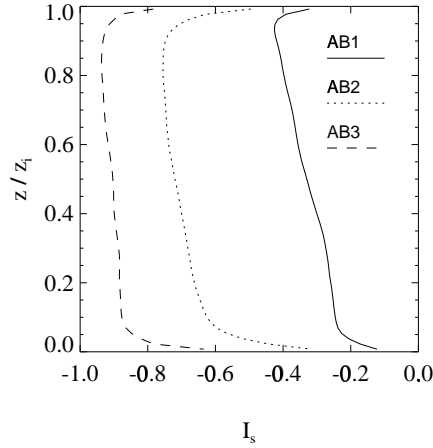


Figure 2.6: Intensities of segregation for bottom-up and top-down diffusing scalars A and B in cases AB1, AB2, and AB3.

of -1 exactly counteracts the increase of Da_t toward infinity. The steady-state concentrations reach a limiting value of $1.4s_*$, corresponding to an effective Damköhler number of 0.5. This limiting value is determined from a manipulation of the scalar fields of the non-reactive case, and no series of runs with increasing reaction-rate coefficients needs to be performed. Molemaker and Vilà-Guerau de Arellano (1998) using direct numerical simulation (DNS) of a convective boundary layer instead of LES did perform such a series of runs with their model. They found an asymptotic value for the effective Damköhler number of about 0.8, 50% higher than our result. The source of this large difference probably lies in the much lower Rayleigh number Ra (and Reynolds number Re) used in DNS compared to LES. In our LES Ra and Re are several orders of magnitude larger than in their DNS and are close to real atmospheric values. Concerning the turbulent control of chemical reactions found here, one should be aware of the fact that we here study a special chemistry case with equal input fluxes and equal boundary-layer averaged concentrations. A similar effect needs not be present in other chemistry cases.

2.5.2 Fluxes $\overline{w's'_A}$ and $\overline{w's'_B}$

In Figs. 2.2a,b also, the fluxes of the bottom-up and top-down scalars A and B in the reactive cases are plotted. The equilibrium between flux divergence and chemical destruction

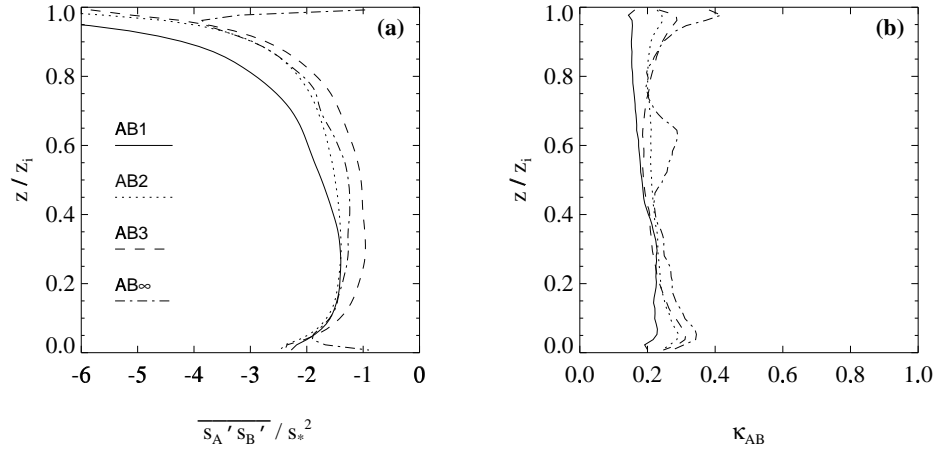


Figure 2.7: (a) Total covariances of reactive bottom-up and top-down diffusing scalars A and B and (b) ratios of top-hat contribution to total covariance, determined from LES.

results in nonlinear flux profiles. The fact that the shape of the flux profiles of the top-down diffusing scalars differs somewhat from that of the bottom-up diffusing scalars indicates that in most of the cases we have not yet reached an exact steady state. However, since we found small tendencies for the boundary-layer averaged concentrations, we consider the scalars to be close enough to steady state for the purposes of this chapter. The nonlinearity of the flux profiles becomes stronger for higher reaction rates. The flux profiles for case AB ∞ (not shown) are close to those of case AB3. Just as there exists a minimum limit on the concentrations there is a maximum limit, for the specific cases studied in this chapter, on the nonlinearity of the flux profiles for higher and higher reaction rates. In other cases, for example with premixed emissions (positive covariances) or in cases where one of the species has a much higher initial concentration than the other species (for the sake of the argument keeping the fluxes fixed), the just-mentioned limits do not have to be present and the nonlinearity of the fluxes can be larger than in the cases studied in this chapter. Preliminary results for other cases with larger flux divergences lead us to expect that the main results of this chapter apply more generally.

2.5.3 Covariance $\overline{s'_A s'_B}$

Figs. 2.7a,b show profiles of the total covariance $\overline{s'_A s'_B}$ and the fractional top-hat contribution $\kappa_{AB} \equiv \overline{s'_A s'_{B\text{top-hat}}}/\overline{s'_A s'_B}$, respectively. In the last column of Table 2.2 the boundary-layer averaged ratios of top-hat contribution to total covariance (weighed with the covariance at each height) are listed. These boundary-layer averaged quantities are the ones that should be modeled correctly by the mass-flux schemes in order to reach the correct boundary-layer averaged steady-state concentrations of scalars A and B. The profile of the total covariance is not very sensitive to the change in reaction rate by a factor of 25 between cases AB1 and AB3: $\overline{s'_A s'_B}$ changes less than 50%. And also κ_{AB} changes less than 50%. Case AB1 has the lowest κ_{AB} , indicating that subplume covariances become largest for Da_i in the order of 1. For nonreacting scalars the covariance $\overline{s'_{BU} s'_{TD}}$ is smallest and the fractional contribution of the subplume covariances is somewhat smaller than for reactive scalars (not shown). In appendix A we show that $\kappa_{12} = 0.25 \pm 0.10$ for all types of scalars in the solid-lid CABL. In the parameterization for the subplume covariances (2.35) and (2.36) in schemes MF1 to MF3 we will use $\kappa_{AB} = 0.25$. On the basis of experiments in the entraining CABL Young (1988a) finds values of $\kappa_{\theta\theta}$ (the fractional top-hat contribution to the total potential temperature variance) in the surface layer and lower mixed layer that lie within the stated range. Also LES results for a case in the entraining CABL (not shown; this case is also based on simulating a steady state in the CABL with equal bulk quantities of reactive bottom-up and top-down diffusing scalars) confirm that one can extrapolate the result to the surface layer and lower mixed layer of the entraining CABL. The top-hat formula for the covariance, however, breaks down for reactions that mainly take place in the entrainment zone. We anticipate that such conditions do not often occur in reality. In future studies we will assess the importance of this problem for realistic cases in atmospheric chemistry.

In order to assess the assumption made in (2.35) and (2.36) that the subplume covariances are equal for updrafts and downdrafts, we have plotted in Fig. 2.8 the terms of the covariance decomposition given in (2.34). Only one case (AB2) is shown; the other cases give similar results. Apparently the subupdraft and subdowndraft contributions are not equal at each height, as assumed in our subplume covariances parameterization, but compared to the large differences found for the subplume contributions to the fluxes, the subplume contributions to the covariance are relatively close to each other in size. We expect that the differences do not have a large influence on the performance of the mass-flux schemes, since the chemical sinks and sources are relatively small terms in (2.18) and (2.19) (not shown) and are only important in the boundary-layer averaged budget, in which they balance the input terms from the boundary fluxes.

Complementary to our updraft–downdraft analyses of $\overline{s'_A s'_B}$, we have also investigated

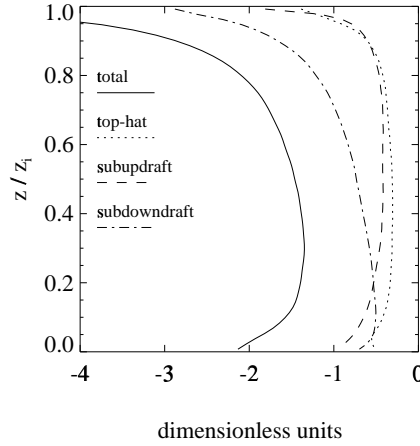


Figure 2.8: Covariance decomposition for bottom-up and top-down diffusing scalars A and B in case AB2, determined from LES. Shown are total resolved covariance, top-hat contribution, subupdraft contribution, and subdowndraft contribution.

the behavior of $\overline{s'_A s'_B}$ for the different cases in spectral space (see appendix B).

2.5.4 Lateral entrainment and detrainment rates E_A , D_A , E_B , and D_B

For the profiles of E_A , D_A , E_B , and D_B (not shown) we find similar results as for E_{BU} , D_{BU} , E_{TD} , and D_{TD} , respectively (shown in Figs. 2.5a,b). The only difference is that near the zero-flux boundaries the profiles do not become negative but only become zero. This is due to the fact that the large chemical sink term near both boundaries prevents strong countergradient fluxes from occurring (see Figs. 2.10a,b for typical LES profiles of scalars A and B, respectively). Nevertheless, we will also use $E = \max(E_{BU}, E_{TD})$ and $D = \max(D_{BU}, D_{TD})$ in scheme MF1 for the reactive cases.

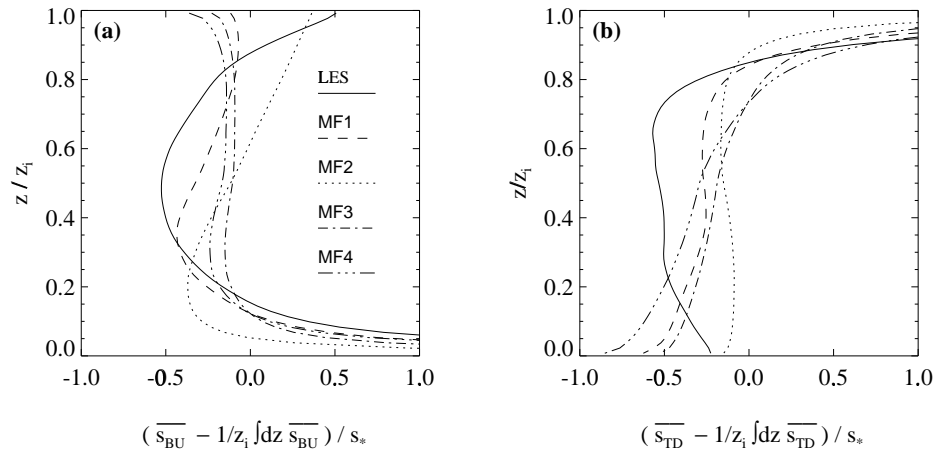


Figure 2.9: Mean quasi-steady profiles of (a) bottom-up diffusing scalar BU and (b) top-down diffusing scalar TD in nonreactive case BUTD, modeled by four mass-flux schemes and compared to LES. The steady deviation from the bulk concentration is plotted.

2.6 Results of mass-flux schemes

2.6.1 Non-reactive case BUTD

The quasi-steady results of four mass-flux schemes are shown in Figs. 2.9a,b (for this case scheme MF5 is identical to scheme MF3). The LES results are also plotted. The effect of using the new subplume-fluxes parameterization (2.26) and (2.27) is a change in the gradient in the bulk of the CABL to a (stronger) countergradient profile. The two schemes containing the new subplume-fluxes parameterization (schemes MF1 and MF2) model gradients in the bulk of the CABL that are closer to the LES results than the modeled gradients by the other two schemes.

Adding subinterface-scale lateral exchange (scheme MF1 compared to scheme MF2) results in larger scalar values near the influx boundaries of the scalars (more in agreement with LES) and a corresponding decrease of scalar values in the bulk of the CABL. The behavior near the influx boundaries is comparable for three of the schemes (MF1, MF3, and MF4) and is closer to LES for these schemes than for scheme MF2.

The discrepancies between all mass-flux schemes and LES near the zero-flux boundaries are due to the two different closure assumptions studied, (2.38) and (2.41). However, as said before, we can argue that for realistic scalar fields consisting of both bottom-up and top-down parts, the problems near the zero-flux boundaries for the purely bottom-up and top-down diffusing scalars are mitigated.

Although none of the schemes matches the LES results, we can conclude that the most comprehensive scheme (MF1) that is closest to the exact plume-budget equations gives the best overall performance of the schemes considered.

2.6.2 Reactive cases AB1, AB2, and AB3

In Table 2.3 the boundary-layer averaged steady-state results for the reactive cases are listed for all five mass-flux schemes. We have added the results for a simple bulk boundary-layer scheme without covariance parameterization, which is also indicative for the results of nonlocal scalar transport schemes without (implicit) covariance parameterization. From Table 2.3 it becomes clear that schemes MF1 through MF3 have a similar good performance for the boundary-layer averaged results. These are the three mass-flux schemes that include the subplume-covariances parameterization (2.35) and (2.36). Scheme MF4 performs worse but still gives a much improved performance compared to the bulk scheme, due to the fact that the updraft–downdraft scalar difference ($\bar{s}^u - \bar{s}^d$) is erroneously overestimated by a factor κ_w^{-1} . Finally, scheme MF5 does not give much improvement in performance compared

Case	LES	BULK	MF1	MF2	MF3	MF4	MF5
AB1	2.76	2.24	2.56	2.51	2.54	2.46	2.32
		(−19%)	(−7.2%)	(−9.1%)	(−8.0%)	(−11%)	(−16%)
AB2	1.78	1.00	1.68	1.62	1.64	1.49	1.21
		(−44%)	(−5.6%)	(−9.0%)	(−7.9%)	(−16%)	(−32%)
AB3	1.43	0.45	1.48	1.41	1.39	1.24	0.86
		(−69%)	(+3.5%)	(−1.4%)	(−2.8%)	(−13%)	(−40%)

Table 2.3: Bulk mean steady-state concentrations of scalars A and B (these are equal), determined from LES and modeled by five mass-flux schemes. In brackets the relative deviation from the LES value is given. For comparison we have also included the results of a bulk boundary-layer scheme without covariance parameterization (BULK).

to the bulk scheme.

For case AB2, Figs. 2.10a,b show the scalar profiles modeled by the five mass-flux schemes in comparison to the LES results. As in the nonreactive case BUTD the profiles modeled by scheme MF1 are closest to the LES profiles near the influx boundaries. And, also as in case BUTD, the effect of including subplume fluxes explicitly is a significant change of the gradient in the bulk of the CABL.

The subplume-covariances parameterization is the determining factor for the performance of the mass-flux schemes in the reactive cases. Therefore we have plotted in Fig. 2.11 the profiles of the intensity of segregation I_s for case AB2. Compared to the profiles of I_s modeled by schemes MF4 and MF5, the profiles modeled by schemes MF1, MF2, and MF3 are relatively close to LES.

Due to the fact that the subplume-covariances parameterization has the largest impact on the boundary-layer averaged steady-state concentrations, the other differences between the mass-flux schemes are irrelevant from the bulk point of view. However, in the studied cases we have prescribed the fluxes at the bottom and top. For a correct interactive modeling of the emission (deposition) at the surface and scalar entrainment (detrainment) fluxes at the top it is also important to correctly model scalar profiles near the bottom and top boundaries of the CABL.

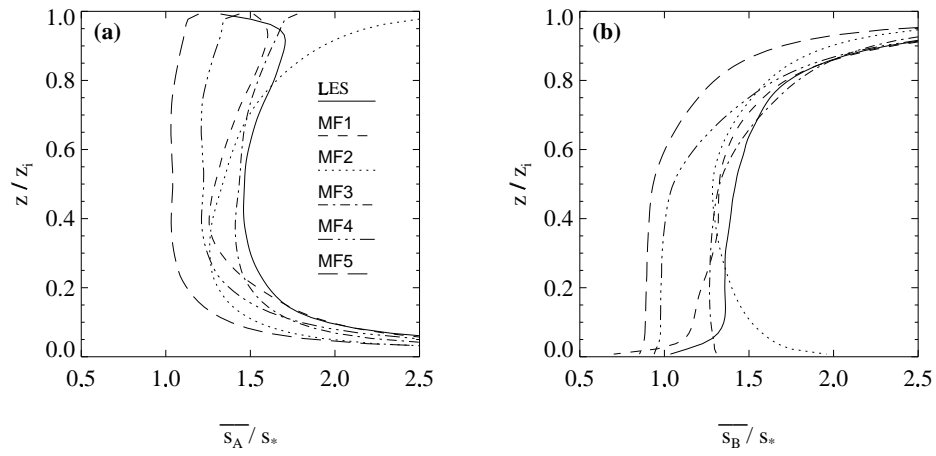


Figure 2.10: Mean steady-state profiles of (a) bottom-up diffusing scalar A and (b) top-down diffusing scalar B in reactive case AB2, modeled by five mass-flux schemes and compared to LES.

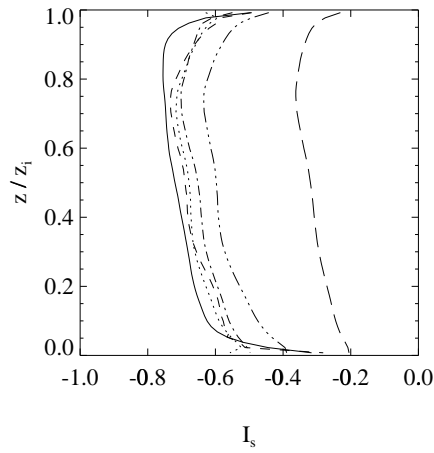


Figure 2.11: Intensity of segregation for bottom-up and top-down diffusing scalars A and B in case AB2, modeled by five mass-flux schemes and compared to LES. The line styles are as in Fig. 2.10.

2.7 Summary and discussion

In this chapter we have studied the mass-flux characteristics of scalar transport in the CABL. We have explicitly evaluated different parameterizations for component processes that can be included in mass-flux schemes for transport of nonreactive and reactive scalars. The best performance is obtained with the mass-flux schemes that is nearly identical to the exact scalar plume-budget equations.

We have shown that a subplume-fluxes parameterization based on the different behaviors of bottom-up and top-down diffusing scalars is best able to model the gradients of bottom-up and top-down diffusing scalars in the bulk of the CABL. Furthermore, we have shown that for an adequate modeling of the lateral-exchange processes between plumes one also has to take into account the subinterface-scale lateral-exchange processes. Mass-flux scheme MF3 gives a satisfactory performance in modeling the boundary-layer averaged concentrations of reactive scalars, the slightly more sophisticated scheme MF2 performs worse, and the most sophisticated scheme MF1 gives the best performance. However, we think that the improvement gained in scheme MF1 is not worth the increase in complexity. We advice using scheme MF3, in which the lateral-exchange terms are parameterized according to (2.38)–(2.40) and the subplume fluxes are parameterized according to (2.22) and (2.23).

For reactive scalars involved in a binary reaction (either as a reactant or as a reaction product) with moderate or fast reaction rates relative to the convective timescale, mass-flux schemes offer the advantage of intrinsically modeling the covariances of reactants. This gives a measure of the intensity of segregation of the scalars, which can give important corrections to the mean reaction rate. The covariance is dominated by the subplume contribution (75% of the total covariance is caused by subplume covariances and the remaining 25% is represented by the top-hat approximation). We have used this result in three of the five mass-flux schemes studied and it turned out to be the determining component process parameterization for correctly modeling the boundary-layer averaged steady-state concentrations. In typical reaction schemes for atmospheric chemistry many important reactions are moderately fast or fast compared to the convective timescale (like the $\text{NO} + \text{O}_3$ and $\text{C}_5\text{H}_8 + \text{OH}$ reactions). However, at present it is not clear whether or not the segregation of chemical species due to convection is an important effect that has to be parameterized in large-scale atmospheric chemistry models. The use of the top-hat approximation for the covariance and the parameterization for the subplume covariances that we propose here, can help in assessing the importance of the effect. The uncertainty of about 40% in the value of κ_{AB} (the fractional top-hat contribution to the total covariance) is acceptable in this light. The primary concern is to model more accurate effective reaction rates in large-scale atmo-

spheric chemistry–transport models than is currently the case. The effective reaction rates modeled with mass-flux schemes that include the subplume covariances parameterization are more accurate than the mean reaction rates calculated without this parameterization, even with the large uncertainty in κ_{AB} .

One must be aware that one can not directly include the mass-flux scheme MF3 in large-scale atmospheric models. In this chapter we have prescribed the profiles related to boundary-layer dynamics that are needed to drive the mass-flux schemes (i.e., the mass flux and the updraft area fraction, or, equivalently, the second and third moments of the turbulent vertical velocity; see appendix C). In practice not all of these dynamical quantities are available in large-scale atmospheric models, and it must be recognized that it is not yet clear whether adding them to the models will lead to a scalar transport scheme that is at least as accurate and robust as the schemes that are currently used for scalar transport in the CABL. In future studies we will address this issue.

Chapter 3

A first-order closure for covariances and fluxes of reactive species in the convective boundary layer*

*The material contained in this chapter has been accepted for publication in *Journal of Applied Meteorology*, with A. A. M. Holtslag as co-author.

Abstract

Covariances and fluxes of reactive species in the clear convective atmospheric boundary layer (CABL) are studied and parameterized. The covariances result from correlations between reactive species. These may have a significant influence on the modelled reaction rates in atmospheric chemistry models, but are usually neglected. To facilitate the representation of covariance effects in large-scale atmospheric chemistry models, we have developed a new first-order closure for covariances. The closure is based on top-hat distributions as is common in mass-flux schemes. In addition we utilize an existing nonlocal first-order closure expression for the flux, which represents the combined effects of gradient mixing and nonlocal convective mixing. We show how the latter also includes the impact of chemistry on the nonlocal flux contribution. The impact of the closures is illustrated first for artificial, simple chemistry cases. The results are evaluated using large-eddy simulation (LES). By comparing results for the entraining and solid-lid CABL it is established that the covariance closure works satisfactorily away from the inversion. Subsequently, the closures are evaluated against LES for a photochemical case with 10 reactions involving 6 modelled species. The accuracy of the modelled covariances is found to be within a factor of 2, which is sufficient to improve the modelled concentrations.

3.1 Introduction

The turbulent mixing of fast reacting chemical species in the clear convective atmospheric boundary layer (CABL)—here “fast” is taken relative to the turbulent timescale—has been known for quite some time now to require special treatment in large-scale atmospheric chemistry models (e.g., Lamb 1973). An important aspect of the turbulent transport–chemistry problem is the fact that reactive species are not always well-mixed due to short chemical timescales associated with certain important reactions—shorter than or comparable to the convective mixing timescale (see Vilà-Guerau de Arellano and Lelieveld 1998 for a precise definition of chemical timescales).

Reacting species concentrations can be (anti-)correlated. The correlations are represented in the expressions for the mean chemical reaction rates by covariance terms, and can have a significant impact on these rates (e.g., Donaldson and Hilst 1972; Bilger 1978; Schumann 1989; Krol et al. 1999). Covariance effects related to convective boundary-layer mixing can have impacts on large-scale species budgets. However, at present no estimate of large-scale covariance effects exists. This is mostly due to the fact that there is no simple covariance parameterization available that can readily be included in large-scale models. This chapter aims to fill this gap. Future studies can use the covariance parameterization proposed here to perform large-scale assessments.

We develop a first-order closure for the covariance, which is supported with an argument based on the study of mass-flux characteristics of reactive species in the CABL in chapter 2. The closure must be simple, i.e., first order, since for more complex higher-order closures (e.g., Sykes et al. 1994; Verver et al. 1997) too many prognostic variables would have to be added to large-scale models. The proposed closure can readily be included in large-scale models.

The parameterization aims to represent all contributions to the turbulent and chemical production of covariances: from the smallest scale (millimeters) to the largest turbulent scales (several kilometers), assuming uniform emissions of emitted species. These turbulence-related covariances add to the covariances due to nonuniform emissions (e.g.,

Sillman et al. 1990; Krol et al. 1999), taken together they represent the total covariance. The covariances due to nonuniform emissions should be parameterized separately, since the scaling behavior of the covariances depends on the scales on which heterogeneity is present in the emissions. The parameterization of covariance effects related to nonuniform emissions deserve separate study and are not treated in this chapter.

The fluxes of chemically reactive species are modeled with the first-order flux closure given by Cuijpers and Holtslag (1998). This closure represents the combined effects of gradient mixing and nonlocal convective mixing. We make visible how the effect of mean chemical sources and sinks on the nonlocal part of the flux is included in this closure. However, the influence of chemical higher-order moments on the flux through the flux budget (e.g., Fitzjarrald and Lenschow 1983; Hamba 1993; Sykes et al. 1994; Gao and Wesely 1994; Galmarini et al. 1997a; Verver et al. 1997) is not included in the flux closure. Our approach is to treat species for which the chemical terms in the flux budget are dominant as nontransported species, i.e., species whose concentration budget can be adequately described by considering only local chemical production and destruction.

Besides studying simple bimolecular chemistry we put emphasis on daytime photochemistry in the CABL (covariance effects were found by Galmarini et al. 1997b to be typically less than 1% for a nighttime chemistry case). We use results from large-eddy simulation (LES) of the CABL to evaluate the covariance and flux closures in either case. The closures are included in a one-dimensional (1-D) model driven by average vertical profiles for the dynamics obtained from the LES. Two LES-with-chemistry runs, one presented in chapter 2 and another similar to the one presented by Krol et al. (1999), are used, as well as one new LES-with-chemistry run specifically performed for this study. Together these runs cover nearly all types of atmospheric LES cases with chemistry reported in the literature. These are the cases published by Schumann (1989), Sykes et al. (1994), Beets et al. (1996), Molemaker and Vilà-Guerau de Arellano (1998), Petersen et al. (1999, chapter 2 of this dissertation), and Krol et al. (1999, their uniform-emission case). As a reference case we also investigate the behavior of nonreactive bottom-up and top-down diffusing scalar fields.

The theory and background of covariances is discussed in section 3.2. The first-order covariance and flux closures and the different 1-D model versions studied in this chapter are introduced in section 3.3. Simple chemical cases (involving the irreversible, binary reaction $A + B \rightarrow C$) are used to illustrate the effects of the covariance parameterization and the nonlocal flux term in section 3.4. In section 3.5 the photochemistry case is studied and the closures are evaluated for this case. Finally, in section 3.6, the results of this chapter are summarized and discussed.

3.2 Theory and background

The problem of representing atmospheric boundary layer transport and chemical reactions in large-scale models is mathematically described by the budget equation for the mean concentration, which reads

$$\frac{\partial \bar{s}_i}{\partial t} = - \frac{\partial \overline{w's'_i}}{\partial z} + R_i, \quad (3.1)$$

where horizontal homogeneity and zero mean vertical velocity have been assumed for simplicity. We will give a brief review of the covariance terms that form part of the mean chemical reaction rate term R_i (for a more extensive review, see Vilà-Guerau de Arellano and Lelieveld 1998). In this study we limit ourselves to first- and second-order reactions. For second-order reactions, covariances of species occur in the term R_i in (3.1). For example, for the simple irreversible, binary reaction $A + B \rightarrow C$ the mean reaction rate at a certain height is given by

$$R_A = R_B = -k \overline{A B} = -k \overline{(A + A')(B + B')} = -k(\overline{A B} + \overline{A'B'}), \quad (3.2)$$

where k is the reaction rate coefficient and A and B are species concentrations. The overbars denote horizontal averaging and the primed quantities represent deviations from the average. Inclusion of covariance terms like $\overline{A'B'}$ either slows down (if the terms are negative) or speeds up (if the terms are positive) modeled reaction rates for binary reactions, compared to estimates based on mean concentrations.

Following Lamb and Seinfeld (1973) we write R_i in the general case as

$$R_i = \sum_{m=1}^M \eta_{im} k_m \prod_{n=1}^N (\bar{s}_n + s'_n)^{\beta_{nm}}, \quad (3.3)$$

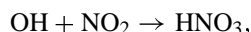
in which η_{im} is the stoichiometric coefficient for species i in reaction m , k_m is the reaction rate coefficient for reaction m , and β_{nm} is the reaction order of species n in reaction m . M is the total number of reactions and N is total number of species. If a covariance for a certain reaction in (3.3) is negative the involved species are said to be “segregated.” Segregation can be partial, and is quantified using the quantity “intensity of segregation” (this can also be positive and then represents the degree of “premixedness”). The intensity of segregation $(I_s)_{ij}$ for the reactive couple of species i and j at a certain height is defined as $\overline{s'_i s'_j} / (\bar{s}_i \bar{s}_j)$, and is bounded on the negative side by the value of -1 (total segregation of the species) and unbounded on the positive side (the value goes to infinity for premixed species emitted from a point source if the background concentrations are zero).¹

¹The fact that in principle the intensity of segregation can go to infinity will be proved here. The intensity of

The possible impact of covariance effects related to convective boundary-layer mixing on large-scale species budgets can be illustrated for the following two important atmospheric oxidation reactions:



and



where RH is a generic hydrocarbon. Isoprene is an important example for our study, since the chemical timescale for the breakdown of this hydrocarbon is comparable to the convective mixing timescale (covariance effects for the OH + isoprene reaction were studied by Davis 1992). For conditions where reactions with hydrocarbons constitute an important sink for OH, the species OH and RH will be strongly anticorrelated. In cases where RH and NO₂ are correlated (for example if they both have upward fluxes) OH and NO₂ will typically also be anticorrelated. Due to the presence of (anti-)correlations the local budgets of RH and NO_x ($\equiv \text{NO} + \text{NO}_2$) are altered, since the mentioned oxidation reactions represent major sinks of RH and NO_x. If patterns of (anti-)correlations extend over larger areas also large-scale budgets are affected by covariances.

It is useful to make a distinction between the “horizontal” and the “vertical” bulk covariance, which are defined here. Proceeding from horizontally averaged covariances towards volume-averaged covariances, we write $\langle A'B' \rangle$ —note that the primes here denote deviations from the volume average—as the sum of the boundary-layer averaged “horizontal bulk covariance” and “vertical bulk covariance”:

$$\langle A'B' \rangle = \langle A'B' \rangle_{\text{hor}} + \langle A'B' \rangle_{\text{vert}}, \quad (3.4)$$

segregation at a certain height can be written as

$$(I_s)_{ij} = \frac{\frac{1}{A} \int_A s'_i s'_j dA}{\frac{1}{A} \int_A s_i dA \frac{1}{A} \int_A s_j dA},$$

in which A is the fixed horizontal area over which averaging takes place. Now supposing we concentrate certain amounts of both species in an infinitesimally small volume (occupying an infinitesimally small area at a certain height), the numerator will be infinite and the denominator will have a finite value (the denominator is independent of the species distribution). The fact that the numerator (the covariance) goes to infinity if the species are concentrated in an infinitesimally small volume can be proved by way of the following argument. Suppose that the small area in which the species are concentrated at a certain height is proportional to ϵ and that the concentrations on this small area are proportional to ϵ^{-1} . The product of concentrations is then proportional to ϵ^{-2} , but this product is still “located” in the same small area that is proportional to ϵ . Hence the numerator is proportional to ϵ^{-1} , which does go to infinity if $\epsilon \downarrow 0$. Note that in this argument we keep the total amount of both species in area A fixed.

with

$$\langle A'B' \rangle_{\text{hor}} \equiv \frac{1}{z_i} \int_0^{z_i} \overline{A'B'} dz \quad (3.5)$$

$$\langle A'B' \rangle_{\text{vert}} \equiv \frac{1}{z_i} \int_0^{z_i} \overline{A} \overline{B} dz - \langle A \rangle \langle B \rangle. \quad (3.6)$$

Likewise we define and decompose the bulk intensity of segregation, $I_{s,\text{total}} = I_{s,\text{hor}} + I_{s,\text{vert}}$, with

$$I_{s,\text{hor}} \equiv \frac{\langle A'B' \rangle_{\text{hor}}}{\langle A \rangle \langle B \rangle} \quad (3.7)$$

$$I_{s,\text{vert}} \equiv \frac{\langle A'B' \rangle_{\text{vert}}}{\langle A \rangle \langle B \rangle}. \quad (3.8)$$

The vertical bulk covariance is related to vertical mean gradients, and can be resolved by choosing a vertical resolution that is fine enough to resolve the gradients, provided that one can model the gradients correctly. The horizontal bulk covariance is unresolved in large-scale models due to computational constraints. Of course, there are computational constraints on the vertical resolution too, but the horizontal resolution needed to resolve covariances that are due to convection in the CABL will not be reached for many years in the future.

The modeling of (horizontal) covariances may start from the budget equation for the covariance $\overline{s'_i s'_j}$ at a certain height (in zero mean flow),

$$\frac{\partial \overline{s'_i s'_j}}{\partial t} = -\overline{w' s'_j} \frac{\partial \overline{s_i}}{\partial z} - \overline{w' s'_i} \frac{\partial \overline{s_j}}{\partial z} - \frac{\partial \overline{w' s'_i s'_j}}{\partial z} - 2D \frac{\partial s'_i}{\partial z} \frac{\partial s'_j}{\partial z} + R_{ij}, \quad (3.9)$$

with D the Fickian diffusion coefficient. The reactive term R_{ij} can be written in the following compact form:

$$R_{ij} = \sum_{m=1}^M \eta_{im} k_m (s'_i + s'_j) \prod_{n=1}^N (\overline{s_n} + s'_n)^{\beta_{nm}}. \quad (3.10)$$

The first two terms on the rhs of the covariance budget (3.9) represent gradient production, the third term represents turbulent transport, the fourth term molecular diffusion, and the last term chemical production or destruction. The molecular diffusion term is small in the CABL and can be neglected.

Different modeling strategies for the covariances have been proposed in the literature. The first articles on the role and the parameterization of covariances in atmospheric chemistry modeling appeared in the 1970s. The budget equation (3.9) was closed in different ways. For example, on the one hand, Donaldson and Hilst (1972), focussing on reactive plumes, neglected the gradient production and the turbulent transport terms, leaving only R_{ij} on the rhs of (3.9)—in which subsequently the third-order moments were neglected. On the other hand, Lamb (1973) neglected the chemical term R_{ij} and only considered gradient production and turbulent transport effects on (co-)variances (using mixing-length theory). Bilger (1978) retained both the gradient production, the turbulent transport, and the chemical terms in (3.9). His strategy was to let turbulence produce fluctuations of relatively slowly reacting species and let chemistry produce fluctuations of relatively fast reacting species. We will use a similar separation—between transported and nontransported species—in our parameterization, as is described in the next section.

To substantiate our claim that currently no applicable parameterization for covariances in large-scale models exists in the literature, we here discuss some classifications and parameterizations that have been presented before. Classifications of reactions that are diffusion-limited have been given by, e.g., Donaldson and Hilst (1972) and Stockwell (1995). However, these classifications deal with the molecular diffusion–chemistry problem instead of the turbulent transport–chemistry problem. The application of classifications based on the molecular diffusion problem to the turbulent CABL is problematic. For the turbulent transport–chemistry problem the use of simple bulk parameterizations has been suggested by, e.g., Thuburn and Tan (1997) and Molemaker and Vilà-Guerau de Arellano (1998). One proposal (Molemaker and Vilà-Guerau de Arellano 1998) is to generate look-up tables of covariance effects for all relevant archetypes of reactive cases. However, it is not clear how this approach should be worked out (which cases to select, how many different cases are needed, etc.), nor how accurate it can be. For completeness we mention two other model approaches here, full second-order closure models that incorporate covariances through (3.9) (Sykes et al. 1994; Verver et al. 1997) and Lagrangian models (Crone et al. 1999). However, these approaches for calculating covariances are too complex to be included in large-scale models.

3.3 First-order closures

3.3.1 Covariances

Our approach to obtain the covariances is a diagnostic one, using a mass-flux argument. Mass-flux schemes (e.g., Chatfield and Brost 1987) are higher-order closure schemes in the sense that they can be written in terms of two prognostic equations, one for the mean concentration and one for the flux. Mass-flux schemes use an updraft–downdraft decomposition for the atmospheric boundary layer and are usually formulated in terms of two prognostic variables, updraft concentration and downdraft concentration, for each species (see chapter 2). The mean concentration and the flux can be written as function of updraft and downdraft concentrations as follows:

$$\overline{s_i} = a \overline{s_i^u} + (1 - a) \overline{s_i^d} \quad (3.11)$$

$$\overline{w' s_i'} = \frac{(M/\rho)}{\kappa_0} (\overline{s_i^u} - \overline{s_i^d}), \quad (3.12)$$

in which a is the updraft area fraction, the indices u and d denote that the horizontal averaging is done over updrafts and downdrafts, respectively, M is the mass flux in the atmospheric boundary layer, $M \equiv a\rho(\overline{w^u} - \overline{w})$, and ρ is the density. The mean vertical velocity \overline{w} is typically small and will be neglected in the following. The parameter κ_0 in (3.12) typically varies with the species and with height. The mass-flux approximation employed here assumes that κ_0 is a constant equal to 0.64, which follows from both theoretical considerations (Wynngaard and Moeng 1992), experimental evidence (Young 1988a; Businger and Oncley 1990; de Laat and Duynkerke 1998), and LES results (Schumann and Moeng 1991a; Wynngaard and Moeng 1992; chapter 2 of this dissertation). Note that (3.11) and (3.12) are valid for both nonreactive and reactive species.

For the surface layer and mixed layer of the dry CABL, we proposed in chapter 2 the following estimate for the covariance:

$$\overline{s_i' s_j'} = \frac{1}{\kappa_1} \left\{ a \overline{s_i^u} \overline{s_j^u} + (1 - a) \overline{s_i^d} \overline{s_j^d} - \overline{s_i} \overline{s_j} \right\}, \quad (3.13)$$

with κ_1 a species and height dependent parameter, here taken to be a constant equal to 0.25. This value of κ_1 is justified in chapter 2, considering several cases. Expression (3.13) is analogous to the top-hat formula for the variance derived by Randall et al. (1992), the difference being that we take the empirically determined factor κ_1 into account. The accuracy of the estimate of κ_1 was reported in chapter 2 to be about 40%, reflecting the scalar dependence of (3.13). Even with this relatively low accuracy it is guaranteed for the given value

of κ_1 that the inclusion of (3.13) in the R_i term in (3.1) leads to an improved estimate of R_i , as far as covariance effects are concerned.

In order to use (3.13) to determine the covariance, we need the updraft and downdraft concentrations of the reacting species. To obtain expressions for updraft and downdraft concentrations we invert (3.11) and (3.12), yielding

$$\overline{s_i^u} = \overline{s_i} + \frac{(1-a)\kappa_0}{(M/\rho)} \overline{w's_i'} \quad (3.14)$$

$$\overline{s_i^d} = \overline{s_i} - \frac{a\kappa_0}{(M/\rho)} \overline{w's_i'}. \quad (3.15)$$

Substituting (3.14) and (3.15) in (3.13), and using $(M/\rho) = \frac{1}{2} \sqrt{\kappa_0} \sigma_w$ (see appendix C) we arrive at

$$\overline{s_i's_j'} \cong \alpha \frac{\overline{w's_i'} \overline{w's_j'}}{\sigma_w^2}, \quad (3.16)$$

where

$$\alpha = \frac{4\kappa_0 a (1-a)}{\kappa_1} \approx 2.6. \quad (3.17)$$

We have used $a = 0.5$ in the approximating step in (3.17). The error associated with this approximation is smaller than 10% in the mixed layer, since there typically $0.35 < a < 0.5$; in the surface layer a is close to 0.5 (see Young 1988a; Schumann and Moeng 1991a; Nieuwstadt et al. 1993).

Tests with LES data leads to the conclusion that (3.16) is valid for all species—if one substitutes the fluxes taken from LES. However, in models that use a first-order closure for the flux—which do not include the chemical higher-order moments that appear in the flux budget (discussed below)—the fluxes of reactive species with a very short lifetime (in the order of seconds) cannot be accurately modeled. This is due to the importance of the chemical higher-order moments in the flux budget for such species. Therefore we employ the following method in our covariance parameterization to solve this problem (details can be found in appendix D). We make a separation between transported and nontransported species. The transported species are defined as those species for which the turbulent flux divergence in the concentration budget (3.1) cannot be neglected, and the nontransported species as those for which it can. Ideally one should make the distinction on the basis of a certain value for the Damköhler number (for instance, 10). Species that are not both chemically produced and destroyed and species that are emitted or deposited should be treated

as transported species. The covariance parameterization makes use of (3.14) and (3.15) for the concentrations of transported species and subsequently determines the concentrations of nontransported species from a chemistry calculation. Eq. (3.13) finally gives the covariances based on the calculated updraft and downdraft concentrations of all reacting species. Thus only for the special case of two reacting transported species (3.16) can be used directly to calculate the covariance. Note that from the updraft and downdraft concentrations of nontransported species we can determine the fluxes through (3.12). Only if we use fluxes of nontransported species calculated in that way, (3.16) can be used to calculate covariances—this is then equivalent to using (3.13).

As said before the accuracy of about 40% for κ_1 reflects the species and height dependence of the ratio that was neglected in the approximation. This leads to an accuracy of about a factor of 2 in α . This accuracy is also found when one compares estimates of α in the literature (determined from measurements of θ and q in the lower CABL). For example, evaluating the similarity relations from Stull (1988, pp. 371–373) for $\overline{\theta'q'}$ and w'^2 at $z/z_i = 0.1$ and assuming that $\overline{w'\theta'} = 0.9 \overline{w'\theta'}|_0$ and $\overline{w'q'} = 0.9 \overline{w'q'}|_0$ at that height, gives $\alpha = 2.6$, while evaluation of the similarity relations for the same quantities in a nonentraining boundary layer from Sorbjan (1989, pp. 113–115) gives $\alpha = 1.5$ (independent of height, since it concerns local scaling relations). However, from the results given by Wang and Stevens (1999) for the stratocumulus-topped CABL we can conclude that for the covariance $\overline{q'_t\theta'_i}$ of total water content q_t and liquid water potential temperature θ_i the closure (3.13) only works well in the surface layer and not in the mixed layer. In this chapter we will determine with which accuracy the covariance closure works in the surface layer and mixed layer of the entraining and solid-lid clear CABL.

The form of (3.16) allows us to deduce that

$$\alpha = \frac{\rho_{s_i s_j}}{\rho_{w s_i} \rho_{w s_j}}, \quad (3.18)$$

where the ρ 's are the correlation coefficients, defined in the standard way:

$$\rho_{s_i s_j} \equiv \frac{\overline{s'_i s'_j}}{\sigma_{s_i} \sigma_{s_j}}, \quad \rho_{w s_i} \equiv \frac{\overline{w' s'_i}}{\sigma_w \sigma_{s_i}}, \quad \rho_{w s_j} \equiv \frac{\overline{w' s'_j}}{\sigma_w \sigma_{s_j}}.$$

According to the above we have that α is scalar-independent within a factor of 2. A similar assumption has been used by Vilà-Guerau de Arellano et al. (1993b) to estimate the covariances of reacting species in the neutral surface layer: they assumed constant values for the separate ρ 's, also leading to a constant estimate of α . The differences between our approach and theirs are that we apply it for the CABL and that we can also deal with nontransported species. Appendix A provides an overview of the implementation of the current proposal in atmospheric chemistry models.

3.3.2 Fluxes

To model the fluxes for our purpose we follow Cuijpers and Holtslag (1998), who propose for the vertical flux $\overline{w's'_i}$ of a scalar s_i :

$$\overline{w's'_i} = -K \frac{\partial \overline{s_i}}{\partial z} + \overline{w's'_{i\text{NL}}}, \quad (3.19)$$

where K is a diffusivity, $\overline{s_i}$ the mean scalar profile, and

$$\overline{w's'_{i\text{NL}}} = \beta_1 \frac{L}{z_i} \frac{w_\star}{\sigma_w} \frac{1}{z_i} \int_0^{z_i} \overline{w's'_i} dz. \quad (3.20)$$

Here β_1 is assumed to be a constant (in general this parameter can vary with height), L is a length scale, z_i the boundary-layer height, w_\star the convective vertical velocity scale, and σ_w the standard deviation of the vertical velocity fluctuations. The term $\overline{w's'_{i\text{NL}}}$ represents the nonlocal contribution to the flux. For more details on the background of expression (3.20) we refer to Cuijpers and Holtslag (1998).

The eddy diffusivity and the length scale are given by $K = c_k \sigma_w L$ and $L = c_l z (1 - z/z_i)$, respectively, with the constants $c_k = 0.4$ and $c_l = 1.8$. Furthermore we take $\beta_1 = 1.6$. This combination of constants was chosen since it gives the most satisfying performance of nonreactive scalar dispersion in the CABL. Note that these values are somewhat different compared to Cuijpers and Holtslag (1998). This is related to the different length-scale formulation used.

For a scalar with a linear flux profile (3.20) provides:

$$\overline{w's'_{i\text{NLB}}} = \beta_1 \frac{L}{z_i} \frac{w_\star}{\sigma_w} \frac{1}{2} \left(\overline{w's'_i} \Big|_0 + \overline{w's'_i} \Big|_{z_i} \right), \quad (3.21)$$

where $\overline{w's'_i} \Big|_0$ and $\overline{w's'_i} \Big|_{z_i}$ are the surface flux and the entrainment flux, respectively, and “B” is added to the subscript to make clear that this nonlocal contribution to the flux is related to the fluxes at the boundaries of the CABL. In this chapter we are studying reactive species and therefore we will evaluate the performance of (3.19) and (3.20) for cases with nonlinear flux profiles. In fact (3.19) and (3.20) have not been rigorously tested for such cases before, because nearly all scalar fields studied by Cuijpers and Holtslag (1998) have linear flux profiles in the CABL.

To emphasize the difference between (3.20) and (3.21) we decompose the flux as follows:

$$\overline{w's'_i} = -K \frac{\partial \overline{s_i}}{\partial z} + \overline{w's'_{i\text{NLB}}} + \overline{w's'_{i\text{NLI}}}, \quad (3.22)$$

with $\overline{w's'_{i\text{NLB}}}$ already given by (3.21) and $\overline{w's'_{i\text{NLI}}} \equiv \overline{w's'_{i\text{NL}}} - \overline{w's'_{i\text{NLB}}}$. The additional subscript “I” denotes the internal net chemical source or sink, represented by the term R_i , that causes a nonlinear flux profile in the CABL (note that $\overline{w's'_{i\text{NLI}}} = 0$ for linear flux profiles). Within the first-order closure this nonlinearity is caused by the chemistry through (3.1). The condition for $\overline{w's'_{i\text{NLI}}}$ to be nonzero, assuming (quasi-)steady conditions, is that $\partial R_i / \partial z \neq 0$, i.e., vertical inhomogeneity of the reaction rate is needed.

The nonlocal flux expression (3.20) proposed by Cuijpers and Holtslag (1998) is an extension of the expression proposed earlier by Holtslag and Moeng (1991), since it includes the additional effect of the nonlinearity of the flux profile on the nonlocal flux contribution. Since this is a first-order closure no chemical higher-order moments, that appear in higher-order closures, are modeled. For scalars with a linear flux profile Cuijpers and Holtslag (1998) amounts to a simplification of Holtslag and Moeng (1991), since its formulation is scalar-independent, while Holtslag and Moeng (1991) applied a bottom-up/top-down decomposition of the scalar field (Wyngaard and Brost 1984), which resulted both in a scalar-dependent K and different contributions to the nonlocal flux (3.21) related to $\overline{w's'_i}]_0}$ and $\overline{w's'_i}]_{z_i}$, respectively. Moreover, Holtslag and Moeng (1991) assumed the contribution of $\overline{w's'_i}]_{z_i}$ to be zero. A preliminary study for the solid-lid CABL indicated that if a scalar-independent K is used, inclusion of a contribution related to $\overline{w's'_i}]_{z_i}$ (symmetrical to the contribution related to $\overline{w's'_i}]_0}$) in the nonlocal flux expression leads to a significant improvement of the modeled profiles (Petersen et al. 1997). This was confirmed for the entraining CABL by Cuijpers and Holtslag (1998).

3.3.3 Incorporation in a 1-D model

Different combinations of closures are tested in this chapter by including them in a 1-D model. The 1-D model solves the species budget equation (3.1). The differences between the model versions show the impact of either the covariance parameterization or the nonlocal flux term. The closures are combined in three versions of the 1-D model, as given in Table 3.1. The “covariance–nonlocal” version of the 1-D model is the standard version, which includes the covariance expression (3.13) and the full nonlocal flux expression (3.22). The second version does not contain the covariance closure (“no-covariance–nonlocal” version). And the third 1-D model version does not contain the covariance closure and the nonlocal flux contribution (“no-covariance–local” version). It only contains the local flux contribution $-K \partial \overline{s_i} / \partial z$ and no covariance closure.

The LES profiles of σ_w are used both to construct the profiles of K through $K = c_k \sigma_w L$ and to determine (M/ρ) through $(M/\rho) = \frac{1}{2} \sqrt{\kappa_0} \sigma_w$, which is needed in (3.14) and (3.15)

1-D model version	Description
“Covariance–nonlocal”	standard version: covariance closure (3.13) and nonlocal flux closure (3.22)
“No-covariance–nonlocal”	no covariance closure and nonlocal flux closure (3.22)
“No-covariance–local”	no covariance closure and only local flux contribution in (3.22)

Table 3.1: 1-D model versions.

as part of the covariance parameterization (see Appendix A). The eddy diffusivity profile K is typical for local first-order closure schemes for the flux, i.e., it does not have lower values than usual.

Results of the 1-D model are shown for two cases in this chapter: one simple chemistry case (SL1, introduced in section 3.4) and the photochemistry case (introduced in section 3.5). The vertical resolution of the 1-D model varies depending on the case. The vertical resolution is the same as that of the the LES model used for the specific case, that is, 66 and 64 layers in CABL for case SL1 and the photochemistry case, respectively. For the photochemistry case also a high-resolution version of the 1-D model is used (with 17 additional layers in the surface layer, see section 3.5). The following averaging procedures are applied: for case SL1 the 1-D model is integrated towards steady state and for the photochemistry case the instantaneous 1-D model results in the middle of the LES averaging interval are used (see appendix E).

3.4 Simple cases with one irreversible, binary reaction

3.4.1 Description and LES results

We simulate two types of CABLs, the entraining CABL and the solid-lid CABL. The difference between the two types is that for the solid-lid CABL there is no entrainment of heat at the top of the CABL, and this top is fixed at height z_i by a solid lid. The solid-lid CABL was studied with LES by Schumann (1993). He found that LES compares favorably with laboratory measurements. The main differences between entraining and solid-lid CABLs were studied by Sorbjan (1996). The major difference is a higher skewness of the vertical velocity fluctuations (equivalent to a lower updraft area fraction, see section 3.3) in

Case	k	w_\star [m/s]	z_i [m]	t_\star [s]	$\langle A \rangle$	$\langle B \rangle$	$Da_{t,A}$	$Da_{t,B}$	$I_{s,hor}$	$I_{s,vert}$	$I_{s,total}$
E0		1.1	720	650							
E1	1.2	1.1	720	650	2.0	2.2	2.6	2.4	-0.46	-0.40	-0.86
SL0		1.5	1500	1000							
SL1	1.0	1.5	1500	1000	1.8	1.8	1.8	1.8	-0.60	-0.08	-0.68

Table 3.2: Bulk quantities for simple cases with one irreversible, binary reaction: dimensionless reaction-rate coefficients k , convective velocity scales w_\star , boundary-layer heights z_i , time scales t_\star , mean concentrations of species A and B, turbulent Damköhler numbers $Da_{t,A}$ and $Da_{t,B}$, and bulk intensities of segregation I_s (horizontal and vertical contributions, and the total). Additionally the nonreactive cases E0 and SL0 are listed.

the top half of the entraining CABL. The second (and third) moments in the surface layer (and for some variables also in the lower mixed layer) do not differ between the entraining and solid-lid CABL. The main advantage of the solid-lid CABL is that we can directly prescribe the fluxes at the top of the CABL, which makes integrations towards steady states possible.

All cases studied in this section concern the injection of a species at the surface (denoted by BU or A) and another species at the top of the CABL (denoted by TD or B) until a (quasi-)steady state is attained. Table 3.2 lists some of the bulk quantities, and fluxes and concentrations are shown in Figs. 3.1 and 3.2. Cases E0 and E1 are entraining CABL cases, and SL0 and SL1 are solid-lid CABL cases. For each case we take the surface flux of the bottom-up diffusing species as the flux scale F_\star , hence all fluxes in Fig. 3.1a are equal to F_\star at the surface. The concentration scale $s_\star \equiv F_\star/w_\star$ is derived from this flux scale. If no dimensions are given in this chapter for certain quantities, we have used z_i , w_\star , and s_\star to make the quantities dimensionless.

Cases E0 and SL0 are used as reference cases for transport without reaction. They consist of the nonreactive bottom-up diffusing species BU and top-down diffusing species TD. The flux profiles $\overline{w'BU'}$ and $\overline{w'TD'}$ are linear (see Fig. 3.1), since the fields are in quasi-steady state. The concentration profiles plotted in Fig. 3.2a show a clear asymmetry between bottom-up and top-down transport in the entraining CABL. While some countergradient transport is observed for species BU, it does not occur for species TD in the entraining CABL. As was already found by Petersen et al. (1997) and Cuijpers and Holtslag (1998) we also find here that inclusion of a nonlocal flux term for the top-down diffusing species

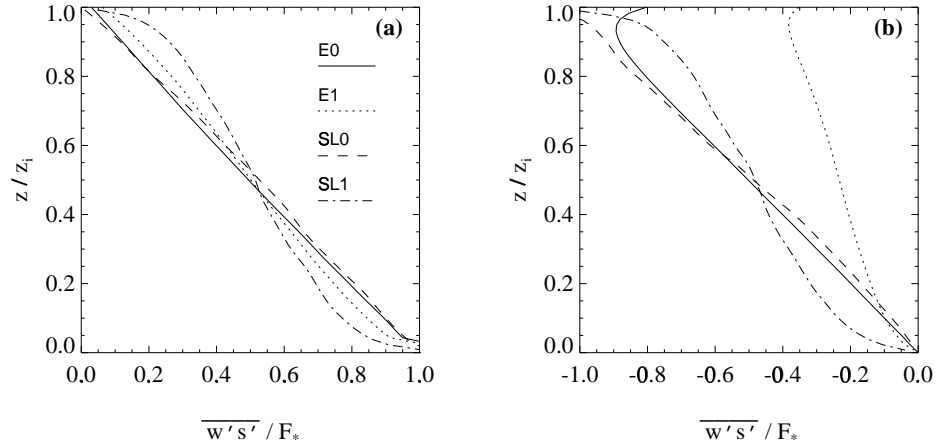


Figure 3.1: Fluxes of (a) bottom-up diffusing species BU or A and (b) top-down diffusing species TD or B.

improves the estimated flux given the LES concentration profile (not shown). Compared to the entraining CABL bottom-up and top-down transport are more symmetrical in the solid-lid CABL. This symmetry is reflected in the vertically symmetric profile of the updraft area fraction a in the solid-lid CABL (see chapter 2). Even countergradient transport occurs for the TD species in case SL0.

The chemistry cases E1 and SL1 consist of the two species A and B, denoting reactive bottom-up and top-down diffusing species, respectively. These cases are similar in the sense that both are “unmixed” cases (cf. Schumann 1989), in which species A and B have about equal concentrations (exactly equal in the solid-lid CABL case). To achieve this situation in the third hour of the entraining CABL run (see appendix E), we initialize the field of the species at $t = 0$ s with zero concentration for species A and a concentration of $7.3s_*$ below height z_{i0} and $73s_*$ above height z_{i0} for species B. Furthermore the dimensionless reaction rate k is nearly equal for the cases E1 and SL1 (see Table 3.2). The “turbulent Damköhler numbers,” defined as $Da_{t,A} \equiv k \langle B \rangle$ and $Da_{t,B} \equiv k \langle A \rangle$, are also given in Table 3.2 are close enough to each other so that one can consider the cases to be similar with respect to the chemistry, keeping as only relevant difference the type of CABL. Here both the concentrations and the reaction rate coefficient k are assumed to be dimensionless (e.g., $k = s_* t_* k'$ with k' the dimensional reaction rate coefficient). The turbulent Damköhler number is the ratio of the turbulent timescale and the the chemical destruction timescale of

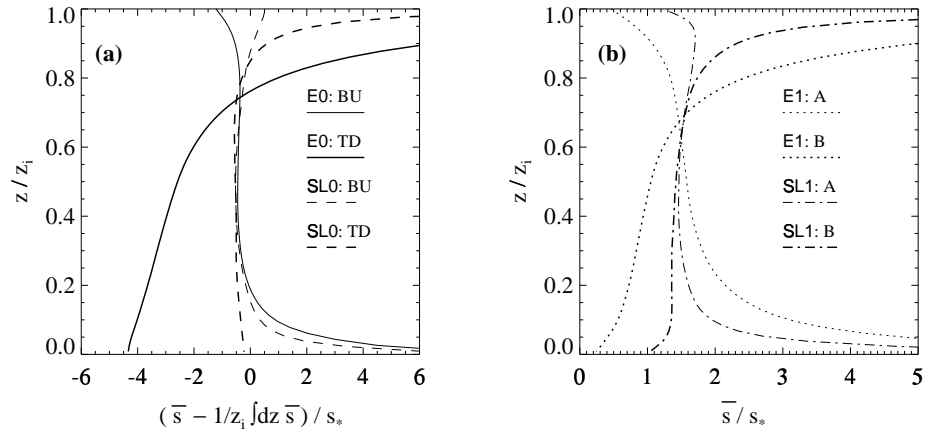


Figure 3.2: Concentrations of (a) inert bottom-up and top-down diffusing species BU and TD, (b) reactive bottom-up diffusing species A, and (c) reactive top-down diffusing species B. For the inert species the steady deviation from the bulk value is plotted as calculated by subtracting the vertically integrated (and steadily increasing) scalar concentration from the vertical profiles.

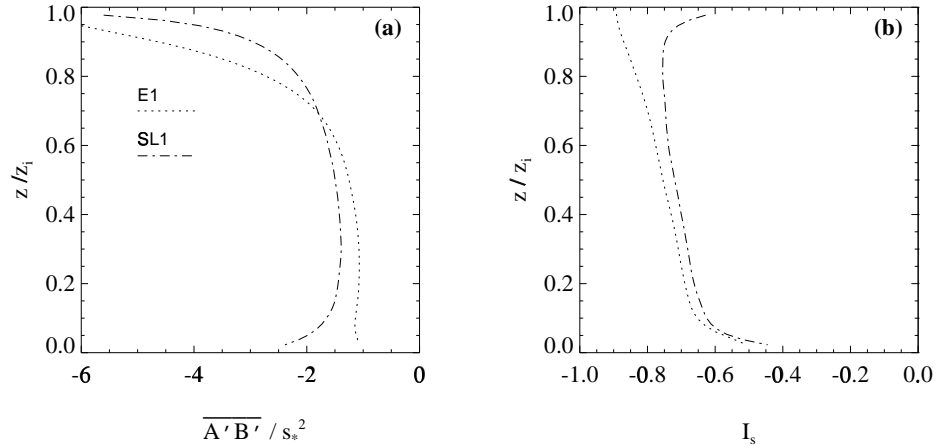


Figure 3.3: (a) Covariances of reactive bottom-up and top-down diffusing species A and B and (b) intensities of segregation for species A and B.

the species based on the boundary-layer averaged concentration—the actual ratio is given by the “effective Damköhler number” $Da_{\text{eff}} \equiv (1 + I_{s,\text{total}}) Da_t$. Since the Damköhler numbers are in the order of 1 the chemical reaction has a time scale that is comparable to the time scale of turbulent convective mixing.

There are some differences between entraining and solid-lid CABLs for the reactive cases too. Differences between cases E1 and SL1 in the nonlinearity of the flux profiles are related to differences in the profiles of the mean reaction rate at $-k(1 + I_s)\overline{A}\overline{B}$, and thus to differences in the profiles of the species concentrations and the intensity of segregation (the difference in the latter is small, as can be seen in Fig. 3.3b, discussed below). Another difference is that the entraining CABL case E1 does not show the countergradient transport for the bottom-up diffusing species found in case E0, while the solid-lid CABL case SL1 does show countergradient transport for species A (see Fig. 3.2b). The differences in the concentration profiles between the cases E1 and SL1 are due to the difference in symmetry between bottom-up and top-down transport (as was already found for the nonreactive case) and the fact that the entrainment flux in case E1 is smaller than the entrainment flux in case SL1.

The profiles of covariance and intensity of segregation are plotted in Fig. 3.3. We find that the differences between cases E1 and SL1 are relatively small. In both cases most reaction occurs near the top of the CABL (not shown; it can be checked by combining Figs.

3.3a,b and the covariances show a maximum near the CABL top. In Table 3.2 the horizontal, vertical, and total bulk intensities of segregation for the reactive cases are listed. We find a large difference between the otherwise very similar cases E1 and SL1 for the relative contributions of $I_{s,\text{hor}}$ and $I_{s,\text{vert}}$. In the solid-lid CABL the vertical bulk covariance is much smaller than in the entraining CABL. This is due to the fact that the concentration of the top-down diffusing species in the solid-lid CABL stays relatively constant in the lower CABL. The implication for large-scale atmospheric chemistry modeling of a large negative value of $I_{s,\text{vert}}$ is that the ability of large-scale models to resolve the vertical gradients of the reacting species in the CABL is also important for an accurate modeling of the boundary-layer averaged reaction rate. Comparing Fig. 3.3b to Table 3.2 we observe that $I_{s,\text{hor}}$, the contribution of the horizontal covariances to the bulk intensity of segregation, is systematically lower than the values of I_s at each height. This is due to the significant, negative contribution of $I_{s,\text{vert}}$ to the total bulk intensity of segregation.

3.4.2 Closure evaluations

The crucial parameter in the covariance parameterization is α , defined in (3.17). In the implementation of the covariance parameterization (3.13), as is described in appendix D, we effectively assume that α is constant equal to 2.6. Here we evaluate this assumption for a simple chemistry case in the entraining and solid-lid CABL. The profiles of α based on LES results are plotted in Fig. 3.4. For case SL1 α is close to the constant value of 2.6 that is used for α in this dissertation. The fact that α is higher for case E1 is due to a higher value of κ_0 for the top-down diffusing species (not shown). The higher value of κ_0 is related to the bottom-up/top-down asymmetry in the entraining CABL and was also found for the inert case E0 by Wyngaard and Moeng (1992). From Fig. 3.4 we conclude that in the surface layer and most of the mixed layer (below $z/z_i \approx 0.8$) the accuracy of the estimate $\alpha=2.6$ is about a factor of 2. The effect of entrainment on the performance of the covariance parameterization is significantly larger than the stated accuracy range around the inversion ($z/z_i \gtrsim 0.8$).

To illustrate the sort of effects associated with the covariance and flux closures, we show 1-D model results for case SL1 in Fig. 3.5. We first discuss the effects of the non-local flux term. Since for this case $\overline{w'A'}_{\text{NLI}}$ and $\overline{w'B'}_{\text{NLI}}$ are practically zero (which can be checked by inspecting the flux profiles shown in Fig. 3.1), the effect of including the nonlocal term can be attributed to the $\overline{w'A'}_{\text{NLB}}$ and $\overline{w'B'}_{\text{NLB}}$ term. We find much too large concentration gradients for both species with the no-covariance–local 1-D model version, that models only the local flux term, resulting in an erroneous bulk vertical intensity of segregation $I_{s,\text{vert}}$ —which compensates for the lack of a horizontal covariance closure in this

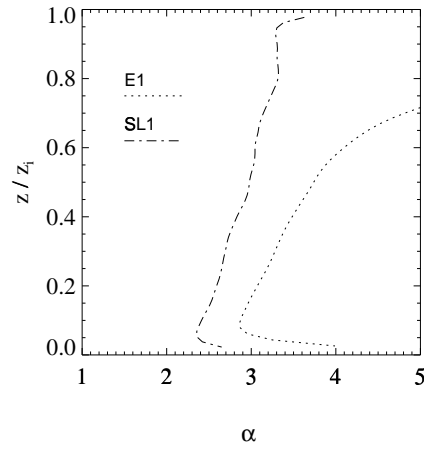


Figure 3.4: Profiles for the parameter α , as calculated directly from LES using $\alpha \equiv \frac{\overline{A'B'} \sigma_w^2}{\overline{w'A'} \overline{w'B'}}$.

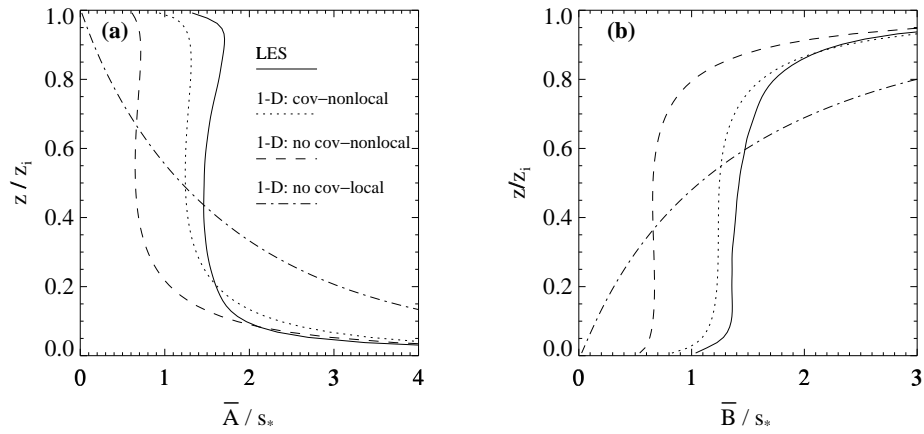


Figure 3.5: Steady-state concentrations of (a) reactive bottom-up diffusing species A and (b) reactive top-down diffusing species B in case SL1. Results are shown for LES (see also Figs. 3.2b,c) and three 1-D model versions.

1-D model version (the concentration equals $2.0s_*$, which is only 10% too high). Of course, one could choose higher values of K for which local downgradient transport alone could produce well-mixed profiles that are very close to the profiles plotted in Figs. 3.5a,b for the no-covariance–nonlocal 1-D model version. In this well-mixed limit the above-mentioned erroneous compensation disappears and a significant underestimation of the concentration results (the concentration being $1.1s_*$, 40% too low). Inclusion of the covariance closure improves the modeled concentration in the standard 1-D model version (the concentration is $1.7s_*$, only 7% too low). One could also combine the local downgradient flux closure with an unrealistic high value for K and the covariance closure to obtain this result. However, such an approach cannot model the countergradient transport as is obvious for species A in Fig. 3.5a.

3.5 Photochemistry case

3.5.1 Description and LES results

The simple chemistry case studied in the previous section is meant as an illustration of covariance and nonlocal flux effects. We here turn to the study of a photochemistry case, that is more representative for tropospheric chemistry than the case of the previous section. The bulk intensities of segregation found for a comparable photochemistry case by Krol et al. (1999) are typically small (at most a 5% decrease in reaction rate was found). Below we will study how well the concentrations and fluxes for the photochemistry case are represented by the different 1-D model versions. Although the intensities of segregation are small for this case, we mainly use it to assess the ability of our covariance closure to model the intensities of segregation, especially for reactions involving nontransported species which are locally in a chemical steady state. A satisfactory performance of the covariance closure makes it possible for future studies to use it in assessing the importance of covariances for large-scale atmospheric chemistry modeling. We also perform two sensitivity runs with the high-resolution version of the covariance–nonlocal 1-D model version under chemical conditions for which the covariance effects are expected to be larger.

The photochemical reaction scheme is a slightly simplified version of the scheme used by Krol et al. (1999) and is reproduced in Table 3.3. We will here describe the elements of importance for the current chapter. The basic O_3 -producing and -destroying reactions are included in the scheme, involving the species NO, NO_2 (in the analysis often taken together as $NO_x \equiv NO + NO_2$), CO (prescribed at a fixed concentration), and RH (a generic hydrocarbon, with an adjustable reaction rate, proportional to the parameter f : f is for the

Constant	Value	Consumed	Produced
j_1	2.7×10^{-6}	O_3	$\rightarrow 2 \text{OH} + \text{O}_2$
j_2	8.9×10^{-3}	NO_2	$\rightarrow \text{NO} + \text{O}_3$
k_1	4.75×10^{-4}	$\text{O}_3 + \text{NO}$	$\rightarrow \text{NO}_2 + \text{O}_2$
k_2	6.0×10^{-3}	$\text{OH} + \text{CO}$	$\rightarrow \text{HO}_2 + \text{CO}_2$
$k_2 \times f$	$6.0 \times 10^{-3} \times f$	$\text{OH} + \text{RH}$	$\rightarrow \text{HO}_2 + \text{products}$
k_3	2.1×10^{-1}	$\text{HO}_2 + \text{NO}$	$\rightarrow \text{OH} + \text{NO}_2$
k_4	5.0×10^{-5}	$\text{HO}_2 + \text{O}_3$	$\rightarrow \text{OH} + 2 \text{O}_2$
k_5	7.25×10^{-2}	2HO_2	$\rightarrow \text{H}_2\text{O}_2 + \text{O}_2$
k_6	2.75×10^{-1}	$\text{OH} + \text{NO}_2$	$\rightarrow \text{HNO}_3$
k_7	1.75×10^{-3}	$\text{OH} + \text{O}_3$	$\rightarrow \text{HO}_2 + \text{O}_2$

Table 3.3: Reaction scheme and constants for the photochemistry case, adapted from Krol et al. (1999). Photolysis frequencies j_1 and j_2 are given in s^{-1} . Reaction rates k_1 through k_7 are given in $\text{ppb}^{-1}\text{s}^{-1}$. The CO concentration is fixed at 100 ppb and the factor f is 100 for the standard case.

standard case taken equal to 100). Furthermore the radicals OH and HO₂ are included. Where in the LES model only OH is considered as a nontransported species, we also treat HO₂ as a nontransported species in the 1-D model. A steady-state tropical background chemistry case is studied, and both LES and 1-D models are initialized with the steady-state box model concentrations given in Table 3.4. NO and RH are emitted into the CABL from the surface. Most species undergo deposition, which is modeled using the concept of deposition velocity. The deposition flux (by definition a positive quantity) of a certain species i is given by

$$F_{d,s_i} = v_{d,s_i}(z) \overline{s_i}(z), \quad (3.23)$$

in which $v_{d,s_i}(z)$ is the height-dependent deposition velocity. In the LES study by Krol et al. (1999) the most important deposition velocities, those of O₃ and NO₂, were both taken to be 0.5 cm s^{-1} , and were physically prescribed at a height of 8 m, the center of the lowest LES model level. The fluxes at the top of the CABL are zero for all species in the photochemistry case.

The LES results for the fluxes and concentrations of the species are plotted as the solid lines in Figs. 3.6 and 3.7. The main features are the following. O₃ is chemically produced and removed from the CABL by deposition. The flux profile is linear, hence the chemical

Model	O ₃ [ppb]	NO [ppb]	NO ₂ [ppb]	RH [ppb]	HO ₂ [ppt]	OH [ppt]
Box model	78.8	0.0990	0.520	2.43	47.5	0.685
LES	78.7	0.0990	0.514	2.52	47.7	0.687
1-D: covariance–nonlocal	78.8	0.0989	0.512	2.50	47.7	0.694
1-D: no-covariance–nonlocal	78.8	0.0979	0.510	2.45	47.7	0.688
1-D: no-covariance–local	78.8	0.0977	0.509	2.51	47.8	0.696
1-D: covariance–nonlocal (high resolution)	78.8	0.0985	0.510	2.54	47.7	0.695

Table 3.4: Bulk species concentrations for the photochemistry case.

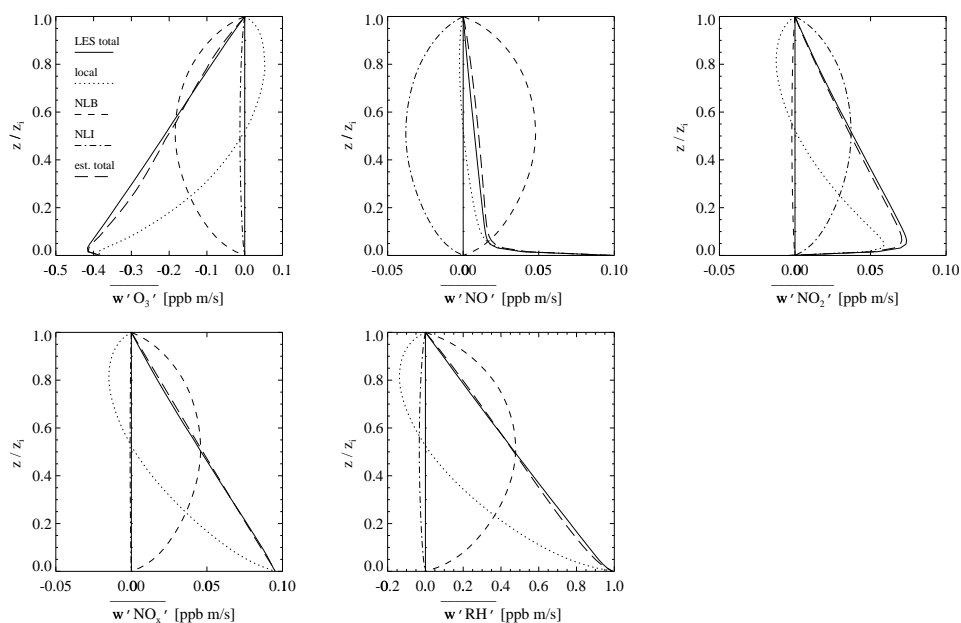


Figure 3.6: Different contributions to the total fluxes in the photochemistry case. The results are modeled with the 1-D model version “covariance–nonlocal” (standard). The LES results for the total flux are also shown.

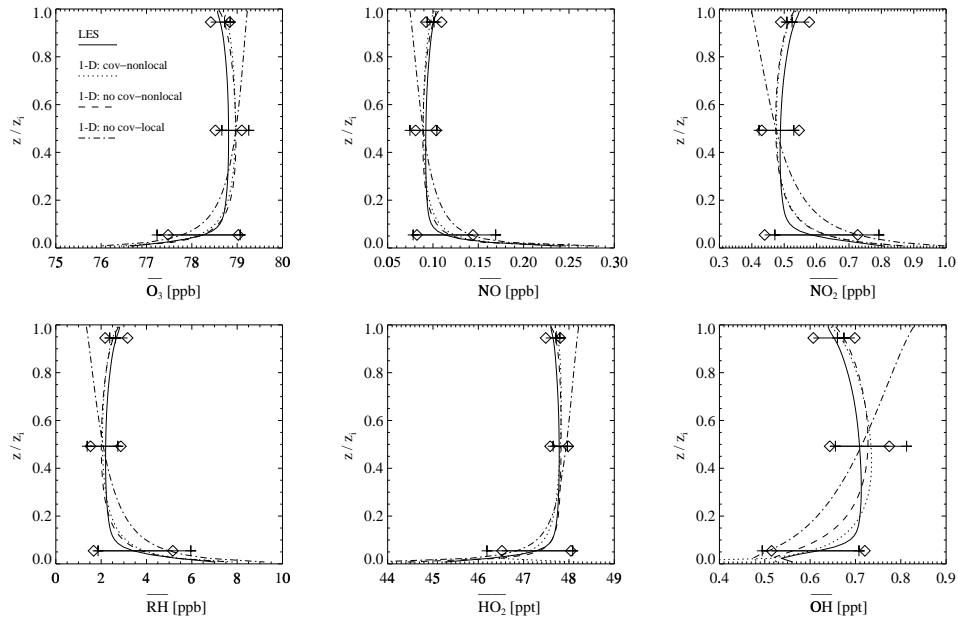


Figure 3.7: Concentrations in the photochemistry case. Results are shown for LES and three 1-D model versions. The diamonds and crosses denote the standard deviation interval at three heights for the LES and the standard 1-D model version, respectively.

Model	$I_{s,\text{OH+RH}}$ $\times 100$			$I_{s,\text{OH+NO}_2}$ $\times 100$		
	total	hor	vert	total	hor	vert
LES	-4.9	-3.5	-1.4	-2.0	-1.5	-0.5
1-D: covariance-nonlocal	-5.4	-1.7	-3.6	-2.6	-1.3	-1.3
1-D: no-covariance-nonlocal	-2.3		-2.3	-0.9		-0.9
1-D: no-covariance-local	-6.4		-6.4	-2.7		-2.7
1-D: covariance-nonlocal (high resolution)	-7.4	-4.0	-3.3	-3.0	-1.8	-1.2

Table 3.5: Bulk intensities of segregation for the photochemistry case.

production is about equal at each height in the CABL. NO is effectively transformed into NO₂ near the surface, and NO and NO₂ are in photostationary state from the top of the surface layer to the top of the CABL. The large flux divergences of NO and NO₂ near the surface are consequences of the just-mentioned fact that the chemistry is not in equilibrium near the surface. The flux profile of NO_x is linear, since the loss of NO_x through the reaction OH + NO₂ → HNO₃ is slow compared to the turbulent time scale. Also the reaction OH + RH → HO₂ (+ products) is relatively slow with respect to species RH, and therefore the flux of RH is almost linear.

From Fig. 3.7 we observe that all species are well-mixed in the CABL and have large gradients near the surface. In Table 3.5 we give the bulk intensities of segregation for two binary reactions in the photochemical scheme (chosen from the seven binary reaction since their intensities of segregation were highest). The negative vertical bulk intensities of segregation $I_{s,\text{vert}}$, which can be calculated from the concentration profiles shown in Fig. 3.7, reflect the anticorrelation of the surface-layer gradients of the species involved. For the two reactions OH + RH → HO₂ (+ products) and OH + NO₂ → HNO₃ more than 25% of the bulk intensity segregation is related to the mean vertical gradients of the species. The largest part (75%) is related to the horizontal covariances $\overline{\text{OH}'\text{RH}'}$ and $\overline{\text{OH}'\text{NO}_2}'$, respectively.

3.5.2 Closure evaluations

As a first evaluation of the covariance closure, we have plotted profiles of α based on LES results in Fig. 3.8 for all seven binary reactions. Since for all species κ_0 is fairly constant with height in the surface layer and the mixed layer, and is close to the theoretical value of 0.64 (not shown), κ_1 is the crucial parameter determining the behavior of α . We find that

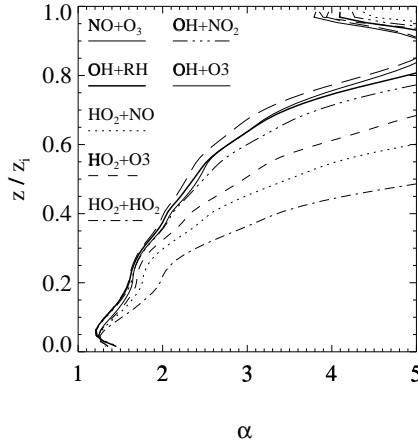


Figure 3.8: Profiles for the parameter α in the photochemistry case, as calculated directly from LES using $\alpha \equiv \overline{s'_1 s'_2} \sigma_w^2 / (\overline{w' s'_1} \overline{w' s'_2})$. The instantaneous LES 3-D fields at the end of the LES run ($t = 7200$ s) have been used.

near the surface, where the variances and covariances are largest (see also Fig. 3.7 for the variances at different heights), κ_1 is about 0.5, resulting in an α of about 1.3. Note that the bulk values of κ_1 (average of κ_1 weighed with the covariance) are at most 0.35, and therefore lie within the range reported in chapter 2. Higher up in the CABL the values of κ_1 diverge depending on whether or not HO_2 is involved in the reaction. For the reactions involving HO_2 the values of κ_1 are significantly lower than for the other reactions, as is also visible in the profiles of α in Fig. 3.8. Hence for those reactions the covariance closure is only valid within the stated uncertainty range below $z/z_i \approx 0.5$ (while for the other reactions—i.e. those not involving HO_2 —the validity extends up to $z/z_i \approx 0.8$). The most important part of the CABL for this case, however, is the surface layer since all fluxes are largest there, and on the basis of Fig. 3.8 we would therefore expect a systematic overestimation of the intensities of segregation by a factor of 2.

In Tables 3.4 and 3.5 the bulk results for concentrations and intensities of segregation are given for all three 1-D model versions. In addition to the standard 64-layer 1-D model, we also ran a model version at a higher resolution. For the high-resolution model we use the analytical profile of σ_w from Holtslag and Moeng (1991) to be able to calculate the fluxes at any height near the surface. This profile is matched with the LES profile of σ_w at height $z/z_i = 0.1$. In the high-resolution model we add 17 layers to the surface layer,

the maximum number of levels that can be added without imposing additional constraints on the time step in the model. The model levels in the surface layer are nonequidistant and the lowest model level has a depth of 1 m (compared to 16 m in the standard model). The deposition velocities in the high-resolution versions are prescribed at 50 cm, and are tuned to give the same deposition velocities at 8 m as the LES and the standard model. The most relevant deposition velocities to mention are $v_{d,O_3}(50 \text{ cm}) = 0.55 \text{ cm s}^{-1}$ and $v_{d,NO_2}(50 \text{ cm}) = 0.33 \text{ cm s}^{-1}$. Note that v_{d,NO_2} at 50 cm differs more from its value at 8 m than v_{d,O_3} . This is due to chemical reactions near the surface. The constant-flux assumption in nonreactive surface-layer similarity theory can thus not be used to calculate the deposition velocity of NO_2 at different heights.

From Table 3.4 we learn that the bulk LES concentrations are accurately reproduced (to within 1%) by the standard 1-D model version. Small differences are found if the covariance closure is not included (no-covariance–nonlocal 1-D model version): NO and NO_2 are about 1% lower and RH is 2% lower than the in the standard 1-D model version. The cause of these differences can be seen in Table 3.5, where a 2 percent point increase in magnitude of $I_{s,total}$ for the NO_x sink reaction ($OH + NO_2 \rightarrow HNO_3$) and a 3 percent point increase in magnitude of $I_{s,total}$ for the RH sink reaction ($OH + RH \rightarrow HO_2 + \text{products}$) are given. Other small differences are found if both the nonlocal flux terms and the covariance closure are excluded (no-covariance–local 1-D model version): NO and NO_2 are 1% lower (this remains the same) and RH shows no change. All differences between the no-covariance–nonlocal and no-covariance–local 1-D model versions are related to the nonlocal flux terms. The absence of these terms in the no-covariance–local 1-D model version results in higher values of $I_{s,vert}$. Compared to the standard model version the bulk $I_{s,OH+RH}$ is decreased by 1 percent point. For the bulk $I_{s,OH+NO_2}$ the increase of $I_{s,vert}$ compensates for the decrease of $I_{s,hor}$ to zero. The observed decrease of NO_x compared to the standard 1-D model version is due to a larger NO_2 deposition flux caused by the 15% higher NO_2 concentration near the surface (see Fig. 3.7). The largest bulk intensities of segregation are found with the high-resolution covariance–nonlocal version of the 1-D model (e.g., 7% for $I_{s,OH+RH}$). This is mostly due to the increased $I_{s,vert}$.

In Table 3.5 it can be seen that $I_{s,hor}$ is higher in the LES model than in the standard 1-D model version. However, from Fig. 3.8, based on the LES, we would expect that $I_{s,hor}$ in the 1-D model versions containing the covariance closure is a factor 2 higher than in the LES. The discrepancy is caused by the much lower variance of NO modeled in the lowest level of the LES, as compared to our (co-)variance closure (not shown). In the LES model used for this case no subgrid-scale covariance model is used. As a result of the higher variance of NO modeled in the standard 1-D model version, high positive values

of $I_{s,\text{OH+RH}}$ and $I_{s,\text{OH+NO}_2}$ are found in the lowest 1-D model level, which are caused by the radical cycling reaction $\text{HO}_2 + \text{NO} \rightarrow \text{OH} + \text{NO}_2$. These positive I_s values are not present in the LES. This effect results in the lower value of the horizontal bulk intensity of segregation observed for the 1-D model. Since on the other hand the vertical gradients near the surface are larger in all 1-D model versions compared to LES, the absolute value of the total bulk intensity of segregation modeled by 1-D model version I is only 14% below the LES result for $I_{s,\text{OH+RH}}$ and even 5% above the LES result for $I_{s,\text{OH+NO}_2}$. The high-resolution model results compare much better to the LES with respect to the horizontal bulk intensity of segregation, but they show an even higher vertical bulk intensity of segregation than for the standard 1-D model version, resulting in an overestimation with more than 35% of $I_{s,\text{total}}$, as compared to LES.

It must be clear from the significant influence of vertical resolution near the surface that the LES model cannot be said to be more accurate than the high-resolution 1-D model version. The applicability of LES to processes occurring very close to the surface is problematic. Besides the too low vertical resolution to resolve these processes there are some other inaccuracies in the results near the surface of the LES model version used for this case (for some characteristics of this model version see appendix E). For example, the simulated flux–gradient relationship deviates from similarity theory since a constant subgrid diffusivity is used. Furthermore the free-slip boundary condition gives different fluid dynamical patterns close to the surface than the more realistic no-slip boundary condition that was used for the LES simulation of the other cases studied in this chapter. However, the difference between free-slip and no-slip boundary conditions will have only a minor quantitative effect on the boundary-layer averaged properties, since we are dealing with free convection here (see appendix E).

Finally, we evaluate the nonlocal flux closure. For the standard 1-D model version we have plotted the flux decomposition (3.22) in Fig. 3.6. The LES flux profiles of all species are accurately reproduced by the total of the different flux terms. The linearity of the flux profiles of O_3 , NO_x , and RH is reflected in a small $\overline{w's'_{i\text{NLI}}}$ term for these species. The $\overline{w's'_{i\text{NLI}}}$ term is large for the individual species NO and NO_2 , however. The $\overline{w's'_{i\text{NLI}}}$ term is needed to complement the $\overline{w's'_{i\text{NLB}}}$ term for species NO and NO_2 . Still, a run with the no-covariance–nonlocal 1-D model version without $\overline{w's'_{i\text{NLI}}}$ term models virtually the same concentration profiles as the no-covariance–nonlocal 1-D model version with $\overline{w's'_{i\text{NLI}}}$ (not shown). This can be explained by the fact that in most of the CABL NO and NO_2 are in a photostationary state and therefore $\overline{w'\text{NO}'_{\text{NLI}}} \approx -\overline{w'\text{NO}_2'_{\text{NLI}}}$. So even if the flux profiles for NO and NO_2 would be completely wrong, this would have no effect on the concentration profiles if the flux profile of NO_x is correct. From Fig. 3.7 we conclude that the profiles of

Sensitivity run	Parameter variation	$I_{s,OH+RH}$ ×100	$I_{s,OH+NO_2}$ ×100	O ₃ [ppb]	NO _x [ppb]	RH [ppb]
Steady	$f = 300$ (rate coefficient increased by factor 3)	−40 (−28)	−8.4 (−5.9)	78.7 {78.8}	0.608 {0.605}	1.30 {0.97}
	NO emission flux increased by factor 10 to 1 ppb m/s	−15 (−9.0)	−11 (−6.8)	77.3 {77.9}	3.07 {2.99}	2.57 {2.36}

Table 3.6: Results for the steady and nonsteady sensitivity runs with the standard 1-D model version at high resolution. The instantaneous values at $t = 6600$ s or at $t = 3600$ s are given for the respective sensitivity runs. In brackets the horizontal bulk intensities of segregation are given. The concentrations modeled with the no-covariance–nonlocal 1-D model version are also given in parentheses.

all species are accurately modeled by the 1-D model versions that include the nonlocal flux term. The no-covariance–local 1-D model version, which only has local downgradient transport, models too large gradients in the bulk of the CABL. The variances obtained from the (co-)variance closure, and shown at three heights in Fig. 3.7, agree well with the LES values at the heights $z/z_i = 0.05$ and $z/z_i = 0.5$. At $z/z_i = 0.95$ the modeled variances are too small, since κ_1 for the variances is much smaller than 0.25 at that height (not shown).

3.5.3 Sensitivity runs

We use the high-resolution covariance–nonlocal 1-D model version to perform two sensitivity runs for different chemical conditions. In the first run the reaction rate coefficient of the OH + RH reaction is increased by a factor of 3 (by setting $f = 300$, coming closer to the reaction rate coefficient for the OH + isoprene reaction, for which $f = 440$). This first run is done in steady state: first the steady-state box concentrations are calculated before the model is run. The second run is a nonsteady case where, starting with the steady-state box concentrations of the reference photochemical case, suddenly the NO emission is increased by a factor of 10.

In Table 3.6 the results for the sensitivity runs are given. For both runs the largest effect of the covariance parameterization on the concentrations is found for RH (an increase of

more than 30% for the steady run and nearly 10% for the nonsteady run). These effects can be completely attributed to the $I_{s,\text{hor}}$ for the OH + RH reaction. Results for the steady sensitivity run are also available for the LES model: in the LES model an $I_{s,\text{total}}$ of 27% is found, where we find 40% with the 1-D model. Note that we used the high-resolution version of the 1-D model, so the $I_{s,\text{vert}}$ modeled by the 1-D model is larger than that modeled by the LES model. In the nonsteady run also the NO_x budget is influenced (3% higher NO_x concentrations after 1 hour), mainly due to the $I_{s,\text{hor}}$ of nearly 7% for the OH+ NO_2 reaction. Also O_3 is a little influenced (1% lower concentrations after 1 hour).

From these sensitivity runs we conclude that the budgets of RH and NO_x can be significantly influenced by the covariance parameterization, but that the influence on O_3 is relatively small. This hypothesis remains to be tested for different chemical and meteorological conditions, for instance in a large-scale model.

3.6 Summary and discussion

In this chapter we propose and evaluate a new first-order closure for covariances of reactive species in the convective atmospheric boundary layer. Also a closure for fluxes, that has been introduced and evaluated for passive scalars in a variety of convective boundary layers by Cuijpers and Holtslag (1998), is evaluated here for reactive species. The covariance closure is based on mass-flux considerations and is shown to have an accuracy of about a factor of 2. This conclusion has been established using LES results for nearly all LES cases with reactive species that are currently in the literature. As shown in this chapter the concentration profiles modeled with a 1-D model improve when the covariance closure is used.

By extending our analysis from the solid-lid CABL to the entraining CABL in this chapter, we have found that the covariance closure is valid for the surface layer and (lower) mixed layer, but does not perform well in and just below the inversion. Wang and Stevens (1999) showed that this can be understood from the presence of a large variability in the coherent structures that can be identified in the flow, near the top of the CABL, which leads to a much lower top-hat contribution to the total covariance. It is not clear how problematic this breakdown near the inversion is for atmospheric chemistry applications. For instance in the photochemistry case we found that the covariances are most important near the surface, where the closure works fine. However, we only used an LES of the solid-lid CABL for this case and prescribed zero fluxes at the top of the CABL. In an entraining CABL with nonzero entrainment fluxes of chemical species one can imagine chemistry cases for which the covariance around the top of the CABL plays a major role. However, in the real atmo-

sphere it appears unlikely for a top-down diffusing species to have a concentration above the inversion that is much higher than below. But this situation cannot be excluded and more research is needed to assess this problem.

We have only dealt with the convective boundary layer. Since we tested the covariance closure with and without shear, and since Businger and Oncley (1990) showed that the mass-flux approximation for the flux works for all stabilities in the surface layer, we expect that the covariance closure will also work for neutral and stable conditions. For the stable boundary layer one should note that in large-scale atmospheric chemistry models grid-box averaged “vertical” bulk covariances (defined in section 3.2), which are due to a too low vertical resolution to resolve the vertical gradients of the concentrations, are much more important than horizontal covariances (Galmarini et al. 1997b).

We have not touched in detail on the chemical higher-order moments that appear in higher-order flux closures. From the fact that both concentrations and fluxes of the transported species are modeled adequately with the nonlocal flux closure, we conclude that an explicit treatment of these chemical higher-order moments within the context of higher-order closure modeling is not needed in the photochemistry case. Further research on this topic is required to establish that this is also the case for other chemical and meteorological conditions.

Finally, by way of a sensitivity study we have shown that covariances might have an impact on hydrocarbon and NO_x budgets. The proposed covariance parameterization can be used to assess the large-scale impact of covariances on atmospheric chemistry. However, since the number of situations for which the parameterization has been tested is limited, it should be used with care.

Chapter 4

The impact of chemistry on flux estimates in the convective boundary layer*

*The material contained in this chapter has been submitted for publication in *Journal of the Atmospheric Sciences*.

Abstract

Different flux closures are studied for two chemistry cases in the convective boundary layer; a simple chemistry case and a photochemistry case. The cases are simulated using large-eddy simulation. We decompose the flux modelled by higher-order closures into two parts, one independent and the other dependent of chemical higher-order moments. The contribution of the part related to chemical higher-order moments depends on the complexity of the flux closure. This contribution is found to be largest for a second-order closure that contains a scalar–temperature covariance term in the flux budget equation. A simplified second-order closure and a mass-flux closure are shown to be equivalent. For these closures a smaller contribution of chemical higher-moments is found. The error made by applying flux–profile relationships from nonreactive surface-layer similarity theory is smallest, especially near the top of the surface layer. For realistic applications it is expected that the errors for first-order closure associated with modified flux–profile relationships in the surface layer are negligible.

4.1 Introduction

The fluxes of nonreacting scalars near the surface can be described by local K theory. For chemically reacting species, however, the flux–gradient relationships are modified due to chemical reactions. The question is how large the impact of chemistry is on different flux estimates, not only in the surface layer but in the whole boundary layer. In this chapter we will deal with this question for the convective atmospheric boundary layer (CABL).

The effects of chemistry on the fluxes of reactive species are twofold. First, the flux budget is dependent on the profile of mean concentrations (which is affected by the chemistry through the concentration budget). Second, the flux budget (and budgets of all other higher-order moments that contain species concentrations), includes higher-order moment terms related to the chemistry. In this study we aim to present an exact decomposition of the flux budget and we examine the chemical higher-order moment contribution to the flux.

When applied to higher-order flux closures the decomposition leads to different outcomes for different higher-order closures. The typical approach that has been followed to determine the chemical higher-moment contribution is by way of second-order closure modelling (e.g., Fitzjarrald and Lenschow 1983). The purpose of this chapter is to evaluate and compare different formulations for the chemical higher-moment contribution to the flux using large-eddy simulation (LES) of two different chemistry cases in the CABL, a simple chemistry case and a more representative case for atmospheric chemistry. In this evaluation we will compare different higher-order closure estimates, some given by a second-order closure (e.g., Verver et al. 1997) and others based on a mass-flux closure (e.g., chapter 2 of this dissertation; de Roode et al. 1999). In addition we calculate the error made in first-order closure flux estimates near the surface, that are based on the assumption that the flux–profile relationships of surface-layer similarity theory are also valid for reactive cases.

4.2 Theory

The flux budget equation for a chemical species s_i , assuming horizontal homogeneity and $\overline{w} = 0$, reads

$$\frac{\partial \overline{w's'_i}}{\partial t} = -\overline{w'^2} \frac{\partial \overline{s_i}}{\partial z} + \frac{g}{\theta_{v,r}} \overline{\theta'_v s'_i} - \frac{\partial \overline{w'^2 s'_i}}{\partial z} - \frac{1}{\rho_r} \overline{s'_i \frac{\partial p'}{\partial z}} + R_{ws_i}, \quad (4.1)$$

where θ_v is the virtual potential temperature, p is the pressure, $\theta_{v,r}$ and ρ_r are the reference virtual potential temperature and density, respectively, and R_{ws_i} is a term containing chemical reaction rate coefficients (R_{ws_i} will be specified below). The overbar denotes horizontal averages and the primed quantities are deviations from the averages. Following Verver et al. (1997), we decompose the flux into two parts

$$\overline{w's'_i} = \left(\overline{w's'_i}\right)_1 + \left(\overline{w's'_i}\right)_2, \quad (4.2)$$

where the first part $\left(\overline{w's'_i}\right)_1$ is defined as the part that does not include the effect of chemical higher-order moments and the second part $\left(\overline{w's'_i}\right)_2$ as the part that solely contains the effect of the chemical higher-order moments. Compared to Verver et al. (1997) we will generalize the decomposition to any flux closure (of any statistical order). Furthermore, we have changed the labels “inert” and “chem” to “1” and “2”, respectively, to avoid confusion. In the inert case $\left(\overline{w's'_i}\right)_2$ equals zero (for a first-order closure it also equals zero in the reactive case, since no higher-order moments are involved in the flux estimate, by definition). The first part $\left(\overline{w's'_i}\right)_1$ is affected by chemical reactions through the concentration profile $\overline{s_i}$, which is determined by the concentration budget equation,

$$\frac{\partial \overline{s_i}}{\partial t} = -\frac{\partial \overline{w's'_i}}{\partial z} + R_{s_i}. \quad (4.3)$$

The term R_{s_i} represents chemical sources and sinks—note that R_{s_i} can also contain higher-order moments: covariances (these will not be explicitly considered here).

We make decomposition (4.2) explicit here by writing:

$$\frac{\partial \left(\overline{w's'_i}\right)_1}{\partial t} = -\overline{w'^2} \frac{\partial \overline{s_i}}{\partial z} + \frac{g}{\theta_{v,r}} \left(\overline{\theta'_v s'_i}\right)_1 - \frac{\partial \left(\overline{w'^2 s'_i}\right)_1}{\partial z} - \frac{1}{\rho_r} \left(\overline{s'_i \frac{\partial p'}{\partial z}}\right)_1 \quad (4.4)$$

$$\frac{\partial \left(\overline{w's'_i}\right)_2}{\partial t} = \frac{g}{\theta_{v,r}} \left(\overline{\theta'_v s'_i}\right)_2 - \frac{\partial \left(\overline{w'^2 s'_i}\right)_2}{\partial z} - \frac{1}{\rho_r} \left(\overline{s'_i \frac{\partial p'}{\partial z}}\right)_2 + R_{ws_i}, \quad (4.5)$$

and similarly for all other higher-order moments appearing in (4.4) and (4.5). Eqs. (4.4) and (4.5) are coupled through the mean concentration budget (4.3), which contains the total flux $\overline{(w's'_i)_1} + \overline{(w's'_i)_2}$, and the chemical term in (4.5)—specified below for second-order closure—which contains fluxes and concentrations of different species. Eqs. (4.4) and (4.5) and similar equations for other higher-order moments have to be closed retaining only terms up to a certain statistical order. We will consider second-order closure and mass-flux closure here.

4.3 Second-order closure formulation

Nearly all second-order closure models that include contributions of chemical higher-order moments to the flux that are currently in the literature, are essentially the same as the one described by Fitzjarrald and Lenschow (1983). This includes the formulations given by Gao et al. (1991), Hamba (1993), Sykes et al. (1994), Gao and Wesely (1994), Vilà-Guerau de Arellano et al. (1995), Galmarini et al. (1997a), and Verver et al. (1997). The studies by Fitzjarrald and Lenschow (1983), Gao et al. (1991), Vilà-Guerau de Arellano et al. (1995), and Galmarini et al. (1997a) were limited to the surface layer. Gao et al. (1991) considered only neutral conditions, where the other surface-layer studies considered all stabilities. Hamba (1993), Sykes et al. (1994), and Verver et al. (1997) studied the convective boundary layer. Where Hamba (1993) neglected the contribution of the chemical higher-moment term $R_{\theta s_i}$ to the $\overline{\theta'_v s'_i}$ budget (as criticized by Verver 1994), this term was taken into account by Sykes et al. (1994) and Verver et al. (1997). Gao and Wesely (1994) studied only the neutral boundary layer. Of all the above-mentioned authors only Sykes et al. (1994) and Verver et al. (1997) considered the contributions of chemical third-order moments in R_{ws_i} and $R_{\theta s_i}$.

We here present and generalize the formula for the chemical part of the flux given earlier by Verver et al. (1997). Like is done in all other second-order closure models that include chemistry, Verver et al. (1997) neglected the chemical higher-moment contributions to the budgets of the turbulent transport term $\partial w'^2 s'_i / \partial z$ and of the concentration–pressure covariance term $1/\rho_r \overline{s'_i \partial p' / \partial z}$. For the contribution of chemical higher-order moments to the flux the following formulation is derived:

$$\overline{(w's'_i)_2} = \tau_1 R_{ws_i} + \tau_1 \tau_4 \frac{g}{\theta_{v,r}} (1 - b_1) R_{\theta s_i}. \quad (4.6)$$

The local time scales τ_1 and τ_4 are defined by $\tau_1 = \tau_{\text{TKE}}/a_1$ and $\tau_4 = \tau_{\text{TKE}}/a_4$, where $\tau_{\text{TKE}} \equiv 1/a_{\text{TKE}} l/\sigma_w$; a_{TKE} , a_1 , a_4 , and b_1 are constants. The rms of the vertical velocity fluctuations is denoted by σ_w . The length scale in τ_{TKE} is taken as $l = \kappa z(1 - z/z_i)$, where

z_i is the CABL height and κ is the von Kármán constant. The closure constants have the following values: $a_{\text{TKE}} = 0.1$, $a_1 = 4.84$, $a_4 = 2.5$, and $b_1 = 0.4$.

For an irreversible, binary reaction between species A and B the terms R_{ws_i} and $R_{\theta s_i}$ are given by

$$R_{wA} = R_{wB} = -k \left(\overline{A w' B'} + \overline{B w' A'} + \overline{w' A' B'} \right) \quad (4.7)$$

$$R_{\theta A} = R_{\theta B} = -k \left(\overline{A \theta'_v B'} + \overline{B \theta'_v A'} + \overline{\theta'_v A' B'} \right). \quad (4.8)$$

Expressions (4.7) and (4.8) can be generalized for arbitrary chemistry. The term R_{ws_i} is then given by

$$R_{ws_i} = \sum_{m=1}^M \eta_{im} k_m \overline{w' \prod_{n=1}^N (\overline{s_n} + s'_n)^{\beta_{nm}}}. \quad (4.9)$$

Here the compact form of Vilà-Guerau and Lelieveld (1998) is used, which is based on the notation of Lamb and Seinfeld (1973): η_{im} is the stoichiometric coefficient for species i in reaction m , k_m is the reaction rate coefficient for reaction m , and β_{nm} is the reaction order of species n in reaction m . M is the total number of reactions and N is the total number of species. Analogous to (4.9) we write for $R_{\theta s_i}$

$$R_{\theta s_i} = \sum_{m=1}^M \eta_{im} k_m \overline{\theta'_v \prod_{n=1}^N (\overline{s_n} + s'_n)^{\beta_{nm}}}. \quad (4.10)$$

4.4 Mass-flux closure formulation

For comparison with the previous approach we present another formulation for $\overline{(w' s'_i)^2}$, valid for mass-flux closures. Mass-flux closures (e.g., Chatfield and Brost 1987; Randall et al. 1992; chapter 2 of this dissertation; de Roode et al. 1999) are higher-order closure schemes in the sense that they effectively contain a prognostic equation for the flux (a second-order moment) besides a prognostic equation for the concentration of a species, provided that we consider a dynamically steady state. The prognostic flux equation can be derived from the updraft and downdraft species budget equations and reads

$$\frac{\partial \overline{w' s'_i}}{\partial t} = \frac{(M/\rho)}{\kappa_{ws}} \left(\frac{\partial \overline{s_i^u}}{\partial t} - \frac{\partial \overline{s_i^d}}{\partial t} \right), \quad (4.11)$$

where $M = \rho a(\overline{w^u} - \overline{w})$ is the convective mass flux, with a the updraft area fraction, $\overline{w^u}$ the updraft velocity, and \overline{w} the mean vertical velocity; κ_{ws} is the fractional top-hat contribution to the total flux, which can vary with height and with the different species, but is here taken constant to its theoretical Gaussian value of 0.64 (Wyngaard and Moeng 1992). The indices u and d indicate the averaging areas of updrafts and downdrafts, respectively.

Following de Roode et al. (1999) we arrive at a mass-flux estimate of the first part of the flux:

$$\left(\overline{w's'_i}\right)_1 = -\frac{(M/\rho)^2/\kappa_{ws}}{(1-a)(E/\rho) + a(D/\rho)} \left\{ \frac{\partial \overline{s_i}}{\partial z} + (1-2a) \frac{\partial (\overline{s^u} - \overline{s^d})}{\partial z} - (\overline{s^u} - \overline{s^d}) \frac{\partial a}{\partial z} \right\}, \quad (4.12)$$

where E and D are lateral entrainment and detrainment rates. Two separate terms containing contributions from the subplume fluxes have been left out for the sake of readability (they can be found in de Roode et al. 1999). The difference with the expression obtained by de Roode et al. (1999) is the presence of the factor κ_{ws}^{-1} in (4.12) to arrive at the real flux—de Roode et al. (1999) only give the top-hat approximation for the flux (cf. chapter 2). If we take chemical reactions in updrafts and downdrafts into account, the chemical higher-moment contribution to the flux becomes (de Roode et al. 1999):

$$\left(\overline{w's'_i}\right)_2 = \frac{2a(1-a)(M/\rho)/\kappa_{ws}}{(E/\rho) + (D/\rho)} \left\{ (R_{s_i})_u + (R_{s_i})_{u,\text{subplume}} - (R_{s_i})_d - (R_{s_i})_{d,\text{subplume}} \right\}, \quad (4.13)$$

where again the factor κ_{ws}^{-1} has been added. We have added subplume terms in (4.13), which refer to subplume covariances that affect the plume-mean reaction rates (see chapter 2).

If we assume that the vertical velocity skewness is zero (hence that $a = 0.5$) and that the subplume fluxes in updraft and downdraft are equal (cf. chapter 2), the total flux can be written as

$$\overline{w's'_i} = -K \frac{\partial \overline{s_i}}{\partial z} + \left(\overline{w's'_i}\right)_2, \quad (4.14)$$

with

$$\left(\overline{w's'_i}\right)_2 = \frac{K}{4(M/\rho)} \left[\left\{ (R_{s_i})_u + (R_{s_i})_{u,\text{subplume}} \right\} - \left\{ (R_{s_i})_d + (R_{s_i})_{d,\text{subplume}} \right\} \right]. \quad (4.15)$$

Here we have defined the apparent diffusivity K as

$$K = \frac{2(M/\rho)^2/\kappa_{ws}}{(E/\rho) + (D/\rho)}. \quad (4.16)$$

Since one often writes $K = c_k \sigma_w L$ (with L a length scale and c_k a constant), and assuming $(M/\rho) = \frac{1}{2} \sqrt{\kappa_{ww}} \sigma_w$ (appendix C) and $\kappa_{ws} = \kappa_{ww} = 0.64$ (denoted in the following by κ_0), the chemical part of the flux becomes

$$\left(\overline{w's'_i}\right)_2 = \frac{c_k L}{2\sqrt{\kappa_0}} \left\{ (R_{s_i})_u + (R_{s_i})_{u,\text{subplume}} - (R_{s_i})_d - (R_{s_i})_{d,\text{subplume}} \right\}. \quad (4.17)$$

For an irreversible, binary reaction between species A and B the chemical sink terms read

$$(R_A)_u = (R_B)_u = -k \overline{A^u} \overline{B^u} \quad (4.18)$$

$$(R_A)_d = (R_B)_d = -k \overline{A^d} \overline{B^d} \quad (4.19)$$

$$(R_A)_{u,\text{subplume}} = (R_B)_{u,\text{subplume}} = -k \overline{A'B'^u} \equiv -k \overline{(A - \overline{A^u})(B - \overline{B^u})} \quad (4.20)$$

$$(R_A)_{d,\text{subplume}} = (R_B)_{d,\text{subplume}} = -k \overline{A'B'^d} \equiv -k \overline{(A - \overline{A^d})(B - \overline{B^d})} \quad (4.21)$$

We can simplify (4.17), first again considering the simple chemistry case, by neglecting the subplume covariances. We then have

$$\begin{aligned} \left(\overline{w'A'}\right)_2 &= \left(\overline{w'B'}\right)_2 \\ &= \frac{c_k L}{2\sqrt{\kappa_0}} (-k) \left\{ \left(\overline{A} + \frac{2(1-a)\sqrt{\kappa_0}}{\sigma_w} \overline{w'A'} \right) \left(\overline{B} + \frac{2(1-a)\sqrt{\kappa_0}}{\sigma_w} \overline{w'B'} \right) \right. \\ &\quad \left. - \left(\overline{A} - \frac{2a\sqrt{\kappa_0}}{\sigma_w} \overline{w'A'} \right) \left(\overline{B} - \frac{2a\sqrt{\kappa_0}}{\sigma_w} \overline{w'B'} \right) \right\} \\ &= \frac{c_k L}{\sigma_w} (-k) \left(\overline{A} \overline{w'B'} + \overline{B} \overline{w'A'} \right). \end{aligned} \quad (4.22)$$

Generalizing (4.22), we write

$$\left(\overline{w's'_i}\right)_2 = \frac{c_k L}{\sigma_w} (R_{ws_i})_{\text{no 3rd}}, \quad (4.23)$$

with $(R_{ws_i})_{\text{no 3rd}}$ given by (4.9) except for the third moments. Eq. (4.23) has the same form as the first term in (4.6). The time scale $\tau_{\text{MF}} = c_k L / \sigma_w$ replaces τ_1 . The length scale L is here taken proportional to the length scale l used by Verver et al. (1997)—we take $L = c_l z (1 - z/z_1)$ with $c_l = 1.8$, as was used in chapter 3. The ratio $L/l = 4.5$, which leads

to $\tau_{\text{MF}}/\tau_1 = 0.87$. So the time scale that we use in the mass-flux closure formula differs only 13% from that used in the second-order closure formula.

Since we ultimately arrive at similar expressions for the mass-flux closure and the simplified second-order closure (neglecting the third moments and assuming $b_1 = 1$), we have shown that both closures are essentially equivalent under the simplifications mentioned. Therefore, we can attach a simple physical picture to the chemical higher-moment contribution to the flux of a certain species: according to (4.13) it is determined by the difference between the net chemical reaction rates in updraft and downdraft.

4.5 Intercomparison of formulations using LES

4.5.1 Description of cases

Two LES cases are used here to investigate differences in $(\overline{w's'_i})_2$ and to determine the residual error when nonreactive flux–profile relationships in the surface layer are applied. The cases considered are an artificially simple chemistry case and a photochemistry case. For the simple chemistry case we simulate an entraining CABL. Two species are involved that react away by the reaction $A+B \rightarrow C$. Species A is injected at the surface and species B is entrained at the top of the CABL. A nearly steady state is attained during the simulation. The simple chemistry case is a “mixed” case (cf. Schumann 1989), with a much higher concentration of species B. The surface flux of species A is denoted by F_\star . A concentration scale s_\star can be derived from F_\star by putting $s_\star = F_\star/w_\star$, with w_\star the convective velocity scale. The LES model and the simulated CABL are described in chapter 3. Averaging takes place over the third hour of the LES run.

For the simple chemistry case, the convective velocity scale $w_\star = 1.1$ m/s, and the CABL height $z_i = 720$ m. The associated time scale $t_\star \equiv z_i/w_\star = 650$ s. The dimensional reaction rate coefficient, denoted by k' , can be made dimensionless in the following way: $k = s_\star t_\star k'$. We put k equal to 0.39. Species A is initialized with zero concentration and species B has a concentration of $22s_\star$ below height z_{i0} and $220s_\star$ above this height (z_{i0} is the initial inversion height, equal to 680 m). During the averaging interval the flux of species B at height z_i is about $-1.2F_\star$. The concentrations of species A and B are $0.14s_\star$ and $27s_\star$, respectively. As a result of the relatively high concentration of species B the “turbulent Damköhler number” for species A, defined as $\text{Da}_{t,A} \equiv k \langle B \rangle$ (the brackets denote an average over the CABL), is 11, which means that the chemical lifetime of species A is very short compared to the turbulent mixing time. Therefore the flux profile $\overline{w'A'}(z)$, as shown in Fig. 4.1, is strongly nonlinear, decreasing to less than $0.15F_\star$ at the top of the surface layer (z/z_i

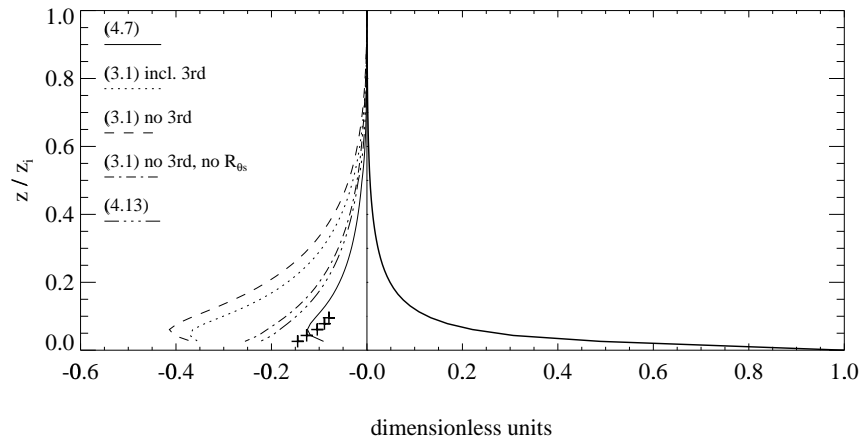


Figure 4.1: Contribution of chemical higher-order moments to the flux for species A and B in the simple chemistry case, estimated by five formulations, and total flux (thick solid line). The crosses denote the residual error when the flux–profiles relationships of surface-layer similarity theory are applied. Averages over the third hour of the LES run have been used.

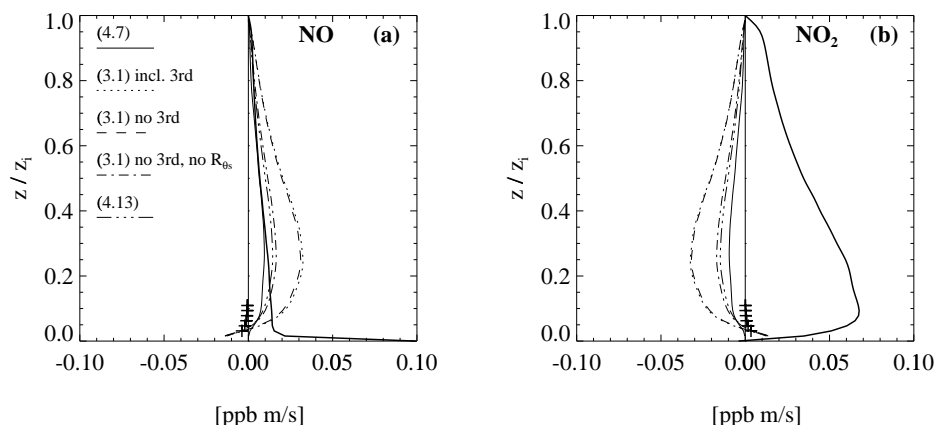


Figure 4.2: Contribution of chemical higher-order moments to the flux for species (a) NO and (b) NO₂ in the photochemistry case, estimated by five different formulations, and total flux (thick solid line). The crosses denote the residual error when the flux–profiles relationships of surface-layer similarity theory are applied. Instantaneous values at the end of the 2-hour LES run have been used—except for the surface-layer similarity theory errors—since for many of the needed quantities averages were not available.

= 0.1).

In the photochemistry case, comparable to the case studied by Krol et al. (1999), a solid-lid CABL is simulated. The case was studied and described in chapter 3. The convective velocity scale for this case is $w_* = 1.5$ m/s and the boundary-layer height $z_i = 1000$ m. More details on the LES model, the simulated CABL, and the chemistry case are described in these sources. Here we will discuss only a few aspects of the case. The photochemical scheme consists of 10 reactions involving 6 modelled species (O₃, NO, NO₂, RH, HO₂, and OH). The species RH is a generic hydrocarbon. The basic O₃-producing and -destroying reactions are included in the scheme. Species NO is emitted with a surface flux of 0.1 ppb m/s and is quickly transformed to NO₂ in the surface layer. This is obvious from the large flux divergences in the surface layer (see Figs. 4.2a and 4.2b). Higher-up in the CABL NO and NO₂ reach a photostationary state with the photolysis reaction $\text{NO}_2 + \text{light} \xrightarrow{\text{O}_2} \text{NO} + \text{O}_3$ being balanced by the reaction $\text{NO} + \text{O}_3 \rightarrow \text{NO}_2 + \text{O}_2$ (both reactions have time scales of minutes).

4.5.2 Results

In order to intercompare the different formulations given above for $\overline{(w's'_i)}_2$ —(4.6), (4.17), and (4.23)—we substitute in these formulations the LES profiles of all quantities that appear in them, except for the length scales (and of course the constants). The resulting profiles of $\overline{(w's'_i)}_2$ for the simple chemistry case are plotted in Fig. 4.1, and for the photochemistry case in Figs. 4.2a (species NO) and 4.2b (species NO₂). For the formula based on the second-order closure scheme (4.6) we also show the profiles of $\overline{(w's'_i)}_2$ for which either the third-order moments in R_{ws_i} and $R_{\theta s_i}$ are neglected or the whole term containing $R_{\theta s_i}$ and the third-order moments in $R_{\theta s_i}$ are neglected. Furthermore surface-layer flux residues for application of nonreactive flux–profile relationships are shown. The method to determine these residues consists of first calculating $K_{\text{inert}} = -\overline{w'BU'}/(\partial\overline{BU}/\partial z)$ from an inert bottom-up diffusing scalar, and subtracting an inert part based on this K_{inert} from the total flux of the reactive species:

$$\overline{(w's'_i)}_{\text{residue}} = \overline{w's'_i} - K_{\text{inert}} \frac{\partial \overline{s_i}}{\partial z}. \quad (4.24)$$

In the simple chemistry case all estimates of the chemical part of the flux give large values compared to the total flux throughout the whole CABL, both where the fluxes are large (near the surface) and where the fluxes are small (in the top half of the CABL). In the photochemistry case all estimates of the chemical part of the NO flux are small where the total flux is large (near the surface) and large where the total flux is small (around the middle of the CABL and higher-up). For NO₂ the situation is comparable but somewhat less pronounced.

In both cases we see a consistent grouping of results into two groups, which leads to the following conclusions. Regarding the first group, the second-order closure of Verver et al. (1997) gives the largest values of $\overline{(w's'_i)}_2$. The impact of third-order moments in (4.6) is small. And regarding the second group, a simplified version of the second-order closure—equivalent to mass-flux closure formulation (4.23)—gives significantly smaller values for $\overline{(w's'_i)}_2$. The results lie also close to mass-flux closure formulation (4.17), leading to the conclusion that the difference between updraft and downdraft subplume covariance is small and the approximating steps to arrive at (4.23) are valid.

The residual error identified in the surface layer when using nonreactive flux–profile relationships tends to be smaller than the different corrections $\overline{(w's'_i)}_2$ estimated by the higher-order closure schemes, especially near the top of the surface layer. Although $\overline{(w's'_i)}_2$ and the residual error for first-order closure are different quantities, we do want to point at the fact that the chemical corrections needed on the flux are smaller in first-order closure

than in the full second-order closure.

One should note that we here prescribed most profiles in the evaluation of the higher-order closures. If we let the higher-order closures themselves model all profiles other differences can be found. For instance, in addition to the cases studied in this note, we simulated similar bottom-up/top-down cases with LES as were studied by Verver et al. (1997), and arrived at conflicting results for the contribution of chemical higher-order moments to the flux: the effective transport to mid-levels of the CABL is decreased when LES profiles are substituted in the second-order closure formulation for $\overline{(w's'_i)}_2$, while it is increased according to the full second-order closure model results given by Verver et al. (1997). This is a sign that the estimate of the chemical higher-order moments is very sensitive to the parameterization (especially for the constants to calculate the timescales).

4.6 Summary and discussion

The contribution of chemical higher-order moments to the flux has been estimated for two cases by several different closures. A significant difference between the full second-order closure of Verver et al. (1997) and a simplified version of that closure—equivalent to a mass-flux closure—has been found. A simple physical picture of higher-order chemistry corrections to flux comes with the mass-flux closure: these corrections are proportional to the difference in chemical reaction rates between updrafts and downdrafts. The residual error for flux estimates based on nonreactive flux–profile relationships in the surface layer tends to be somewhat smaller than the contribution of chemical higher-order moments to the flux as estimated by higher-order closures, especially near the top of the surface layer.

Although the specific magnitude of the differences found is dependent on the precise values chosen for the different constants, changing these constants will not structurally change our conclusions. This study suggests that the presence of more degrees of freedom in full second-order closures leads to a stronger impact of chemical reactions on the flux estimate. If, for instance, in a full second-order closure the higher-order chemistry terms are not taken into account, a significantly larger error results in the flux estimate compared to if a first-order closure is used. The fact that for a representative photochemical case the higher-order chemistry corrections modeled by higher-order closures become larger with height near the surface, does not mean that the error for first-order closures also increases: we even find a decrease of the first-order closure error with height. We expect that for representative atmospheric chemistry conditions no significant chemical corrections related to higher-order chemical moments in the flux budget are needed for first-order closure estimates of the flux.

Chapter 5

Segregation effects in atmospheric chemistry related to boundary-layer convection

Abstract

A first-order covariance closure is included in a single-column version of a global climate–chemistry model, and the impact of segregation effects due to boundary-layer convection on atmospheric chemistry is studied. The column model is run for several locations with widely varying chemical conditions. The chemical scheme that is used is a modified version of the Carbon Bond Mechanism 4 (CBM-4) and contains 32 species and 71 reactions. For all locations the impact on daytime boundary-layer averaged isoprene, NO_x , O_3 , and OH concentrations is found to be less than 2%. The impact is often smaller than 0.5%. The covariance that plays the most significant role during daytime is the covariance of isoprene and OH , although the magnitude of the intensity of segregation for this reaction is at most -2% . A sensitivity study with turbulence–canopy interactions for the tropical rainforest indicates increases of only 1% or less in the concentrations of isoprene and OH . We conclude that segregation effects related to dry boundary-layer convection can be neglected in atmospheric chemistry modeling. On the other hand, surface heterogeneities affecting emission and deposition processes may be significant.

5.1 Introduction

In atmospheric chemistry models all species are typically assumed to be well mixed in each model grid box (representing an area of 10^2 – 10^6 km²). This assumption might lead to inaccuracies in atmospheric chemistry models, since some measurements show that chemical species are not always well mixed and that segregation effects must be taken into account in atmospheric chemistry models. Concentrations of reacting species can be positively or negatively correlated and these correlations may lead to corrections on the mean reaction rates in model grid boxes. The relative corrections are called “intensities of segregation.” For instance, Vilà-Guerau de Arellano et al. (1993a) calculated an intensity of segregation I_s of -10% at a certain height in the mixed layer of the convective atmospheric boundary layer (CABL) from aircraft measurements over the Netherlands (considering an area of 200×200 km²). They attributed this segregation effect to the turbulent and chemical production of covariances (e.g., Schumann 1989). Davis (1992) studied the importance of the chemically produced covariance between isoprene (C₅H₈) and the hydroxyl radical (OH). He identified conditions for which this covariance could result in a significant intensity of segregation.

The question now is whether intensities of segregation of about -10% or more can be caused by convection and chemistry in the CABL. If not, then nonuniform emission and deposition patterns must be responsible for observed large intensities of segregation. Only a few studies have been done on the turbulent transport–reaction problem for chemical schemes that are representative for atmospheric chemistry in the CABL. For tropical background steady-state conditions Krol et al. (1999) showed, using large-eddy simulation (LES), that the bulk intensity of segregation for NO and O₃ is very small ($\approx 1\%$), but that for nonmethane hydrocarbons (NMHC) and OH it could be as large as 5–30%, depending on the lifetime of the hydrocarbons considered. The sensitivity study for a nonsteady case presented in chapter 3 of this dissertation suggests that segregation effects related to boundary-layer convection may be important in atmospheric chemistry. Finally, Verver et al. (1999) studied a nonsteady tropical rainforest case (ABLE-2A) and found a bulk intensity

of segregation for the reaction of isoprene with OH of a few per cent both in the morning and afternoon, and bulk intensities of segregation of about 10% for the reaction of NO with peroxy radicals. From the small impact on the modeled concentrations they concluded that it is not necessary to include covariances produced by turbulence and chemistry in atmospheric chemistry models.

We here extend the above studies to different chemical and meteorological nonsteady conditions, in order to determine whether conditions exist over the globe for which segregation related to dry boundary-layer convection has a significant effect on atmospheric chemistry. Therefore we implement the covariance parameterization of chapter 3 in a single-column version of a climate–chemistry model. This model is run for two consecutive days at four different locations over the globe: South America (tropical rainforest), Europe (agriculture/industry), North America (agriculture/forest), and Africa (savanna). The initialization of meteorology and chemistry is performed using profiles from global climate and chemistry models.

5.2 Model description

The model used is a single-column version of the global climate model ECHAM4. The global model is described by Roeckner et al. (1996) and the single-column version by Christensen et al. (1996). We will not give the details of its physical parameterization here. The standard vertical resolution of 19 layers is used. All relevant model variables are initialized using global model output (also the necessary land-surface parameters are taken from global data sets).

Chemical species have been added to the single-column model: 34 species are modeled, of which 29 are transported. The chemical scheme is a modified version of the Carbon Bond Mechanism 4 (CBM-4), taken from Houweling et al. (1998), and describes 71 reactions (including 3 sulfur reactions that have been added to the scheme of Houweling et al. 1998). The scheme is representative of global tropospheric NO_y –CO–CH₄–NMHC–O₃ chemistry.

The initial meteorological conditions are derived from ECHAM4 and the initial chemical conditions are obtained for the specific month studied from the global chemical tracer model TM3 (see Houweling et al. 1998). Both global models are driven by analyses from the European Centre for Medium-Range Weather Forecasts (ECMWF)—ECHAM4 through Newtonian relaxation, and TM3 directly.

The nonbiogenic surface emissions are similar to the climatological values used for the specific locations in the chemistry version of ECHAM4 (Roelofs and Lelieveld 1995). The biogenic emissions are calculated explicitly, using the available physical variables,

Case	Continent	Latitude	Longitude	Period
Tropical rainforest	South America	4° N	55° W	March 1–2, 1993
Agriculture/industry	Europe	50° N	10° E	July 1–2, 1993
Agriculture/forest	North America	35° N	87.5° W	July 1–2, 1993
Savanna	Africa	7.5° N	10° E	October 1–2, 1993

Table 5.1: Locations and periods for four cases.

Case	Isoprene [ppbv]	OH [10 ⁶ molec cm ⁻³]	NO _x [ppbv]	O ₃ [ppbv]
Tropical rainforest	1.9	1.9	0.12	23
Agriculture/industry	0.03	16	1.1	40
Agriculture/forest	0.3	10	0.2	50
Savanna	0.3	7	0.07	30

Table 5.2: Boundary-layer averaged concentrations around noon on the second day of the simulation (one-hour average).

and based on a land cover database. Dry deposition is modeled following Ganzeveld and Lelieveld (1995).

5.3 Results for different cases

To study the impact of covariances for different chemical and meteorological conditions, four locations and periods were selected to run the single-column model (see Table 5.1). In all cases a CABL develops during daytime. Different emissions of NMHC and NO_x result in a range of chemical conditions. We run the single-column model for two consecutive days, both with and without covariance closure, and compare the results around noon local time on the second day. Note that the studied locations are representative for large areas. Therefore local advection effects are not taken into account (although in the initial concentration fields some effects of monthly-mean advection are present). In Table 5.2 the boundary-layer averaged concentrations are given. As is evident, a large range of concentrations is covered by the four cases. Realistic concentrations are modeled for the different cases; for the tropical rainforest case this was accomplished by reducing the isoprene emission flux,

Case	$I_{s,OH+isop}$ $\times 100$	$\frac{\Delta[\text{isoprene}]}{[\text{isoprene}]_{\text{no cov}}}$ $\times 100$	$\frac{\Delta[\text{OH}]}{[\text{OH}]_{\text{no cov}}}$ $\times 100$	$\frac{\Delta[\text{NO}_x]}{[\text{NO}_x]_{\text{no cov}}}$ $\times 100$	$\frac{\Delta[\text{O}_3]}{[\text{O}_3]_{\text{no cov}}}$ $\times 100$
Tropical rainforest	-2	+0.4	+0.4	+0.4	-0.08
Agriculture/ industry	+0.2	+0.2	-0.5	-0.6	-0.07
Agriculture/ forest	-2	+2	+0.02	-0.6	+0.2
Savanna	-2	+2	-0.2	-0.6	-0.15

Table 5.3: Boundary-layer averaged horizontal intensity of segregation for the OH–isoprene reaction and relative changes in concentrations due to covariances around noon at the second day of the simulation (one-hour average). $\Delta[\text{conc}]$ is defined as the difference between the model results with and without covariance parameterization: $\Delta[\text{conc}] \equiv [\text{conc}]_{\text{cov}} - [\text{conc}]_{\text{no cov}}$.

which is resolved in the model according to Guenther et al. (1995), by 50%. Two chemical regimes can be discerned for the four cases: an NO_x -rich (agriculture/industry case) and an NO_x -poor regime (all other cases).

The boundary-layer averaged horizontal intensity of segregation for the reaction of isoprene with OH and the impact of the covariance parameterization on some species concentrations are given in Table 5.3. The impact of covariances is very small at all locations. The other intensities of segregation are typically also very small; some reactions involving radicals, NO, NO_2 , and NO_3 , show somewhat larger effects for early morning conditions (evident from a 0.6% impact on the NO_x concentration during the day for the agriculture cases). The largest relative impact is found for the two cases with moderate isoprene concentrations (agriculture/forest and savanna case), where the isoprene concentrations are increased by 2% due to a -2% intensity of segregation for the reaction of isoprene with OH. For the tropical rainforest case the effects on the isoprene concentration of the segregation between OH and isoprene is much smaller (0.5%).

To deduce an upper limit for covariance effects related to convective boundary-layer mixing in the tropical rainforest case, we performed a sensitivity run where the covariance of isoprene and OH is enhanced to account for covariances produced by turbulence–canopy interactions (Patton et al. 1999). We assume a fixed value of -20% for this covariance in the lowest grid box (with a height of 60 m) of the model. This grid box largely extends above the canopy top—its bottom is at the displacement height, 20 m for our case. The results for

Sensitivity run	$I_{s,OH+isop}$ $\times 100$	$\frac{\Delta[\text{isoprene}]}{[\text{isoprene}]_{\text{no cov}}}$ $\times 100$	$\frac{\Delta[\text{OH}]}{[\text{OH}]_{\text{no cov}}}$ $\times 100$	$\frac{\Delta[\text{NO}_x]}{[\text{NO}_x]_{\text{no cov}}}$ $\times 100$	$\frac{\Delta[\text{O}_3]}{[\text{O}_3]_{\text{no cov}}}$ $\times 100$
turbulence–canopy interactions	–4	+1.3	+0.7	+1.6	–0.08

Table 5.4: Sensitivity run (the same quantities are given as in Table 5.3).

this sensitivity study are given in Table 5.4. The intensity of segregation and the impact on the isoprene concentration increase—but still the impact is only about 1%.

5.4 Summary and discussion

We have addressed the question on the significance of turbulently and chemically produced covariances leading to segregation effects in atmospheric chemistry models. Only a small influence was found for the inclusion of these covariances in an atmospheric chemistry model that was run for several different conditions. In general, in low- NO_x environments (tropical rainforest, agricultural/forest, and savanna cases) increases of at most 2% were found for the concentrations of isoprene, while the effect on O_3 concentrations was negligible. For high- NO_x conditions the covariance of isoprene and OH seems to be even less important. A sensitivity run suggests that taking turbulence–canopy interactions into account does not significantly alter the conclusion that covariances produced in the CABL have only a minor impact on chemistry in the atmospheric boundary layer. However, this conclusion is probably not valid for the concentrations within the canopy (and the effective emissions from the canopy).

Subgrid-scale covariances for grid sizes typical of mesoscale or global atmospheric chemistry models can be important, however. Sillman et al. (1990) have shown, for instance, that a large subgrid-scale variability exists in the range from 40 to 400 km. And, as another example, Vilà-Guerau de Arellano et al. (1993a) found a –10% intensity of segregation for NO and O_3 above the Netherlands. This intensity of segregation was not produced, as the authors suggested, by turbulence and chemistry, but by the nonuniformity of the emissions. Indeed, from the cospectrum of NO and O_3 presented by Vilà-Guerau de Arellano et al. (1993a)—with scales ranging from 50 km down to 1 km—it is evident that most of the –10% intensity of segregation for NO and O_3 is located at the 15 km scale and that the contribution of scales of order 1 km or less (approaching the boundary-layer turbulence scales) is negligible. We conclude that subgrid-scale surface heterogeneities affecting

emission and deposition patterns are the cause of the measured intensity of segregation for NO and O₃. We expect that in general it is more important to incorporate subgrid-scale surface heterogeneities in atmospheric chemistry models than turbulently and chemically produced subgrid-scale covariances.

Chapter 6

Summary and discussion

6.1 Summary

The mixing of chemical species in the convective boundary layer has been studied. An LES investigation of the mass-flux characteristics of both reactive and nonreactive scalars reveals that 65% of the flux is captured by the updraft–downdraft decomposition and about 25% of the covariance between two arbitrary scalars. The CABL profiles of scalars are modeled accurately by an off-line mass-flux scheme that has two major simplifying assumptions in it, as compared to the exact plume-budget equations. First, only one-way lateral exchange is considered, and second, the subplume-scale fluxes are taken into account by an increase of the mass flux. The accuracy of the mass-flux estimate of the covariance is estimated to be a factor of 2, which is accurate enough to improve modeled reaction rates by taking the estimated covariance into account.

Based on the mass-flux characteristics of scalars a simple covariance parameterization has been developed which can be used in atmospheric chemistry models to assess the importance of turbulent covariances for atmospheric chemistry. The parameterization considers both turbulent and chemical production of covariances. It makes use of a distinction between short-lived and long-lived species. The short-lived species do not have to be transported by the flux closure that is used in combination with the covariance closure. The evolution of the updraft and downdraft concentrations of nontransported species is completely determined by chemical reactions also involving longer-lived species (that are transported).

It is not necessary to combine this covariance parameterization with a mass-flux parameterization for the flux. A nonlocal first-order flux closure suffices to model accurately the flux and concentration profiles of reactive species in the CABL, provided that the flux divergence due to chemistry is also taken into account in the nonlocal contribution to the flux. Concerning the potential error related to the neglect of the higher-order chemical terms in the flux budget it has been found that this error is the largest for relatively complex flux closures (like full second-order flux closure) and the smallest for very simple flux closures (like the nonlocal first-order flux closure). This explains why a simple flux closure can model the fluxes in the photochemistry case accurately whereas in a second-order flux closure a large

flux correction due to higher-order chemical terms is indicated.

The covariance closure, developed using nonreactive and simple chemistry cases, has been found to compare well with LES for a more complex photochemistry case. This provides support for the actual application of the covariance parameterization in a full climate–chemistry model. In this dissertation a study has been presented where a single-column version of a global climate–chemistry model has been used to study the impact of the covariance parameterization. The model has been run for several locations on the globe. It has been found that the impact of turbulent covariances on the modeled concentrations is very small (less than 1%) everywhere.

In summary, the main conclusions are the following (cf. section 1.4):

- The updraft–downdraft decomposition is very useful for solving the turbulent transport–reaction problem. More specifically we found that:
 1. sufficiently accurate estimates of covariances can be made on the basis of the updraft–downdraft decomposition.
 2. the tool that was used to study this decomposition, LES, showed no problems relating to LES subgrid-scale covariances (these subgrid-scale covariances were typically negligible, even near the bottom and top of the CABL).
- The mass-flux approach for calculating covariances can be combined with any flux closure. A first-order covariance closure can be formulated that takes both turbulent and chemical production of covariances into account.
- The contribution of chemical higher-order moments to the flux in higher-order closures is typically larger than the error that is made by using a first-order flux closure. The latter error is expected to be small in atmospheric chemistry.
- Turbulently and chemically produced covariances contribute at most 2% to the day-time species budget of the NMHC species isoprene. The impact on concentrations is typically only 0.5%. Other species are often even less affected by the modeled covariances. One must note, however, that in reality covariances are also produced by subgrid-scale surface heterogeneity (affecting emission and deposition patterns). This heterogeneity is expected to lead to considerable effects for large-scale models with grid sizes that are significantly larger than 10 km.

6.2 Discussion

Using the LES technique it has been found here that reactive scalars largely behave like nonreactive scalars as far as their turbulent characteristics are concerned. From the discussion in chapter 2 related to the spectra shown in Fig. B.1 it can be concluded that although (anti-)correlations persist up to the smallest resolved scales, the contribution to the total covariance by the smallest scales is negligible. In fact, for very high reaction rates—considering a one-way, binary reaction between two scalars with comparable CABL-averaged concentrations—the (anti-)correlation even drops to zero at the smallest scales. Such fast-reacting scalars do not put additional constraints on the LES technique.

It is simple to imagine a chemical regime for which the LES technique breaks down: two species reacting very quickly where one species has a much higher concentration than the other. But for such a case the turbulent transport–chemistry problem becomes the molecular transport–chemistry problem. A central claim of this dissertation is that the molecular transport–chemistry problem is not relevant for atmospheric chemistry: chemical species with such short lifetimes (in the order of seconds or less) can be considered to be in a steady state—they are *both* quickly produced *and* quickly destroyed. The turbulent spectra of short-lived species therefore follow the spectra of their longer-lived precursors and reactants. Furthermore, the small shift toward smaller scales that is found in the turbulent spectra for reactive scalars, still takes place in the part of the spectral domain that is well-resolved by LES. It should be noted here that the cautions given in the literature about chemistry in LES are sometimes based on low-Re experiments with a one-way binary reaction. For the real atmosphere with its very high Re and with the presence of back reactions, LES of atmospheric chemistry does not suffer from special problems related to the chemistry.

Retrospectively, it is the large intensity of segregation found for the simple reaction considered for years in the literature (the one-way reaction $A + B \rightarrow C$), e.g., by Schumann (1989), Sykes et al. (1994), Verver et al. (1997), Molemaker and Vilà-Guerau de Arellano (1998), and Petersen et al. (1999, chapter 2 of this dissertation), that supported the hypothesis that turbulent covariance effects might be important. We conclude, however, that significant intensities of segregation might be present in the atmosphere at scales ranging from 10 to 1000 km, but that the contribution of smaller (turbulent) scales to the intensities of segregation is negligible. Intensities of segregation caused by larger-scale variability are related to inhomogeneities at the surface—as opposed to turbulent and chemical production. To give an outlook on future research, we think that it is now interesting to establish a broader experimental basis on subgrid-scale covariances. The following question should be addressed: How large is the error that is made by neglecting horizontal subgrid-scale

covariances as a function of the spatial resolution of atmospheric chemistry models? If the errors are then subsequently considered to be too large for specific modeling purposes, two strategies can be followed: either to increase the horizontal resolution (at 10 km the intensities of segregation could probably already be reduced to magnitudes of a few per cent) or to continue the development of parameterizations for the effects of subgrid-scale heterogeneity in surface emission and deposition (and in meteorologically relevant parameters, since also the dynamics and thermodynamics of the CABL can significantly vary on these scales).

It should be made clear that all the above considerations are valid for the dry CABL only. In the cases of the stratocumulus-topped or the (shallow-)cumulus-topped CABL it is still expected that the turbulent transport–chemistry problem contains features that should be parameterized in atmospheric chemistry models. This subject awaits further research. We expect that the proposed covariance parameterization will also work for the stratocumulus-topped CABL, since it has been shown that also within the stratocumulus cloud 65% of the flux is described by the mass-flux approximation. First, however, tests for several reactive cases will have to be performed to determine if the accuracy of the parameterization is still a factor of 2 in the stratocumulus case.

Finally, it must be stressed that, although CABL turbulence is not important for the covariances in atmospheric chemistry, it is important for the vertical fluxes. Due to the fact that the spectrum of vertical velocity has a peak at scales of the order of the CABL height, the turbulent scales are dominant for vertical transport of chemical species in the CABL.

Appendix A

Fractional top-hat contribution to the covariance κ_{12}

In this appendix we want to generalize the work of Wyngaard and Moeng (1992) from fluxes to variances and covariances. Wyngaard and Moeng (1992) determined a theoretical value of κ_{ws} , assuming a Gaussian probability density function (pdf) $P(w', s')$. We here determine an expression for κ_{12} , the top-hat fraction of the covariance of two (arbitrary) scalars, assuming Gaussian pdf's $P_1(w', s'_1)$ and $P_2(w', s'_2)$. Furthermore, we would like to demonstrate that $\kappa_{12} = 0.25$ is a best-guess value for all possible scalars, thereby generalizing from the pure bottom-up and top-down diffusing scalar fields studied in chapter 2. Finally, this appendix aims to determine the uncertainty in this value of κ_{12} .

We start with the definition of κ_{12} :

$$\kappa_{12} \equiv \frac{a\overline{s_1^u s_2^u} + (1-a)\overline{s_1^d s_2^d} - \overline{s_1} \overline{s_2}}{\overline{s_1 s_2}}. \quad (\text{A.1})$$

We rewrite the updraft and downdraft quantities in terms of the joint pdf $P(w', s')$ of vertical velocity and scalar fluctuations, analogous to Wyngaard and Moeng (1992):

$$\overline{s_1^u} \equiv \frac{\int_{-\overline{s_1}}^{\infty} \int_0^{\infty} s'_1 P(w', s'_1) dw' ds'_1}{\int_{-\overline{s_1}}^{\infty} \int_0^{\infty} P(w', s'_1) dw' ds'_1} \quad (\text{A.2})$$

$$\overline{s_1^d} \equiv \frac{\int_{-\overline{s_1}}^{\infty} \int_{-\infty}^0 s'_1 P(w', s'_1) dw' ds'_1}{\int_{-\overline{s_1}}^{\infty} \int_{-\infty}^0 P(w', s'_1) dw' ds'_1}, \quad (\text{A.3})$$

with similar expressions for $\overline{s_2^u}$ and $\overline{s_2^d}$. The lower integration limit $-\overline{s_1}$ for s_1' follows from the fact that the scalar values cannot become negative ($\overline{s_1}$ is the horizontally averaged value of scalar s_1 relative to which the fluctuations s_1' are defined).

We define the correlation coefficients ρ in the following way:

$$\overline{w's_1'} \equiv \rho_{ws_1} \sigma_w \sigma_{s_1} \quad (\text{A.4})$$

$$\overline{w's_2'} \equiv \rho_{ws_2} \sigma_w \sigma_{s_2} \quad (\text{A.5})$$

$$\overline{s_1's_2'} \equiv \rho_{s_1s_2} \sigma_{s_1} \sigma_{s_2}, \quad (\text{A.6})$$

where the σ 's denote the rms values of the indicated quantities.

If $P(w', s_1')$ and $P(w', s_2')$ have a Gaussian form, it follows that

$$\overline{s_1^u} = \frac{2\sigma_{s_1} \rho_{ws_1}}{\sqrt{2\pi}} \quad (\text{A.7})$$

$$\overline{s_1^d} = -\frac{2\sigma_{s_1} \rho_{ws_1}}{\sqrt{2\pi}}, \quad (\text{A.8})$$

and similar expressions are obtained for scalar s_2 . Furthermore, it follows under Gaussian assumptions that $a = \frac{1}{2}$. Combining all above equations we arrive at

$$\kappa_{12, \text{Gauss}} = \frac{4}{2\pi} \frac{\rho_{ws_1} \rho_{ws_2}}{\rho_{s_1s_2}}. \quad (\text{A.9})$$

Contrary to what was found earlier for κ_{ws} (the top-hat flux fraction) in the case of a Gaussian joint pdf $P(w', s')$, that is, that $\kappa_{ws} = 4/(2\pi)$ is independent of the correlation coefficient ρ_{ws} , (A.9) states that κ_{12} is dependent on all three correlation coefficients defined in (A.4)–(A.6). We can also see that if we substitute w for either s_1 or s_2 , the result $\kappa_{ws} = 4/(2\pi)$ for the top-hat flux fraction comes out again. If we assume $s_1 = s_2 \equiv s$ we find for the top-hat variance fraction $\kappa_{ss, \text{Gauss}} = 4/(2\pi) \rho_{ws}^2$.

In order to empirically investigate the sensitivity of κ_{12} to different cases we have used the superposition hypothesis of Wyngaard and Brost (1984) to construct different types of scalars s_1 and s_2 (without chemical reaction) from the BU and TD scalars in the following manner:

$$s_1 = \alpha_1 s_{\text{BU}} + \beta_1 s_{\text{TD}} \quad (\text{A.10})$$

$$s_2 = \alpha_2 s_{\text{BU}} + \beta_2 s_{\text{TD}}. \quad (\text{A.11})$$

Description	α_1	β_1	α_2	β_2	$\frac{\int \kappa_{12,\text{Gauss}} \overline{s'_1 s'_2} dz}{\int \overline{s'_1 s'_2} dz}$	$\frac{\int \kappa_{12} \overline{s'_1 s'_2} dz}{\int \overline{s'_1 s'_2} dz}$
s_1 : Pure bottom-up						
s_2 : Pure top-down	1.0	0.0	0.0	1.0	0.41	0.36
s_1 : 20% detrained at top						
s_2 : No deposition at bottom	1.0	-0.2	0.0	1.0	0.17	0.16
s_1 : 20% detrained at top						
s_2 : 20% deposited at bottom	1.0	-0.2	-0.2	1.0	0.19	0.18
s_1 : 20% detrained at top						
s_2 : 100% deposited at bottom	1.0	-0.2	-1.0	1.0	0.23	0.22
Both pure bottom-up	1.0	0.0	1.0	0.0	0.28	0.29
Both bottom-up						
20% detrained at top	1.0	-0.2	1.0	-0.2	0.27	0.27
s_1 : 20% entrained at top						
s_2 : 20% detrained at top	1.0	0.2	1.0	-0.2	0.32	0.33
Both pure top-down	0.0	1.0	0.0	1.0	0.07	0.09

Table A.1: Bulk ratios of top-hat contribution to total covariance for different combinations of nonreactive bottom-up and top-down scalar fields, determined from LES.

We do not have to perform additional LES runs in order to calculate κ_{12} and $\kappa_{12,\text{Gauss}}$. In Table A.1 we present the bulk values of κ_{12} and $\kappa_{12,\text{Gauss}}$ for a host of different cases, together spanning a large range of possibilities. We can conclude that in general the bulk value of $\kappa_{12,\text{Gauss}}$ does not deviate much from the bulk value of κ_{12} . Furthermore, $\kappa_{12} = 0.25 \pm 0.10$ seems to be a good estimate of the range of values that κ_{12} can attain. From the experimental LES results presented in section 2.5 we infer that chemical reactions cannot cause large changes in this range.

Appendix B

Spectral behavior of $\overline{s_1' s_2'}$

In this appendix we describe the spectral behavior of the covariance for cases studied in chapter 2. The bottom-up scalars BU and A are denoted by s_1 and the top-down scalars TD and B by s_2 . Using the 2-D Fourier transforms \widehat{s}_1 and \widehat{s}_2 , normalized in a proper way, we have

$$\overline{s_1' s_2'} = \sum_{i=-N}^N \sum_{j=-N}^N (\widehat{s}_1^{ij})^* \widehat{s}_2^{ij} = \sum_{k=1}^N S_{12}^k, \quad (\text{B.1})$$

where S_{12} is the discrete cospectrum of s_1 and s_2 (for the resolution of 130×130 we have $N = 63$). Another spectral quantity that we investigate is the spectral correlation, defined as

$$\rho_{12}^k = \frac{S_{12}^k}{\sqrt{S_{11}^k S_{22}^k}}, \quad (\text{B.2})$$

where S_{11} and S_{22} are the discrete spectra of s_1 and s_2 , respectively. The spectral correlation obeys $\rho_{12}^k \in [-1, 1]$, $k = 1, \dots, N$.

In Figs. B.1a,b we have plotted ρ_{12} and S_{12} for different cases at height $z/z_i = 0.14$. The spectral behavior at other heights is qualitatively similar (not shown). We see that case $\text{AB}\infty$ behaves as case BUTD: the correlation drops to near-zero values for higher wavenumbers (smaller scales), while the reactive cases AB1 and AB3 (and AB2, not shown) maintain constant correlations as low as -0.35 at all scales for case AB1. This difference is due to the chemical reaction that proceeds at a moderate reaction rate in case AB1, acting at all scales as a source of negative covariance and counteracting the tendency toward near-zero correlations (which is dominant at the smaller scales for nonreactive or fast-reactive cases). From the cospectra S_{12} we can furthermore conclude that the small scales have a larger

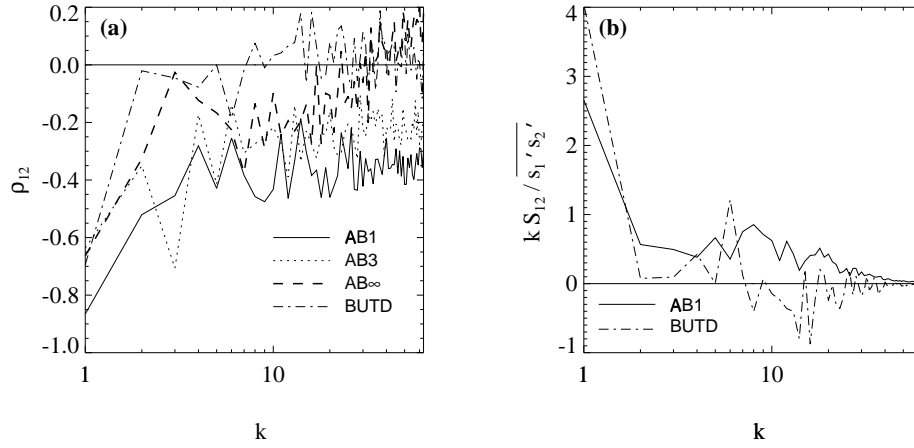


Figure B.1: (a) Spectral correlations and (b) cospectra of bottom-up diffusing scalars BU or A (scalar values denoted by s_1) and top-down diffusing scalars TD or B (scalar values denoted by s_2), determined from LES. The plotted quantities have been calculated at height $z/z_i = 0.14$. The normalization in (b) is chosen such that $\int_{\ln 1}^{\ln 63} k S'_{12} d(\ln k) = 1$, with $S'_{12} \equiv S_{12} / \overline{s_1' s_2'}$.

contribution to the total covariance in case AB1 with a moderate reaction-rate coefficient than in the nonreactive case BUTD.

Appendix C

Top-hat formulas for a and M

In order to drive a mass-flux scheme, one needs to know the updraft area fraction a and the mass flux M . Use can be made of top-hat formulas that relate a and M to the turbulent vertical velocity statistics $\overline{w'^2}$ and $\overline{w'^3}$. In this appendix we will present these top-hat formulas and evaluate their performance, given that we already know the profiles of $\overline{w'^2}$ and $\overline{w'^3}$.

Using the following top-hat formulas for a and M from Randall et al. (1992),

$$a = \frac{1}{2} - \frac{S_{w,\text{top-hat}}}{2\sqrt{4 + S_{w,\text{top-hat}}^2}} \quad (\text{C.1})$$

$$M = \frac{(\overline{w'^2})_{\text{top-hat}}^{1/2}}{\sqrt{4 + S_{w,\text{top-hat}}^2}}, \quad (\text{C.2})$$

where the top-hat skewness is used, defined as $S_{w,\text{top-hat}} \equiv \overline{w'^3}_{\text{top-hat}} / (\overline{w'^2})_{\text{top-hat}}^{3/2}$, and relating all top-hat quantities in (C.1) and (C.2) to the total quantities using κ -factors, we

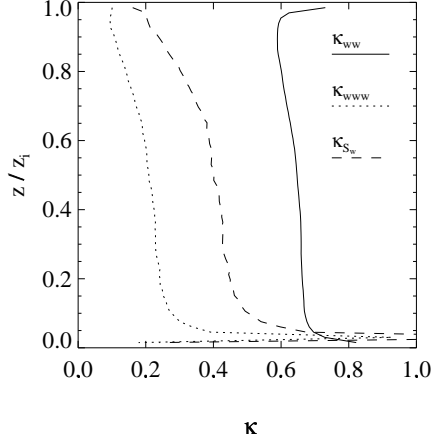


Figure C.1: Ratios of top-hat contribution to total quantity for $\overline{w'^2}$, $\overline{w'^3}$, and S_w determined from LES.

can write the following equations:

$$a = \frac{1}{2} - \frac{\kappa_{S_w}(z)S_w}{2\sqrt{4 + \kappa_{S_w}^2(z)S_w^2}} \approx \frac{1}{2} - \frac{\kappa_{S_w}S_w}{4} \quad (\text{C.3})$$

$$M = \frac{\sqrt{\kappa_{ww}(z)} (\overline{w'^2})^{1/2}}{\sqrt{4 + \kappa_{S_w}^2 S_w^2}} \approx \frac{\sqrt{\kappa_{ww}} (\overline{w'^2})^{1/2}}{2}. \quad (\text{C.4})$$

The κ factors are defined as $\kappa_{ww} \equiv \overline{w'^2}_{\text{top-hat}}/\overline{w'^2}$ and $\kappa_{S_w} \equiv S_{w,\text{top-hat}}/S_w$. In the approximating step of (C.3) and (C.4), it is assumed that the κ factors are independent of height and that $\kappa_{S_w}^2 S_w^2/4 \ll 1$. In Fig. C.1 we plot the profiles of the κ factors. The top-hat fraction of the total vertical velocity variance κ_{ww} turns out to have small variation with height (it decreases from 0.7 near the bottom to 0.6 near the top of the CABL) and on average it is close to the theoretical value for a Gaussian pdf $P(w', s')$, namely 0.64. However, the top-hat fraction of the total third moment of the turbulent vertical velocity $\kappa_{w'w'w'}$ is much lower (about 0.2) and less constant with height. Note that under Gaussian assumptions $\kappa_{w'w'w'}$ is undefined, since in that case $\overline{w'^3} = 0$. The top-hat fraction of the total skewness κ_{S_w} is found to be about 0.4.

In Figs. C.2a,b we show a and M calculated with and without the κ factors and com-

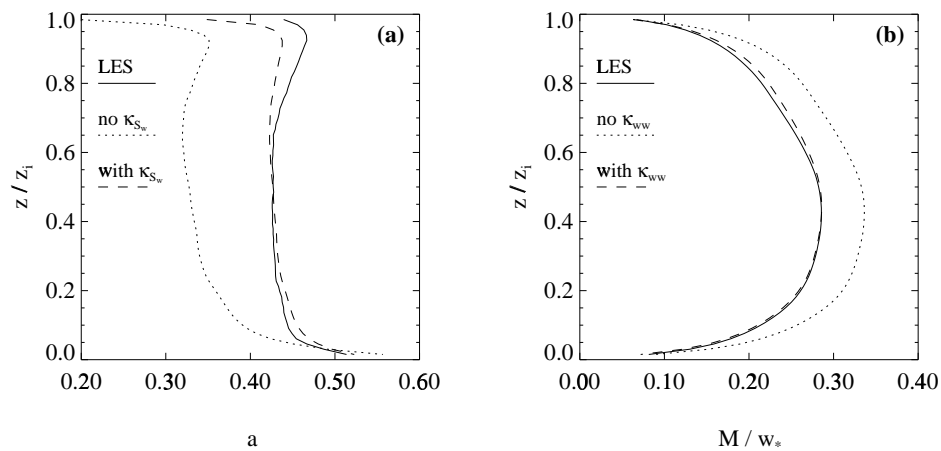


Figure C.2: (a) Updraft area fraction and (b) mass flux, determined from LES. The lines labeled “with κ_{S_w} ” and “with κ_{w_w} ” correspond to Eqs. (C.3) and (C.4), respectively, and the lines labeled “no κ_{S_w} ” and “no κ_{w_w} ” correspond to the same equations but without the κ ’s (or, equivalently, with the κ ’s put equal to 1).

pared to LES. The LES profiles were used to drive the mass-flux schemes in this chapter. Consistent with Sorbjan (1996) the LES result for a shows a roughly constant value of 0.43 in the bulk of the CABL. The LES result for M shows a profile that is nearly symmetrical around its maximum of $0.29w_*$. We can conclude from Figs. C.2a,b that (C.3) and (C.4), using $\kappa_{S_w} = 0.4$ and $\kappa_{w_w} = 0.64$, give a good performance. However, if we do not use the κ factors the minimum of a becomes 0.33 and the maximum of M becomes $0.34w_*$. So, large errors in the estimation of a and M are made if one does not take the κ factors into account.

Appendix D

Implementing the covariance closure

The proposed covariance closure of chapter 3 should be applied in the atmospheric boundary layer only. The covariance parameterization uses the following information on the boundary-layer dynamics: the boundary-layer height z_i , the vertical profile of the rms of turbulent vertical velocity σ_w , and the vertical profile of the updraft area fraction a . If z_i is not available in a model an estimation formula can be used (e.g., Vogelezang and Holtslag 1996), and if σ_w is not available a parameterized profile can be used (e.g., Holtslag and Moeng 1991). We assume that a is equal to 0.5.

In the parameterization a distinction is made between, on the one hand, species for which the turbulent flux divergence term in (3.1) is important—transported species—and, on the other hand, species for which the turbulent flux divergence term is not important, and is neglected—nontransported species. We choose not to calculate fluxes of such species, since first-order flux closures that do not contain chemical higher-order moments which are dominating the flux budget of these species. The species OH and HO₂ are examples of nontransported species in the photochemistry scheme used in this paper.

Turbulent vertical fluxes at each height for the transported species are used as input to the covariance parameterization. The turbulent vertical fluxes must be specified on full levels, where the concentrations are defined. Any (first- or higher-order) flux closure can be used to calculate the fluxes—in this paper we use a first-order nonlocal flux closure (section 3b).

The parameterization uses (3.14) and (3.15) for the transported species. Substitution of

$a = 0.5$, $\kappa_0 = 0.64$, and $(M/\rho) = \frac{1}{2}\sqrt{\kappa_0}\sigma_w$ in (3.14) and (3.15) leads to

$$\overline{s_i^u} = \overline{s_i} + 0.80 \frac{\overline{w's_i^u}}{\sigma_w} \quad (\text{D.1})$$

$$\overline{s_i^d} = \overline{s_i} - 0.80 \frac{\overline{w's_i^d}}{\sigma_w}. \quad (\text{D.2})$$

Also (3.13) is used in the parameterization. Here substituting $a = 0.5$ and $\kappa_1 = 0.25$ results in

$$\overline{s_i^u s_j^u} = 4.0 \left(0.5 \overline{s_i^u s_j^u} + 0.5 \overline{s_i^d s_j^d} - \overline{s_i} \overline{s_j} \right). \quad (\text{D.3})$$

We here present two methods of implementation, a general method and a simplified method. The results shown in this paper were calculated with the simplified method. We have verified that the difference between the two methods is very small. The major difference between the two methods is the use of steady-state formulas for the nontransported species in the simplified method. In the general method, where all chemical species are treated equally by the chemical solver, the nontransported species de facto reach steady state during the chemistry step (if this turns out not to be the case for a certain species, the flux divergence should be taken into account for the species, i.e., they should be transported).

In the general method (D.3) is not used directly, while it is in the simplified method. In order to prevent for the latter method intensities of segregation from occurring that are larger in magnitude negative than -1 , $\overline{s_i^u s_j^u}$ should be limited to the value of $-\overline{s_i} \overline{s_j}$. However, in the cases studied in this paper and—as we expect—also in practical applications such low values of I_s do not occur and limitation does not have a significant effect. In the limit of I_s approaching -1 , the concentrations modeled by the parameterization (including the mentioned limiter) approach limit values, as should be the case (Molemaker and Vilà-Guerau de Arellano 1998; chapter 2 of this dissertation).

Subplume (subupdraft and subdowndraft) covariances and updraft and downdraft intensities of segregation appear in both methods. Subplume covariances are defined as $\overline{s_i^u s_j^u} \equiv \overline{(s_i - \overline{s_i^u})(s_j - \overline{s_j^u})}$ and $\overline{s_i^d s_j^d} \equiv \overline{(s_i - \overline{s_i^d})(s_j - \overline{s_j^d})}$. By assuming their contribution to the total covariance is equal, they can be determined from substitution of (D.3) and $a = 0.5$ in

$$\overline{s_i^u s_j^u} = \left\{ a \overline{s_i^u s_j^u} + (1-a) \overline{s_i^d s_j^d} - \overline{s_i} \overline{s_j} \right\} + a \overline{s_i^u s_j^u} + (1-a) \overline{s_i^d s_j^d}, \quad (\text{D.4})$$

an exact expression for the total covariance, which is given in chapter 2. The result is

$$\overline{s_i^u s_j^u} = \overline{s_i^d s_j^d} = 3.0 \left(0.5 \overline{s_i^u s_j^u} + 0.5 \overline{s_i^d s_j^d} - \overline{s_i} \overline{s_j} \right). \quad (\text{D.5})$$

Updraft and downdraft intensities of segregation are defined as $(I_{s,u})_{ij} \equiv \overline{s'_i s'_j}^u / \overline{s_i}^u \overline{s_j}^u$ and $(I_{s,d})_{ij} \equiv \overline{s'_i s'_j}^d / \overline{s_i}^d \overline{s_j}^d$. Also here, in order to prevent updraft and downdraft intensities of segregation that are larger in magnitude negative than -1 from occurring, $\overline{s'_i s'_j}^u$ and $\overline{s'_i s'_j}^d$ should be limited to the values of $-\overline{s_i}^u \overline{s_j}^u$ and $-\overline{s_i}^d \overline{s_j}^d$, respectively.

Here we give the steps for both methods:

General method

1. Determine updraft and downdraft concentrations of transported species from (D.1) and (D.2).
2. Determine subupdraft and subdowndraft covariances from (D.5), using updraft and downdraft concentrations of nontransported species from the previous time step.
3. Change updraft and downdraft reaction rate coefficients with factors $(1 + I_{s,u})$ and $(1 + I_{s,d})$, respectively.
4. Call chemistry solver separately for updraft and downdraft concentrations.
5. Determine average concentrations.

Simplified method

1. Determine updraft and downdraft concentrations of transported species from (D.1) and (D.2).
2. Determine updraft and downdraft concentrations of nontransported species from steady-state formulas (use is made of subupdraft and subdowndraft covariances, determined from (D.5), using updraft and downdraft concentrations of nontransported species from previous time step).
3. Determine average covariances from (D.3).
4. Change average reaction rate coefficients with factor $(1 + I_s)$.
5. Determine average concentrations of nontransported species.
6. Call chemistry solver for average concentrations (concentrations of nontransported species are fixed).

Appendix E

Specification of LES runs used in chapter 3

We here give the relevant details on the different LES models used in chapter 3 to simulate the CABL (see Table E.1). Two LES model versions, derived from the LES model of Nieuwstadt and Brost (1986), are used to simulate both the entraining and solid-lid CABL for the simple chemistry cases. The solid-lid CABL is simulated using the model version described in Beets et al. (1996) and chapter 2 of this dissertation. The LES results for the cases SL0 and SL1 shown in chapter 3 have been presented also in chapter 2, and were denoted in chapter 2 by BUTD and AB2, respectively. The model version used for the entraining CABL is, except for the numerical method for the time integration of the scalar advection and the part related to chemical reactions, documented by Cuijpers and Duynkerke (1993) and Cuijpers and Holtslag (1998).

We summarize the changes that were made in the model version used for the entraining CABL compared to Cuijpers and Holtslag (1998). The time integration scheme for the scalars has been changed from leap frog to second-order Runge–Kutta (as in the solid-lid CABL model version) in order to retain the positivity of the limited $\kappa = \frac{1}{3}$ scheme (Koren 1993). The part related to the chemical species is identical to that in the solid-lid CABL model version, except for the fact that in the entraining CABL model version only one subgrid diffusivity is calculated, instead of three subgrid diffusivities (one for each spatial dimension) in the solid-lid CABL model version (the subgrid diffusivity is used for calculating both subgrid fluxes and subgrid covariances). Finally, in the upper third of the entraining CABL model version a sponge layer is present, which was omitted by Cuijpers

Reference	Cases	CABL	\mathbf{v}_g [m s^{-1}]	Domain [km]	Grid points
-	E0, E1	entraining	$u_g = -2,$ $v_g = -10$	$3.2 \times 3.2 \times 1.5$	$128 \times 128 \times 120$
chapter 2	SL0, SL1	solid-lid	$u_g = 0,$ $v_g = 0$	$6.0 \times 6.0 \times 1.5$	$130 \times 130 \times 66$
Krol et al. (1999)	photo- chemistry case	solid-lid	$u_g = 0,$ $v_g = 0$	$4.0 \times 4.0 \times 1.0$	$128 \times 128 \times 64$

Table E.1: LES model versions: references to the sources with LES model description, case acronyms used in chapter 3, CABL type, geostrophic wind, domain sizes, and resolutions.

and Holtslag (1998).

In both the entraining and solid-lid LES model versions used to simulate the simple chemistry cases a no-slip boundary condition is prescribed at the surface. The surface flux of momentum is prescribed in the entraining CABL by putting u_* equal to 0.3 m s^{-1} and in the solid-lid CABL by putting the surface roughness length z_0 equal to 0.16 m . At the top of the solid-lid LES model version a free-slip boundary condition is prescribed. The surface heat flux $\overline{w'\theta'}|_0$ is 0.052 K m s^{-1} for the entraining CABL and 0.069 K m s^{-1} for the solid-lid CABL. We apply a geostrophic wind for the entraining CABL only, so that the flow is strongly buoyant with a small shear, and initialize the model with a relatively weak temperature inversion of 2.7 K at height z_{i0} (680 m). We also take humidity into account for the entraining CABL. The initial humidity profile is 1 g/kg for $z/z_{i0} \leq 1$ and 0 g/kg for $z/z_{i0} > 1$; the surface flux of humidity is specified to be zero, therefore humidity behaves as a top-down diffusing scalar. For our purpose humidity in this case can be considered to be a passive scalar.

The third LES model of which we show results in chapter 3 is the one that was used by Krol et al. (1999) to simulate the solid-lid CABL for the photochemistry case. This LES model is described by Molemaker and Vilà-Guerau de Arellano (1998). It uses a constant subgrid diffusivity and therefore simulates too little small-scale variability compared to an LES with a more sophisticated subgrid model, but it is able to represent the large-scale characteristics of the CABL (Beets et al. 1996). Free-slip boundary conditions are prescribed at bottom and top of the CABL and the surface heat flux $\overline{w'\theta'}|_0$ is 0.1 K m s^{-1} .

The initialization procedures for the dynamics and thermodynamics and the durations of

the runs for the different LES model versions can be found in Cuijpers and Holtslag (1998), chapter 2 of this dissertation, and Krol et al. (1999). The domain sizes and resolutions of the different LES model versions are listed in Table E.1. All LES results given in chapter 3 for cases E0 and E1 are averages over the third hour of the run and all results for cases SL0 and SL1 are 2000 s averages in (quasi-)steady state. For the photochemistry case the LES is run for 7200 s and the results presented in chapter 3 are 1200 s averages around $t = 6600$ s. For the simple chemistry cases the boundary-layer heights z_i , convective vertical velocity scales w_* , and the resulting time scales $t_* \equiv z_i/w_*$ are shown in Table 3.2. For the photochemistry case the CABL height z_i is 1000 m and the convective velocity scale w_* is 1.5 m s^{-1} . The boundary-layer height z_i is determined as the height at which the buoyancy flux attains a minimum. Note that the aspect ratios of the simulated CABLs and the resolutions within the CABLs are approximately equal for all model versions. The aspect ratio is 4; the resolution is relatively high and guarantees small subgrid covariances for all cases studied (which were neglected in the LES model used by Krol et al. 1999).

Bibliography

- Arakawa, A., and W. H. Schubert, 1974: Interaction of a cumulus cloud ensemble with the large-scale environment, Part I. *J. Atmos. Sci.*, **31**, 674–701.
- Beets, C., M. J. Molemaker, and J. Vilà-Guerau de Arellano, 1996: Direct numerical simulation and large-eddy simulation of a non-premixed binary reaction in a turbulent convective boundary layer. *Engineering Turbulence Modelling and Experiments 3*, W. Rodi and G. Bergeles, Eds., Elsevier, 279–287.
- Bergé, P., Y. Pomeau, and C. Vidal, 1984: *Order Within Chaos: Towards a Deterministic Approach to Turbulence*. Wiley, 329 pp.
- Bilger, R. W., 1978: The effect of admixing fresh emissions on the photostationary state relationship in photochemical smog. *Atmos. Environ.*, **12**, 1109–1118.
- Brown, A. R., 1996: Evaluation of parametrization schemes for the convective boundary layer using large-eddy simulation results. *Bound.-Layer Meteor.*, **81**, 167–200.
- Businger, J. A., and S. P. Oncley, 1990: Flux measurement with conditional sampling. *J. Atmos. Oceanic Technol.*, **7**, 349–352.
- Busse, F. H., 1978: Non-linear properties of thermal convection. *Rep. Prog. Phys.*, **41**, 1929–1967.
- Cantwell, B. J., 1990: Future directions in turbulence research and the role of organized motion. *Whither Turbulence? Turbulence at the Crossroads*, Lecture Notes in Physics, Vol. 357, J. L. Lumley, Ed., Springer-Verlag, 97–131.
- Chatfield, R. B., and R. A. Brost, 1987: A two-stream model of the vertical transport of trace species in the convective boundary layer. *J. Geophys. Res.*, **92**, 13263–13276.
- Christensen, J. H., O. B. Christensen, P. Lopez, E. van Meijgaard, and M. Botzet, 1996: The HIRHAM4 Regional Atmospheric Climate Model. Sci. Rep. 96-4, Danish Meteorological Institute, 51 pp. [Available from Danish Meteorological Institute, Lyngbyvej 100, 2100 Copenhagen Ø, Denmark.]
- Crone, G. C., N. Dinar, H. van Dop, and G. H. L. Verver, 1999: A Lagrangian approach for

- modelling turbulent transport and chemistry. Submitted to *Atmos. Environ.*
- Crutchfield, J. P., and K. Kaneko, 1988: Are attractors relevant to turbulence? *Phys. Rev. Lett.*, **60**, 2715–2718.
- Crutzen, P. J., and P. H. Zimmermann, 1991: The changing photochemistry of the troposphere. *Tellus*, **43AB**, 136–151.
- Cuijpers, J. W. M., and P. G. Duynkerke, 1993: Large eddy simulation of trade wind cumulus clouds. *J. Atmos. Sci.*, **50**, 3894–3908.
- , and A. A. M. Holtslag, 1998: Impact of skewness and nonlocal effects on scalar and buoyancy fluxes in convective boundary layers. *J. Atmos. Sci.*, **55**, 151–162.
- Danckwerts, P. V., 1952: The definition and measurement of some characteristics of mixtures. *Appl. Sci. Res.*, **A3**, 279–296.
- , 1958: The effect of incomplete mixing on homogeneous reactions. *Chem. Eng. Sci.*, **8**, 93–99.
- Davis, K. J., 1992: Surface fluxes of trace gases derived from convective-layer profiles. Ph.D. dissertation, University of Colorado, NCAR Cooperative Thesis No. 139, 281 pp.
- Deardorff, J. W., 1966: The counter-gradient heat flux in the lower atmosphere and in the laboratory. *J. Atmos. Sci.*, **23**, 503–506.
- , 1970: Convective velocity and temperature scales for the unstable planetary boundary layer and for Rayleigh convection. *J. Atmos. Sci.*, **27**, 1211–1213.
- , 1972: Numerical investigation of neutral and unstable planetary boundary layers. *J. Atmos. Sci.*, **29**, 91–115.
- , 1973: Three-dimensional numerical modeling of the planetary boundary layer. *Workshop on Micrometeorology*, D. A. Haugen, Ed., American Meteorological Society, 271–311.
- de Laat, A. T. J., and P. G. Duynkerke, 1998: Analysis of ASTEX-stratocumulus observational data using a mass-flux approach. *Bound.-Layer Meteor.*, **86**, 63–87.
- de Roode, S. R., P. G. Duynkerke, and A. P. Siebesma, 1999: Analogies between mass-flux and Reynolds-averaged equations. Submitted to *J. Atmos. Sci.*
- Donaldson, C. duP., and G. R. Hilst, 1972: Effect of inhomogeneous mixing on atmospheric photochemical reactions. *Environ. Sci. Technol.*, **6**, 812–816.
- Ertel, H., 1942: Der vertikale Turbulenz-Wärmestrom in der Atmosphäre. *Meteorol. Zeitsch.*, **59**, 250–253.
- Fitzjarrald, D. R., and D. H. Lenschow, 1983: Mean concentration and flux profiles for chemically reactive species in the atmospheric surface layer. *Atmos. Environ.*, **17**, 2505–2512.

- Frisch, U., 1995: *Turbulence: The Legacy of A. N. Kolmogorov*. Cambridge University Press, 296 pp.
- Galmarini, S., J. Vilà-Guerau de Arellano, and P. G. Duynkerke, 1997a: Scaling the turbulent transport of chemical compounds in the surface layer under neutral and stratified conditions. *Quart. J. Roy. Meteorol. Soc.*, **123**, 223–242.
- , P. G. Duynkerke, and J. Vilà-Guerau de Arellano, 1997b: Evolution of nitrogen oxide chemistry in the nocturnal boundary layer. *J. Appl. Meteor.*, **36**, 943–957.
- Ganzeveld, L. N., and J. Lelieveld, 1995: Dry deposition parameterization in a chemistry general circulation model and its influence on the distribution of reactive trace gases. *J. Geophys. Res.*, **100**, 20999–21012.
- Gao, W., and M. L. Wesely, 1994: Numerical modeling of the turbulent fluxes of chemically reactive trace gases in the atmospheric boundary layer. *J. Appl. Meteor.*, **33**, 835–847.
- , ———, and I. Y. Lee, 1991: A numerical study of the effects of air chemistry on fluxes of NO, NO₂, and O₃ near the surface. *J. Geophys. Res.*, **96**, 18761–18769.
- Garratt, J. R., 1992: *The Atmospheric Boundary Layer*. Cambridge University Press, 316 pp.
- Guckenheimer, J., 1986: Strange attractors in fluids: Another view. *Ann. Rev. Fluid Mech.*, **18**, 15–31.
- Guenther, A., et al., 1995: A global model of natural volatile organic compound emissions. *J. Geophys. Res.*, **100**, 8873–8892.
- Hamba, F., 1993: A modified *K* model for chemically reactive species in the planetary boundary layer. *J. Geophys. Res.*, **98**, 5173–5182.
- Hardy, K. R., and H. Ottersten, 1969: Radar investigations of convective patterns in the clear atmosphere. *J. Atmos. Sci.*, **26**, 666–672.
- Holtslag, A. A. M., and P. G. Duynkerke, Eds., 1998: *Clear and Cloudy Boundary Layers*, Koninklijke Nederlandse Akademie van Wetenschappen, 372 pp.
- , and C.-H. Moeng, 1991: Eddy diffusivity and countergradient transport in the convective atmospheric boundary layer. *J. Atmos. Sci.*, **48**, 1690–1698.
- Houweling, S., F. J. Dentener, and J. Lelieveld, 1998: The impact of nonmethane hydrocarbon compounds on tropospheric photochemistry. *J. Geophys. Res.*, **103**, 10673–10696.
- Hundsdoerfer, W., B. Koren, M. van Loon, and J. G. Verwer, 1995: A positive finite-difference advection scheme. *J. Comp. Phys.*, **117**, 35–46.
- Hunt, J. C. R., J. C. Kaimal, and J. E. Gaynor, 1988: Eddy structure in the convective boundary layer: New measurements and new concepts. *Quart. J. Roy. Meteorol. Soc.*, **114**, 827–858.

- Jonker, H. J. J., P. G. Duynkerke, and J. W. M. Cuijpers, 1999: Mesoscale fluctuations in scalars generated by boundary layer convection. *J. Atmos. Sci.*, **56**, 801–808.
- Kaimal, J. C., J. C. Wyngaard, D. A. Haugen, O. R. Coté, Y. Izumi, S. J. Caughey, and C. J. Readings, 1976: Turbulence structure in the convective boundary layer. *J. Atmos. Sci.*, **33**, 2152–2169.
- Koren, B., 1993: A robust upwind discretization method for advection, diffusion and source terms. *Numerical Methods for Advection-Diffusion Problems*, Notes on Numerical Fluid Mechanics 45, C. B. Vreugdenhil and B. Koren, Eds., Vieweg, 117–138.
- Krol, M. C., M. J. Molemaker, and J. Vilà-Guerau de Arellano, 1999: Photochemistry in the convective boundary layer. Submitted to *J. Geophys. Res.*
- Lamb, R. G., 1973: Note on the application of *K*-theory to diffusion problems involving nonlinear chemical reactions. *Atmos. Environ.*, **7**, 257–263.
- , and J. H. Seinfeld, 1973: Mathematical modeling of urban air pollution: General theory. *Environ. Sci. Technol.*, **7**, 253–261.
- Lanford, O. E., III, 1982: The strange attractor theory of turbulence. *Ann. Rev. Fluid Mech.*, **14**, 347–364.
- Lenschow, D. H., 1982: Reactive trace species in the boundary layer from a micrometeorological perspective. *J. Meteor. Soc. Japan*, **60**, 472–480.
- Lesieur, M., 1997: *Turbulence in Fluids*. 3d ed. Kluwer Academic, 515 pp.
- Lorenz, E. N., 1963: Deterministic nonperiodic flow. *J. Atmos. Sci.*, **20**, 130–141.
- Lumley, J. L., 1990: The utility and drawbacks of traditional approaches, Comment 1. *Whither Turbulence? Turbulence at the Crossroads*, Lecture Notes in Physics, Vol. 357, J. L. Lumley, Ed., Springer-Verlag, 49–58.
- Mason, P. J., 1994: Large-eddy simulation: A critical review of the technique. *Quart. J. Roy. Meteorol. Soc.*, **120**, 1–26.
- Moeng, C.-H., 1998: Large eddy simulation of atmospheric boundary layers. *Clear and Cloudy Boundary Layers*, A. A. M. Holtslag and P. G. Duynkerke, Eds., Koninklijke Nederlandse Akademie van Wetenschappen, 67–83.
- , and R. Rotunno, 1990: Vertical-velocity skewness in the buoyancy-driven boundary layer. *J. Atmos. Sci.*, **47**, 1149–1162.
- Molemaker, M. J., and J. Vilà-Guerau de Arellano, 1998: Control of chemical reactions by convective turbulence in the boundary layer. *J. Atmos. Sci.*, **55**, 568–579.
- Müller, J.-F., and G. Brasseur, 1995: IMAGES: A three-dimensional chemical transport model of the global troposphere. *J. Geophys. Res.*, **100**, 16445–16490.
- Nieuwstadt, F. T. M., 1990: Direct and large-eddy simulation of free convection. *Proc. 9th International Heat Transfer Conf.*, Vol. 1, Jerusalem, Israel, Amer. Soc. Mech. Eng.,

- 37–47.
- , and R. A. Brost, 1986: The decay of convective turbulence. *J. Atmos. Sci.*, **43**, 532–546.
- , and H. van Dop, Eds., 1982: *Atmospheric Turbulence and Air Pollution Modelling*. Reidel, 358 pp.
- , P. J. Mason, C.-H. Moeng, and U. Schumann, 1993: Large-eddy simulation of the convective boundary layer: A comparison of four computer codes. *Turbulent Shear Flows 8*, F. Durst, R. Friedrich, and B. E. Launder, Eds., Springer-Verlag, 532–546.
- Ottino, J. M., 1989: *The Kinematics of Mixing: Stretching, Chaos, and Transport*. Cambridge University Press, 364 pp.
- Patton, E. G. K. J. Davis, M. C. Barth, and C.-H. Moeng, 1999: Large-eddy simulation of convective boundary-layer mixing of decaying scalars emitted by a forest canopy. Preprints, *13th Symposium on Boundary Layers and Turbulence*, Dallas, TX, Amer. Meteor. Soc., 533-534.
- Peters, L. K., et al., 1995: The current state and future direction of Eulerian models in simulating the tropospheric chemistry and transport of trace species: A review. *Atmos. Environ.*, **29**, 189-222.
- Petersen, A. C., 1999a: Philosophy of climate science. Submitted to *Bull. Amer. Meteor. Soc.*
- , 1999b: The impact of chemistry on flux estimates in the convective boundary layer. Submitted to *J. Atmos. Sci.* (chapter 4 of this dissertation).
- , and A. A. M. Holtslag, 1999: A first-order closure for covariances and fluxes of reactive species in the convective boundary layer. *J. Appl. Meteor.*, in press (chapter 3 of this dissertation).
- , C. Beets, and M. C. Krol, 1997: Parametrization of segregation effects due to convective boundary-layer mixing in atmospheric chemistry models. *Phys. Chem. Earth*, **21**, 445–450.
- , E. J. Spee, H. van Dop, and W. Hundsdorfer, 1998: An evaluation and intercomparison of four new advection schemes for use in global chemistry models. *J. Geophys. Res.*, **103**, 19253–19269.
- , C. Beets, H. van Dop, P. G. Duynkerke, and A. P. Siebesma, 1999: Mass-flux characteristics of reactive scalars in the convective boundary layer. *J. Atmos. Sci.*, **56**, 37–56 (chapter 2 of this dissertation).
- Piacsek, A. P., and G. P. Williams, 1970: Conservation properties of convection difference schemes. *J. Comp. Phys.*, **6**, 392–405.
- Randall, D. A., and B. A. Wielicki, 1997: Measurements, models, and hypotheses in the

- atmospheric sciences. *Bull. Amer. Meteor. Soc.*, **78**, 399–406.
- , Q. Shao, and C.-H. Moeng, 1992: A second-order bulk boundary-layer model. *J. Atmos. Sci.*, **49**, 1903–1923.
- Rayleigh, Lord, 1916: On convection currents in a horizontal layer of fluid, when the higher temperature is on the under side. *Phil. Mag.*, **32**, 529–546. [Reprinted in Rayleigh, Lord (John William Strutt), 1964: *Scientific Papers*, Vol. 6, Dover Publications, 432–446.]
- Roeckner, E., K. Arpe, L. Bengtsson, M. Christoph, M. Claussen, L. Dümenil, M. Esch, M. Giorgetta, U. Schlese, and U. Schulzweida, 1996: The atmospheric general circulation model ECHAM-4: Model description and simulation of present-day climate. Rep. 218, Max-Planck-Institut für Meteorologie, 90 pp. [Available from Max-Planck-Institut für Meteorologie, Bundesstrasse 55, 20146 Hamburg, Germany.]
- Roelofs, G. J., and J. Lelieveld, 1995: Distribution and budget of O₃ in the troposphere calculated with a chemistry general circulation model. *J. Geophys. Res.*, **100**, 20983–20998.
- , ———, H. G. J. Smit, and D. Kley, 1997: Ozone production and transports in the tropical Atlantic region during the biomass burning season. *J. Geophys. Res.*, **102**, 10637–10651.
- Ruelle, D., and F. Takens, 1971: On the nature of turbulence. *Commun. Math. Phys.*, **20**, 167–192.
- Schmidt, H., and U. Schumann, 1989: Coherent structure of the convective boundary layer derived from large-eddy simulations. *J. Fluid Mech.*, **200**, 511–562.
- Schumann, U., 1989: Large-eddy simulation of turbulent diffusion with chemical reactions in the convective boundary layer. *Atmos. Environ.*, **23**, 1713–1727.
- , 1993: Large eddy simulation of turbulent convection over flat and wavy surfaces. *Large Eddy Simulation of Complex Engineering and Geophysical Flows*, B. Galperin and S. A. Orszag, Eds., Cambridge University Press, 399–421.
- , and C.-H. Moeng, 1991a: Plume fluxes in clear and cloudy convective boundary layers. *J. Atmos. Sci.*, **48**, 1746–1757.
- , and ———, 1991b: Plume budgets in clear and cloudy convective boundary layers. *J. Atmos. Sci.*, **48**, 1758–1770.
- Siebesma, A. P., 1997: On the mass flux approach for atmospheric convection. *New Insights and Approaches to Convective Parametrization*, ECMWF Workshop Proceedings, 25–57. [Available from European Centre for Medium-Range Weather Forecasts, Shinfield Park, Reading RG2 9AX, U.K.]
- , and J. W. M. Cuijpers, 1995: Evaluation of parametric assumptions for shallow

- cumulus convection. *J. Atmos. Sci.*, **52**, 650–666.
- Sillman, S., J. A. Logan, and S. C. Wofsy, 1990: A regional scale model for ozone in the United States with subgrid representation of urban and power plant plumes. *J. Geophys. Res.*, **95**, 5731–5748.
- Sorbjan, Z., 1989: *Structure of the Atmospheric Boundary Layer*. Prentice Hall, 317 pp.
- , 1996: Numerical study of penetrative and “solid lid” nonpenetrative convective boundary layers. *J. Atmos. Sci.*, **53**, 101–112.
- Spee, E. J., 1998: Numerical methods in global transport–chemistry models. Ph.D. dissertation, University of Amsterdam, The Netherlands, 150 pp.
- Stockwell, W. R., 1995: Effects of turbulence on gas-phase atmospheric chemistry: Calculation of the relationship between time scales for diffusion and chemical reaction. *Meteorol. Atmos. Phys.*, **57**, 159–171.
- Stull, R. B., 1988: *An Introduction to Boundary Layer Meteorology*. Kluwer Academic, 666 pp.
- , 1993: Review of non-local mixing in turbulent atmospheres: Transilient turbulence theory. *Bound.-Layer Meteor.*, **62**, 21–96.
- , 1998: Introduction to clear and cloudy boundary layers. *Clear and Cloudy Boundary Layers*, A. A. M. Holtslag and P. G. Duynkerke, Eds., Koninklijke Nederlandse Akademie van Wetenschappen, 17–42.
- Sykes, R. I., S. F. Parker, D. S. Henn, and W. S. Lewellen, 1994: Turbulent mixing with chemical reaction in the planetary boundary layer. *J. Appl. Meteor.*, **33**, 825–834.
- Tennekes, H., 1970: Free convection in the turbulent Ekman layer of the atmosphere. *J. Atmos. Sci.*, **27**, 1027–1034.
- , and J. L. Lumley, 1972: *A First Course in Turbulence*. MIT Press, 300 pp.
- Thuburn, J., and D. G. H. Tan, 1997: A parameterization of mixdown time for atmospheric chemicals. *J. Geophys. Res.*, **102**, 13037–13049.
- Tiedtke, M., 1989: A comprehensive mass flux scheme for cumulus parameterization in large-scale models. *Mon. Wea. Rev.*, **117**, 1779–1800.
- van Haren, L., and F. T. M. Nieuwstadt, 1989: The behavior of passive and buoyant plumes in a convective boundary layer, as simulated with a large-eddy model. *J. Appl. Meteor.*, **28**, 818–832.
- Verver, G. H. L., 1994: Comment on “A modified K model for chemically reactive species in the planetary boundary layer” by Fujihira Hamba. *J. Geophys. Res.*, **99**, 19021–19023.
- , H. van Dop, and A. A. M. Holtslag, 1997: Turbulent mixing of reactive gases in the convective boundary layer. *Bound.-Layer Meteor.*, **85**, 197–222.

- , ———, and ———, 1999: Turbulent mixing and the chemical breakdown of isoprene in the atmospheric boundary layer. Submitted to *J. Geophys. Res.*
- Verwer, J. G., and D. Simpson, 1995: Explicit methods for stiff ODEs from atmospheric chemistry. *Appl. Num. Math.*, **18**, 413–430.
- Vilà-Guerau de Arellano, J., and P. G. Duynkerke, 1993: Second-order closure study of the covariance between chemically reactive species in the surface layer. *J. Atmos. Chem.*, **16**, 145–155.
- , and J. Lelieveld, 1998: Chemistry in the atmospheric boundary layer. *Clear and Cloudy Boundary Layers*, A. A. M. Holtslag and P. G. Duynkerke, Eds., Koninklijke Nederlandse Akademie van Wetenschappen, 267–286.
- , P. G. Duynkerke, P. J. Jonker, and P. J. H. Builtjes, 1993a: An observational study on the effects of time and space averaging in photochemical models. *Atmos. Environ.*, **27A**, 353–362.
- , ———, and P. J. H. Builtjes, 1993b: The divergence of the turbulent diffusion flux in the surface layer due to chemical reactions: the NO–O₃–NO₂ system. *Tellus*, **45B**, 23–33.
- , ———, and K. F. Zeller, 1995: Atmospheric surface layer similarity theory applied to chemically reactive species. *J. Geophys. Res.*, **100**, 1397–1408.
- Vogelezang, D. H. P., and A. A. M. Holtslag, 1996: Evaluation and model impacts of alternative boundary-layer height formulations. *Bound.-Layer Meteor.*, **81**, 245–269.
- Wang, S., and B. Stevens, 1999: On top-hat representation of turbulence statistics in cloud-topped boundary layers: A large-eddy simulation study. Submitted to *J. Atmos. Sci.*
- Willis, G. E., and J. W. Deardorff, 1974: A laboratory model of the unstable planetary boundary layer. *J. Atmos. Sci.*, **31**, 1297–1307.
- Wyngaard, J. C., 1982: Boundary-layer modeling. *Atmospheric Turbulence and Air Pollution Modelling*. F. T. M. Nieuwstadt and H. van Dop, Eds., Reidel, 69–106.
- , 1998a: Experiment, numerical modeling, numerical simulation, and their roles in the study of convection. *Buoyant Convection in Geophysical Flows*, E. J. Plate, E. E. Fedorovich, D. X. Viegas, and J. C. Wyngaard, Eds., Kluwer Academic, 239–251.
- , 1998b: Boundary-layer modeling: History, philosophy, and sociology. *Clear and Cloudy Boundary Layers*, A. A. M. Holtslag and P. G. Duynkerke, Eds., Koninklijke Nederlandse Akademie van Wetenschappen, 325–332.
- , and R. A. Brost, 1984: Top-down and bottom-up diffusion of a scalar in the convective boundary layer. *J. Atmos. Sci.*, **41**, 102–112.
- , and C.-H. Moeng, 1992: Parameterizing turbulent diffusion through the joint probability density. *Bound.-Layer Meteor.*, **60**, 1–13.

- Young, G. S., 1988a: Turbulence structure of the convective boundary layer, Part II: Phoenix 78 aircraft observations of thermals and their environment. *J. Atmos. Sci.*, **45**, 727–735.
- , 1988b: Turbulence structure of the convective boundary layer, Part III: The vertical velocity budgets of thermals and their environment. *J. Atmos. Sci.*, **45**, 2039–2049.

Samenvatting

Convectie en chemie in de atmosferische grenslaag

De samenstelling van de atmosfeer is in de laatste 200 jaar geleidelijk aan het veranderen ten gevolge van menselijk handelen. Dit heeft regionaal geleid tot aantasting van het milieu (verzuring en smogvorming) en mondiaal tot het additionele broeikas-effect. Om verwachtingen te maken voor verzuring, smogvorming en veranderingen in het broeikas-effect en om de bepalende processen te bestuderen, wordt met computermodellen de luchtsamenstelling berekend in grote delen van de atmosfeer, zoals de lucht boven Europa, een ander werelddeel of de hele wereld. Hierbij worden de concentratie en de chemische productie en afbraak van gassen zoals ozon en het hydroxylradicaal OH (het schoonmaakmiddel van de atmosfeer) in de verschillende luchtlagen berekend.

Dit proefschrift heeft tot doel een bron van onzekerheid te elimineren die reeds meer dan 25 jaar geleden als zodanig werd gepresenteerd voor grootschalige computermodellen van de chemie van de atmosfeer. De begrensde capaciteit van zelfs de grootste computers, maakt dat niet alle details van de atmosferische stroming en samenstelling kunnen worden berekend met als gevolg dat processen onder een bepaalde ruimtelijk schaal (de "subgrid schaal") slechts bij benadering kunnen worden bepaald. De onzekerheid betreft de veronderstelde grote invloed die subgrid-schaal turbulentie en chemie in de atmosferische grenslaag zouden hebben op de schatting van chemische reactiesnelheden in grootschalige computermodellen. Er moet rekening worden gehouden met het feit dat de turbulente processen die zich afspelen op een schaal die kleiner is dan de afmetingen van de roostercellen, grote invloed kunnen hebben op de gemiddelde reactiesnelheden in de roostercellen.

Een groot deel van de atmosferische chemie van kortlevende sporengassen (met een levensduur van enkele uren) vindt in de atmosferische grenslaag, een (dunne) laag van de atmosfeer die direct beïnvloed wordt door het aardoppervlak. In deze laag, die zich overdag vormt wanneer de hemel helder is en het oppervlak opwarmt, worden belangrijke reactieve gassen uitgestoten en voor een groot deel afgebroken, o.a. onder invloed van zonlicht. Vanaf het oppervlak stijgen warme luchtbellens op, waarbij ze koudere lucht omlaag drukken. Dit convectieve proces zorgt ervoor dat de laag overdag een dikte bereikt van 1 à 2 kilometer. De concentratie van aan het oppervlak uitgestoten gassen is hoger in de stijgende luchtbellens dan in de dalende luchtstromen. Deze concentratieverschillen leiden in principe tot verschillende reactiesnelheden in dalende en stijgende lucht.

Zelfs de allergrootste supercomputers hebben niet genoeg rekencapaciteit om in modellen voor de grootschalige (bijvoorbeeld mondiale) atmosferische chemie de concentratieverschillen op de schalen van de turbulente stijgende en dalende luchtbellens (tussen 10 meter en 1 kilometer) mee te nemen. In de mondiale computermodellen is de atmosfeer namelijk verdeeld in gelijke roostercellen met zijdes van tweehonderd tot duizend kilometer en een hoogte van enkele honderden meters. Hierbij wordt aangenomen dat de concentratie van chemische stoffen in deze roostercellen overal hetzelfde is. De hypothese die in dit proefschrift wordt onderzocht, is dat de concentratieverschillen tussen stijgende en dalende luchtbellens belangrijk zijn voor de gemiddelde grootschalige afbraaksnelheden in de grenslaag.

In hoofdstuk 2 van dit proefschrift wordt nauwkeurig berekend hoe gassen die worden uitgestoten aan het oppervlak of ingemengd aan de bovenkant van de grenslaag, zich verspreiden in een klein turbulent gebied van de atmosfeer van enkele kilometers groot. Zo wordt de kans geschat dat gasdeeltjes met elkaar reageren. Daarbij worden de gemiddelde reactiesnelheden bepaald. De op gedetailleerde wijze bepaalde reactiesnelheid wijkt af van de schatting van de reactiesnelheid op basis van gemiddelde concentraties. Voor de analyse van dit aspect van het turbulente transportreactie probleem is de tweestromenbenadering zeer geschikt, waarbij expliciet onderscheid wordt gemaakt tussen op- en neerwaartse luchtstromen. In het bijzonder kunnen op basis van de tweestromenbenadering voldoende nauwkeurige schattingen worden gemaakt van de bovengenoemde afwijking van de gemiddelde reactiesnelheid.

Op grond van de resultaten van hoofdstuk 2 wordt in hoofdstuk 3 een eenvoudig model geformuleerd en getest voor veranderende gemiddelde reactiesnelheden ten gevolge van turbulentie. De resultaten verhouden zich goed tot de resultaten van fjnschalige modellen voor verschillende onderzochte condities en reactieschema's. Het eenvoudige model is geschikt om te worden ingebouwd in grootschalige chemiemodellen. Ook wordt in hoofdstuk 3 een

bestaand model voor het turbulente verticale transport (flux), een zogenaamde “eerste-orde niet-lokale sluiting”, getest voor reactieve gassen. Het blijkt dat dit model tot goede resultaten leidt in verhouding tot de fjnschalige modellen. In hoofdstuk 4 wordt aangetoond dat de fout die met dit model gemaakt wordt door de zogenaamde “hogere-orde chemietermen” in de berekening van de flux te verwaarlozen, een stuk kleiner is dan in meer complexe “tweede-orde sluitingsmodellen”.

Tenslotte wordt in hoofdstuk 5 een impactstudie verricht voor verschillende plekken op de aarde met een eenkolomsversie van een uitgebreid chemieklimaatmodel, met daarin opgenomen het in hoofdstuk 3 ontwikkelde model voor veranderende reactiesnelheden ten gevolge van turbulentie. Uit de berekeningen blijkt dat zelfs de gassen die het snelst reageren, zoals isopreen (C_5H_8 , uitgestoten door vegetatie) en de stikstofdioxiden, gemiddeld veel minder snel reageren dan de levensduur van een stijgende luchtbel. De bellen blijven hoogstens tien tot vijftien minuten in stand; het afbreken van isopreen en stikstofdioxiden kost gemiddeld een paar uur. Hierdoor blijken concentratieverschillen door turbulente op- en neerwaartse luchtstromen de snelheid waarmee de gassen gemiddeld over grotere gebieden worden afgebroken, met niet meer dan 2 procent te veranderen (en de concentraties van de verschillende betrokken gassen met niet meer dan 1 procent). Dit is verwaarloosbaar in vergelijking met andere modelonzekerheden, zoals de subgrid-schaal variabiliteit ten gevolge van inhomogene emissies.

De conclusie van dit proefschrift is dat de gemiddelde reactiesnelheden nauwelijks veranderen onder invloed van turbulentie in de convectieve atmosferische grenslaag en dat de bestaande berekeningen van de luchtkwaliteit op Europese of mondiale schaal betrouwbaarder blijken te zijn dan aan begin van dit onderzoek was verwacht. Andere oorzaken van subgrid-schaal variabiliteit van gassen, zoals de inhomogeniteit van emissies, dragen echter nog steeds significant bij aan de totale modelonzekerheid.

Curriculum vitae

Arthur Caesar Petersen was born in Amsterdam on September 29, 1970. He grew up in Lisse, where he received the first four years of his secondary education at Fioretti College. In 1986 his family moved to Amsterdam, and he finished his pre-university education at Vossius Gymnasium. From 1988 to 1993 he was enrolled in the physics program and from 1991 to 1995 in the philosophy program of Vrije Universiteit, Amsterdam. He did his MSc thesis research in theoretical physics at the National Institute for Nuclear Physics and High-Energy Physics (NIKHEF) on neutrino scattering off nucleons. His MA thesis in philosophy of science was on consensus in the natural sciences. The current dissertation is the product of a PhD project at the Institute for Marine and Atmospheric Research Utrecht (IMAU), Utrecht University from 1995 to 1999. Since April 1, 1999 he has been a postdoctoral research associate in the Faculty of Philosophy at Vrije Universiteit, Amsterdam.